Brain-machine interface using electrocorticography in humans

by Tomislav Milekovic

Thesis submitted for the degree of Doctorate of Philosophy (Ph. D.) at Department of Bioengineering, Imperial College London

Declaration of originality

Work presented in this thesis is my own. All other work discussed here is referenced at the corresponding location in the text. Full citation is given in the Bibliography section at the end of the thesis.

Abstract

Paralysis has a severe impact on a patient's quality of life and entails a high emotional burden and life-long social and financial costs. More than 5 million people in the USA suffer from some form of paralysis and about 50% of the people older than 65 experience difficulties or inabilities with movement. Restoring movement and communication for patients with neurological and motor disorders, stroke and spinal cord injuries remains a challenging clinical problem without an adequate solution.

A brain-machine interface (BMI) allows subjects to control a device, such as a computer cursor or an artificial hand, exclusively by their brain activity. BMIs can be used to control communication and prosthetic devices, thereby restoring the communication and movement capabilities of the paralyzed patients. So far, most powerful BMIs have been realized by extracting movement parameters from the activity of single neurons. To record such activity, electrodes have to penetrate the brain tissue, thereby generating risk of brain injury. In addition, recording instability, due to small movements of the electrodes within the brain and the neuronal tissue response to the electrode implant, is also an issue. In this thesis, I investigate whether electrocorticography (ECoG), an alternative recording technique, can be used to achieve BMIs with similar accuracy.

First, I demonstrate a BMI based on the approach of extracting movement parameters from ECoG signals. Such ECoG based BMI can further be improved using supervised adaptive algorithms. To implement such algorithms, it is necessary to continuously receive feedback from the subject whether the BMI-decoded trajectory was correct or incorrect. I show that, by using the same ECoG recordings, neuronal responses to trajectory errors can be recorded, detected and differentiated from other types of errors. Finally, I devise a method that could be used to improve the detection of error related neuronal responses.

Acknowledgments

Work described in this thesis took part at the Bernstein Centre for Computational Neuroscience (BCCN) Freiburg, a part of University of Freiburg and at Department for Bioengineering, Imperial College London. It was supported by the German Federal Ministry of Education and Research (BMBF) grant 01GQ0420 to BCCN Freiburg, BMBF 01GQ0830 grant to BFNT Freiburg and Tübingen, BMBF GoBio grant 0313891 and the Imperial College London.

I would especially like to thank the subjects for participating in studies described in Chapters 2, 3 and 4. Their participation was not awarded in any way and, without their generosity, most of the presented research would not be possible.

My supervisor, Dr. Carsten Mehring, deserves a special gratitude. He supported my work from the start and without any reservation, often giving important advice and investing time in discussing technical and research issues whenever these occurred. I would also like to thank all people that directly helped with here presented work: Dr. Chloe Huetz, Dr. Tobias Pistohl, Prof. Dr. Ad Aertsen, Dr. Tonio Ball, Prof. Dr. Andreas Schulze-Bonhage, Joerg Fisher, Markus Raab, Dr. Joern Rickert and Johanna Ruescher. Without their help, it would be hard to perform here presented research.

I would like to thank staff of the Freiburg University hospital's Epilepsy Centre for their help. All ECoG recordings were possible only due to their generous cooperation. I would also like to thank the staff of BCCN Freiburg and Imperial College, Department of Bioengineering. Their support made it possible to concentrate on the research.

In addition, I would like to thank International Neuroinformatics Coordinating Facility (INCF), Federation of European Neurosciences (FENS) and Imperial College Fund (ICF) for helping to fund travel to conferences where here described research was presented and discussed.

Contents

Declaration of originality 1

Abstract 2

Acknowledgments 3

1. Introduction 7

1.1. Recording techniques 8

1.2. BMI approaches 11

1.3. BMI algorithms 13

1.4. Outline of the thesis 14

2. An online BMI using decoding of movement direction from the human ECoG 16

2.1. Introduction 17

2.2. Methods 18

2.2.1. Subjects and recordings 18

2.2.2. Task 20

2.2.3. Model building for decoding in brain control sessions 22

2.2.4. Offline data analysis 23

2.2.5. Comparison of electrode selection strategies 23

2.2.6. Significance testing of neural responses 24

2.2.7. Movement onset versus go cue alignment 25

2.2.8. Electrical stimulation mapping (ESM) and neuroanatomical electrode assignment 25

2.3. Results 27

2.3.1. Neuronal responses 28

2.3.2. Decoding accuracy in online closed loop experiments 28

2.3.3. Comparison of electrode selection strategies 30

2.3.4. DA topographies 30

2.3.5. Movement onset versus go cue alignment 30

2.4. Discussion 32

3. Error related neuronal responses 37
3.1. Introduction 38
3.2. Methods 40
3.2.1. Task 40
3.2.2. Error and control events 42
3.2.3. Subjects and recordings 43
3.2.4. Data analysis 44
3.2.5. Neuroanatomical analysis 54
3.3. Results 55
3.3.1. Widespread ERNRs 56
3.3.2. ERNRs latencies 56
3.3.3. Differentiating ERNRs from baseline and between each other 57
3.3.4. Spatial distribution of ERNRs 61
3.3.5. Classification analysis 64
3.4. Discussion 66
3.4.1. Spectro-temporal characteristics of neuronal error responses 68
3.4.2. Comparison to previous ERNR studies and widespread ERNR 69
3.4.3. Relevance for brain machine interfaces 70
4. Detection of ERNRs recorded by ECoG in humans during continuous movements 72
4.1. Introduction 73
4.2. Methods 74
4.2.1. Measures of detection accuracy 74
4.2.2. Signal components 77
4.2.3. Detection algorithm 78
4.2.4. MRNR subtraction 80
4.2.5. Neuroanatomical analysis 80
4.3. Results 80
4.3.1. Detection of error related neuronal responses 80

4.3.2. Topographical distribution of informative signals for error detection 83
4.3.3. Error detection using signals from motor or somatosensory areas 83
4.3.4. Detection from smaller electrode sets 84
4.3.5. Effect of MRNR subtraction on the normalized mutual information 84
4.3.6. Selection of the model type for detection: rLDA vs. rQDA 85
4.4. Discussion 87
4.4.1. Characteristics of signal components used for detection 90
4.4.2. Comparison to previous detection studies 91
4.4.3. Comparison to previous ERNR studies 92
4.4.4. Relevance for brain machine interfaces 92
5. Inference based method for re-alignment of single trial neuronal responses 94
5.1. Introduction 95
5.2. Methods 95
5.2.1. Neuronal response model 96
5.2.2. Difference of average signal standard deviation 98
5.2.3. Reliability of $dTAV$ as a measure of jitter reduction 99
5.2.4. $dTAV$ realignment algorithm 101
5.2.5. Simulated data 104
5.3. Results 106
5.3.1. Analytical analysis 106
5.3.2. Re-alignment of simulated data 107
5.4. Discussion 108
6. Conclusions 111
Bibliography 114

Chapter 1

Introduction

Paralysis, a loss of muscle function of one or more muscles, is a widespread chronic medical condition. A recent study by Christopher and Dana Reeve Foundation (2009) revealed that approximately 1.9% of USA population has some form of paralysis. Main causes for paralysis (Figure 1) are stroke (29%), spinal cord injury (23%) and multiple sclerosis (17%). Patients suffering from paralysis have to rely on help from their friends and family. It is estimated that more than 50 million people in the USA or around 20% of USA population provide this kind of care. Based on a study by Arno (Arno et al., 1999), economic costs of health care for paralyzed patients were estimated to be $306 billion in 2006. In UK, it is estimated that more than 500,000 people suffer from paralysis and special care annual costs are estimated at more than £500 million. These numbers demonstrate that paralysis dramatically affects not only the lives of the patients and their social environment, but society as a whole.

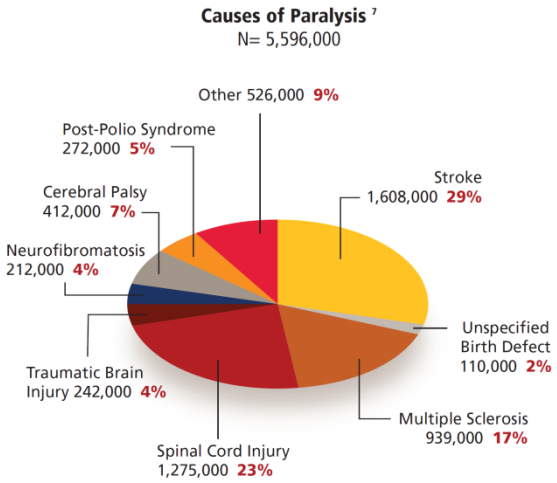

Figure 1. Distribution of causes for paralysis in the USA. Taken from One Degree of Separation: Paralysis and Spinal Cord Injury (2009).

Brain-machine interfaces (BMIs), also called brain-computer interfaces, allow subjects to control a device, such as a computer cursor or an artificial hand, exclusively by their brain activity (Vidal, 1973; Wolpaw et al., 2002). A number of paralyzed patients completely lose the ability to move or speak, thereby losing all means of communication with the outside world. In some studies, BMIs have been used to establish a novel way of communication for such paralyzed patients (Birbaumer, 2006; Krusienski and Shih, 2011; Kubler et al., 2001), restoring their ability for social interaction. In

addition, BMIs can be used to establish the connection between the subject's brain and a prosthetic device (Figure 2), thereby restoring movement capabilities of paralyzed patients (Daly and Wolpaw, 2008; Donoghue et al., 2007; Lebedev and Nicolelis, 2006b; Schwartz et al., 2006).

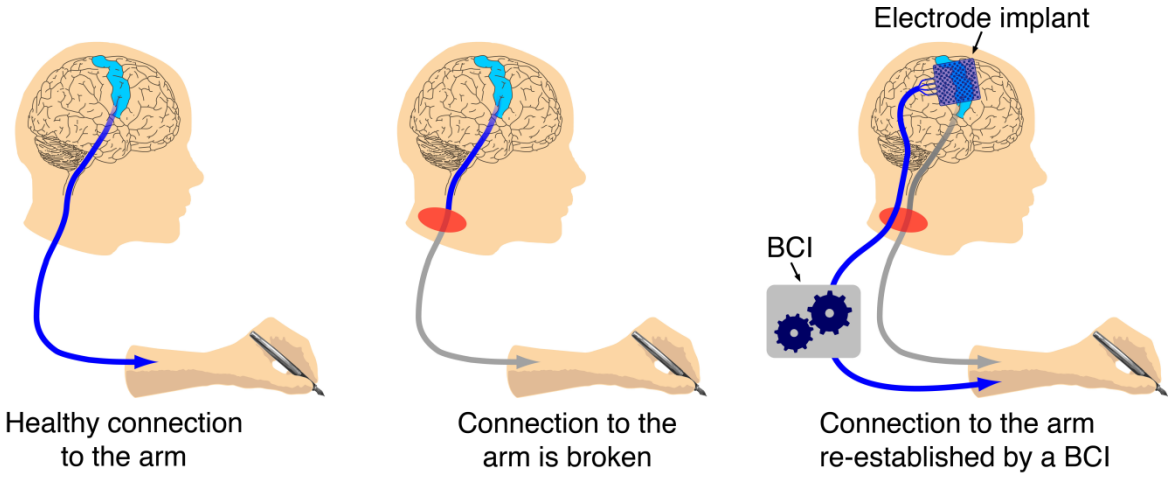

Figure 2. A possible application for a BMI. Here, BMI is used to re-establish the broken nerve connection between the brain and the arm. Figure provided by Mehring, Ball, Rickert and Rau.

BMIs can be characterized by the technique used to record the brain signals and by the approach used to translate brain signals into the control of the external device (Wolpaw et al., 2002; Lebedev and Nicolelis, 2006; Waldert et al., 2009).

1.1. Recording techniques

Different recording techniques have been used to realize BMIs (Figure 3). One can use recordings of spike trains of single neurons (single unit activity; SUA) or several neurons together (multiunit activity; MUA) in the close vicinity of the recording electrode (Carmena et al., 2003; Fraser et al., 2009; Guenther et al., 2009; Hochberg et al., 2006; Moritz et al., 2008; Serruya et al., 2002; Velliste et al., 2008) and local field potentials (LFP) mainly reflecting synaptic activity of a neuronal population around the microelectrode (Hwang and Andersen, 2009; Mehring et al., 2004; Zhuang et al., 2010). To record such signals for BMI use, it is necessary to implant microelectrodes or arrays of microelectrodes into the brain tissue (Figure 4). The process of implantation requires opening the skull and penetrating the cortical tissue, resulting in substantial medical risk. SUA and MUA recordings also exhibit problems with recording stability. Small movements on a micrometre scale of the implanted microelectrodes can move it away from a previously nearby neuron, thereby loosing the signal from this neuron. In addition, tissue reactions at the surface of the implanted electrode (Bjornsson et al., 2006; Shain et al., 2003) creates an insulation layer that can effectively distance the recording electrode from neighbouring neurons, thereby reducing the signal to noise ratio of the recorded signal or losing the signal altogether. Furthermore, neurons can change coding relationship

between their activity and the corresponding behaviour over time (Dickey et al., 2009; Donoghue et al., 2004). For all of these reasons, it is difficult to realize reliable long-term operation of a BMI based on intracortical spike recordings.

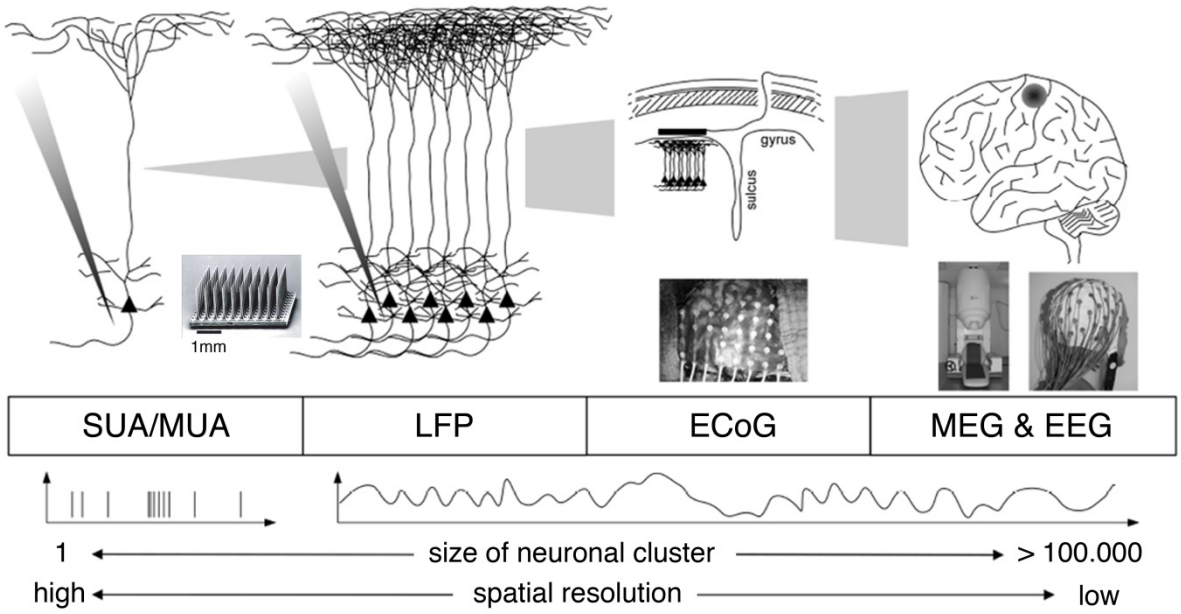

Figure 3. Overview of recording techniques used to achieve BMI control. Microelectrode arrays are used to record activity from multiple single neurons (SUA, MUA) and local field potentials (LFP). Electrocorticography (ECoG) records electrical potentials from the surface of the brain. Non-invasive recording techniques, such as MEG and EEG, record neuronal activity outside of subject's skull. Figure taken from (Waldert et al., 2009).

Alternatively, it is possible to record SUA or MUA signals using neurotrophic electrodes (Bartels et al., 2008). In this technique, recording electrodes reside within glass capillaries filled with neurotrophic factor. Both capillaries and electrodes are implanted in the cortex and, thanks to the neurothophic factor, branches of nearby axons grow into the capillaries and around the electrodes. Such an implant provides stable recordings but, unfortunately, an array of such electrodes, capable of recording signals from a large enough populations of neurons, is still not available. Therefore, BMIs using this recording technique have not yet been realized.

Often, a couple of neurons with similar signals will be recorded by one of the microelectrodes. Therefore, to record SUA, it is necessary to identify and extract signals originating from a particular neuron within the compound signal. This method is called spike sorting (Buzsaki, 2004; Lewicki, 1998; Quiroga, 2012) and, while it can successfully identify different neurons, it occasionally mislabels neuronal spikes (Wood et al., 2004), thereby adding to the instability of the SUA based BMIs.

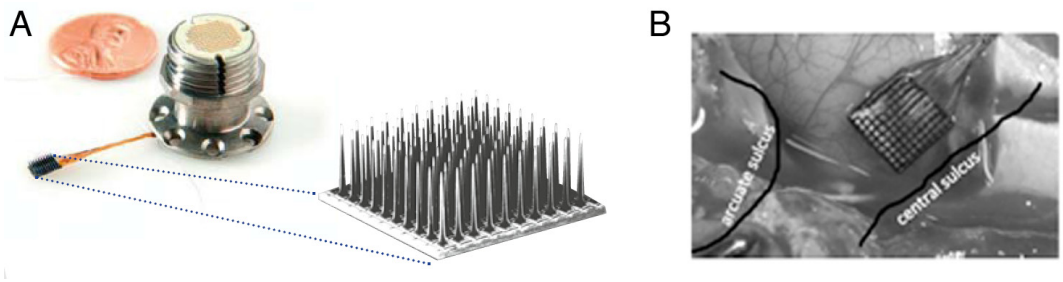

Figure 4. Blackrock microelectrode array used for intracortical recordings of neuronal activity. A: Implant and the scull interface shown next to one United States penny coin for scale. B: Example of implanted Blackrock array. Figure taken from brochure for Blackrock Microsystems™.

Non-invasive recording techniques can also be utilized for a BMI. Electroencephalography (Maulsby et al., 1963; Niedermeyer and Lopes da Silva, 2005; Nunez and Srinivasan, 2006) records electrical potentials from the surface of the subject's scalp. Due to simplicity, low cost and the non-invasiveness of EEG recordings, it has been the most widespread technique to record neural signals from humans. Therefore, it has often been used for BMI research (Birbaumer et al., 1999; Machado et al., 2010; Wolpaw and McFarland, 2004). Magnetoencephalography (MEG; Cohen, 1972) records the magnetic fields from outside of the subject's head. Since magnetic fields, produced by currents in the brain, are rather small, recordings have to be made within a shielded room and using highly sophisticated sensors, which make this technique expensive and immobile (for MEG based BMI see Mellinger et al., 2007). BMIs have also been realized using functional magnetic resonance imaging (fMRI; Huettel et al., 2008; for fMRI based BMI see Weiskopf et al., 2004), a recording technique where neuronal activity is measured indirectly through changes in the blood oxygenation levels (BOLD signal) in small parts of the cortex. fMRI signals are measured using a large superconductive magnet, which also makes the method expensive and immobile. Compared to electrophysiological recording techniques, it has a very low temporal resolution (around 25Hz), but has the ability to record BOLD signals from the whole brain at once. Another recording technique, near infrared spectroscopy (NIRS; Brazy, 1991; Smith, 2011), has recently been utilized for a BMI (Abdelnour and Huppert, 2009). This technique records the absorption of the near infrared light that is passed through the cortex using emitters and sensors on the top of the skull. Absorption depends on the blood oxygenation levels in the part of the cortex light travels through. As in the fMRI, these measurements are correlated to neuronal activity in the corresponding part of the cortex.

In the case of all non-invasive electrophysiological methods, sensors are far from the source of the signal. Therefore, these recording techniques suffer from poor spatial resolution compared to intracortical recording methods (Nunez and Srinivasan, 2006). In addition, the magnitude of noise from the environment is usually comparable to or even higher than the recorded signal, which

makes it challenging to operate it in a mobile BMI system. While recording, subjects' movements can create strong recording artefacts that further hinder the use of non-invasive BMIs.

Another possibility for BMI is to use electrocorticography (ECoG), epicortical implants that record electrical potentials from the surface of the brain (Kellis et al., 2010; Leuthardt et al., 2004; Pistohl et al., 2008; Schalk et al., 2008). As for intracortical implants, an opening of the skull is necessary during the implantation procedure (Figure 5). On the other hand, implanted electrodes reside on the surface of the cortex instead of penetrating the cortex. The recorded signals are analogue and, like the LFP, largely represent synaptic input. Therefore, no spike sorting is required. A recent study by Chao et al. (Chao et al., 2010) showed that ECoG recordings also possess long term stability and that motor coding of these signals does not change even over several months. In comparison to non-invasive recording techniques, ECoG has a higher spatial resolution (Nunez and Srinivasan, 2006; Slutzky et al., 2010), can record signals in higher frequencies (Staba et al., 2002), has a higher signal to noise ratio (Ball et al., 2009a) and is less prone to movement artefacts (Ball et al., 2009a). Therefore, ECoG might provide an adequate compromise of signal quality, information content, and invasiveness between intracortical and non-invasive recording. ECoG recordings are presently used in standard clinical procedures (e.g. presurgical epilepsy assessment, electrical stimulation mapping and stroke assessment) which makes it possible to conduct ECoG studies with human subjects without additional medical risk.

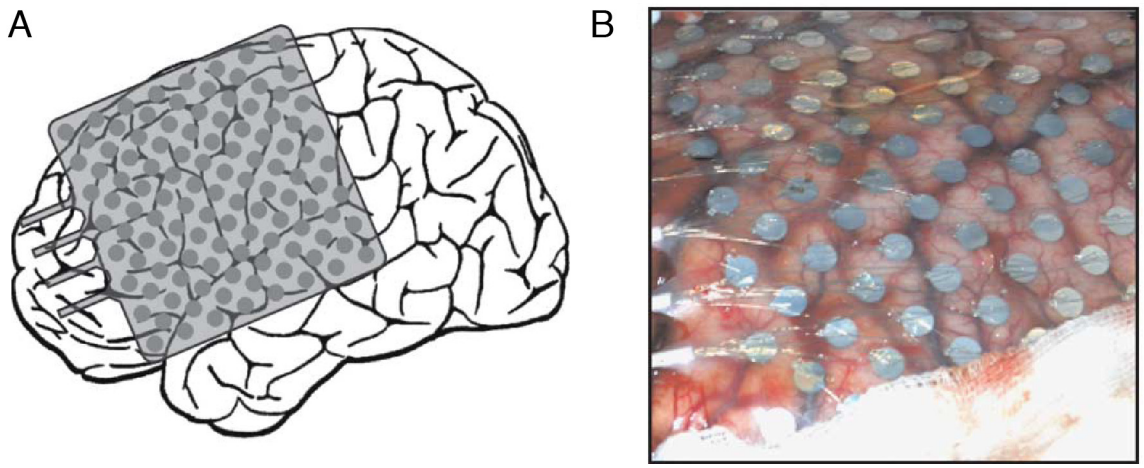

Figure 5. Example of an ECoG implant for epilepsy assessment. A: Scheme of an 112 electrode ECoG grid implant drawn over a planned implantation location. B: Photograph of ECoG implant taken during surgery. Figure taken from (Mehring et al., 2004).

1.2. BMI approaches

A number of approaches can be used to realize BMI control. BMIs can use brain activity elicited in response to external stimuli, such as light flashes or sounds. These BMIs rely on the fact that

neuronal responses to such stimuli can be modulated by attention. By changing the attending from one stimulus to another, a subject can communicate with the surroundings. This approach includes BMIs based on steady state visual evoked potentials (SSVEP; Allison et al., 2008; Middendorf et al., 2000) and visual (Farwell and Donchin, 1988; Hoffmann et al., 2008) and auditory (Sellers et al., 2006) P300 BMIs. It requires little or no training and has already been implemented in a reliable fashion (Birbaumer et al., 1999; Brunner et al., 2011), but exerts constant pressure on the subjects to indirectly communicate their intentions. Therefore, it has mainly been used for BMI speller devices, useful only for the completely paralyzed patient unable to use other ways of communication.

Subjects can also be trained to self-regulate certain aspects of their brain activity. Voluntary up and down regulation of slow cortical potentials (Birbaumer et al., 1999) and voluntary modulation of the amplitude of μ (8-13Hz) or β (13-20Hz) frequency bands (McFarland et al., 2008; McFarland et al., 2010; Moritz et al., 2008; Wolpaw and McFarland, 2004; Wolpaw et al., 1991) have been used in this way. This approach can be used to operate the BMI with three degrees of freedom, but only after an extensive training of several months (McFarland et al., 2010). In addition, many subjects do not show the ability to self-regulate their brain ability. More complex and more reliable control might be possible using this method but extensive training hinders its possible use for paralyzed patients.

Neuronal activity during movement imagination has also been used to control different degrees of freedom of a BMI controlled device (Blankertz et al., 2007; Pfurtscheller et al., 1993; Pfurtscheller and Neuper, 2006; Schalk et al., 2008). In this approach, little or no subject training is needed. On the other hand, such signals are often very noisy and can depend on the subjects' ability to consistently imagine the movement.

Another approach uses the property of neurons in motor related areas to directly code for parameters of active movements. Using this approach, movements of an external effector (e.g. movement of arm prosthesis to the right) are controlled by motor cortical signals that control the equivalent movements of the corresponding body part (e.g. arm movement to the right). This approach was initially motivated by findings in monkey studies (Georgopoulos et al., 1983; Georgopoulos et al., 1986; Moran and Schwartz, 1999) which showed that the direction and speed of arm movements can be inferred from the firing rates of motor cortical neurons. More recently, it has been shown, using offline analysis, that movements of a limb can be inferred from monkey SUA (Vargas-Irwin et al., 2010), monkey MUA (Stark and Abeles, 2007), monkey LFP (Ince et al., 2010; Mehring et al., 2003; Zhuang et al., 2010), human ECoG (Ball et al., 2009b; Leuthardt et al., 2004; Mehring et al., 2004), monkey ECoG (Chao et al., 2010), human EEG (Waldert et al., 2008) and human MEG (Georgopoulos et al., 2005; Waldert et al., 2008). The most powerful BMIs to date,

continuous online BMIs controlling multiple degrees of freedom with high accuracy, have been realized using this approach and SUA signals (Carmena et al., 2003; Fraser et al., 2009; Hochberg et al., 2006; Serruya et al., 2002; Taylor et al., 2002; Velliste et al., 2008). BMIs with the same approach have not yet been realized using less invasive recording method.

1.3. BMI algorithms

BMIs essentially translate the neuronal activity into the control signal for the device that is being interfaced. The part of the BMI that does this translation is called the BMI algorithm. A large number of BMIs are designed to translate neuronal activity into discrete commands. Output of such an interface is a selection amongst several possible choices. In that case, one uses classification algorithms. Algorithms that output a continuous variable are called regression algorithms. To continuously control a complex device, such as a prosthetic hand with the possibility of moving individual fingers, it is necessary to use regression algorithms with several degrees of freedom.

During the active use of a BMI device, subjects receive feedback about its operation. Due to neuronal plasticity, neurons can modify their activity to improve the reliability of BMI control (Fetz, 1969; Ganguly and Carmena, 2009). After only several days, a population of neurons can modify its coding behaviour to achieve two dimensional BMI control (Ganguly and Carmena, 2009). If a larger neuronal population is recorded using EEG, evidence suggests that longer time is needed for modifying neuronal coding behaviour to achieve similar levels of control (McFarland et al., 2010).

One can also allow BMI algorithm to change, thereby incorporating the knowledge gathered during the online operation of the BMI device. Often, a large amount of data is needed to train a BMI algorithm. By re-training the algorithm after a period of time, using the data recorded during the BMI use, it is possible to improve the BMI operation. By using adaptive algorithms, one can continuously incorporate information available from the use of BMI. Adaptive algorithms can be separated into three groups. Unsupervised algorithms receive no feedback on the accuracy of their decoding. They modify the algorithm according to some assumptions about the recorded signals and output variables. For instance, in a two class problem, distributions of neural recordings that code for these classes can start to move. A simple algorithm can continuously fit Gaussian distributions on the last 100 recorded examples, thereby tracking the movements of the distributions (Blumberg et al., 2007).

Reinforcement learning algorithm relies on the binary feedback usually related to the final outcome of the task. For instance, if a subject had BMI control of a computer cursor on the screen and was trying to guide the cursor to one out of several targets, reinforcement algorithms would not receive any feedback about the decoded trajectory, but only whether the correct target was reached or not.

This information is then used to modify the algorithm in such a way to make less incorrect target selections (DiGiovanna et al., 2009).

Supervised adaptive algorithms receive the more informative or full feedback about the decoded outcome. Such feedback can then be used to modify the algorithms in a more direct way, leading to faster improvement of BMI operation. Both reinforcement learning and supervised adaptive algorithms rely on feedback information. Such information is provided either by assuming the intention of the subject or by reading out the discrepancy between the subjects' intention and the decoded outcome from the neuronal activity. Former approach can be used successfully only when the optimal choice or trajectory is obvious and straightforward. For instance, if subject has two possible, equally short trajectories that can be used to reach the target, it will not be possible to reliable estimate subject's intention. Even in the cases where design of the task is such that the optimal trajectory is always easy to predict, subjects might not choose to use such trajectory. Furthermore, during the real-life application, where there are numerous obstacles and target choices are known only to the subject, it is impossible to correctly estimate the subjects' intention.

On the other hand, neuronal responses to errors, such as discrepancy between the subjects' intention and the decoded outcome, have been identified using a number of different recording techniques (Diedrichsen et al., 2005; Krigolson et al., 2008; Ojemann et al., 2004; van Veen and Carter, 2006). This led to several successful uses of the former approach, where neuronal responses to error signals were used to modify BMI classification algorithms, which then improved their accuracy of classification (Blankertz et al., 2003; Buttfield et al., 2006; Ferrez and del R Millan, 2008; Parra et al., 2003). Even though error signals related to trajectory errors have also been recorded (Diedrichsen et al., 2005), the same approach was never used to try to adapt regression BMI algorithms.

1.4. Outline of the thesis

In the second chapter, I will demonstrate an online BMI based on the approach of extracting movement parameters from ECoG signals. Such BMI has not been demonstrated before and is the first step towards ECoG based continuous brain control of a dexterous hand and arm prosthesis. Such device could restore hand and arm movements in paralyzed patients.

To move the ECoG based BMIs further in this direction, I explore the possibility of using error related neuronal signals (ERNRs) as a source of feedback for supervised adaptive trajectory decoding BMI algorithms. To this end, in the third chapter, I demonstrate that it is possible to record neuronal responses to incorrectly achieved goals, called outcome errors, and incorrectly decoded trajectories, called execution errors.

In the fourth chapter, I show that afore identified error types can be reliably detected from ECoG recordings over motor cortex. This is of great importance for BMI applications since motor cortex is a primary target for implants used to drive trajectory decoding BMIs. I also show that, by using only a small subset of 4 electrodes, it is possible to retain most of the detection information compared to using the whole ECoG implant containing 64 electrodes. Using a smaller implant can reduce the size of the wound necessary for the implantation, thereby reducing the medical risk of such a procedure.

Efficient improvement of BMI operation by the adaptive algorithm using detection of error signals depends on the reliable detection. To improve the reliability of detection, I have devised an algorithm that can improve the alignment of ERNRs. Using properly aligned ERNRs for training the detection algorithm could improve the error detection algorithm. This algorithm is presented in chapter 5.

Finally, chapter 6 gives the overview of the presented results and draws conclusion about the future prospects of ECoG as a method for BMIs.

Chapter 2

An online BMI using decoding of movement direction from the human ECoG

Summary. A brain-machine interface (BMI) can be used to control movements of an artificial device, e.g. movements of an arm prosthesis, by motor cortical signals that control the equivalent movements of the corresponding body part, e.g. arm movements. This approach has been successfully applied in monkeys and humans by accurately extracting parameters of movements from the spiking activity of multiple single neurons. I demonstrate that the same approach can be realized using brain activity measured directly from the surface of the human cortex using electrocorticogrpahy (ECoG). Significant BMI control was achieved in 4 out of 5 subjects with correct directional decoding in 69%-86% of the trials (75% on average). The results show the feasibility of an online BMI using decoding of movement direction from human ECoG signals. Thus, to achieve such BMIs, ECoG signals might be used in conjunction with or as an alternative to intracortical neural signals.

2.1. Introduction

A brain-machine interface (BMI) is a device that translates neural activity of the brain into signals controlling a machine. Different techniques exist to record brain activity for BMIs and there are different approaches to translate brain signals into movements of an external effector (Lebedev and Nicolelis, 2006a; Waldert et al., 2009; Wolpaw et al., 2002).

Some of the most powerful BMIs have been realized using the spiking signals of multiple neurons recorded with intracortical electrode implants (Carmena et al., 2003; Fraser et al., 2009; Hochberg et al., 2006; Moritz et al., 2008; Santhanam et al., 2006; Serruya et al., 2002; Velliste et al., 2008). However, recordings from intracortical implants can be unstable due to the response of brain tissue to the implant (Bjornsson et al., 2006; Shain et al., 2003) and due to changes of the neuronal activity - behaviour relationship across time (Dickey et al., 2009; Donoghue et al., 2004). BMIs have also been implemented using non-invasive recording techniques, where the neural activity is recorded outside of the subject's skull using EEG, MEG, fMRI or NIRS (Abdelnour and Huppert, 2009; Birbaumer et al., 1999; McFarland et al., 2010; Mellinger et al., 2007; Weiskopf et al., 2004; Wolpaw and McFarland, 2004).

In addition to afore mentioned recording techniques, ECoG recordings have also been used for BMIs (Leuthardt et al., 2004; Schalk et al., 2008). Compared to intracortical implants, ECoG signals can be recorded without implanting the electrodes into the cortex, do not require spike sorting and exhibit potential advantages with regard to long-term recording stability (Chao et al., 2010). In comparison to non-invasive recording techniques, ECoG has a higher spatial resolution (Freeman et al., 2000; Slutzky et al., 2010), higher bandwidth (Staba et al., 2002), higher signal to noise ratio (Ball et al., 2009a) and is less prone to artefacts (Ball et al., 2009a). In addition, ECoG recordings are presently used in standard clinical procedures making it possible to conduct ECoG studies with human subjects without additional medical risk.

Previous online brain-control studies using ECoG decoded the execution or imagery of different parts of the body (e.g. right vs. left hand) to control an external actuator (Leuthardt et al., 2004; Schalk et al., 2008). In addition, it has been shown that different movements of the same limb (e.g. the direction of an arm movement) can also be inferred from ECoG (Ball et al., 2009b; Chao et al., 2010; Leuthardt et al., 2004; Mehring et al., 2004; Miller et al., 2009; Pistohl et al., 2008; Schalk et al., 2007; Wang et al., 2009). For example, continuous position and velocity of 2D arm movements (Pistohl et al., 2008; Schalk et al., 2007), continuous finger position (Kubanek et al., 2009) and different grasping movements (Pistohl et al., 2012) have been decoded. However, all these studies

decoded these movement parameters offline. An online BMI using the decoding of kinematic movement parameters from ECoG has not been realized until now.

In this chapter, I demonstrate brain-control of a computer cursor using the decoding of movement direction from ECoG recordings in humans.

2.2. Methods

2.2.1. Subjects and recordings

Five subjects (S1-S5) suffering from intractable pharmaco-resistant epilepsy (Table 1) voluntarily participated in the study after having given their informed consent. The study was approved by the Freiburg University Ethics Committee.

For pre-neurosurgical epilepsy diagnostics, the subjects were implanted with an 8×8 grid of subdural surface electrodes (Ad-Tech, Corp., 1cm inter-electrode distance, 4mm electrode diameter) covering parts of the primary and pre-motor cortex (Figure 6). S1, S2, S3 and S4 had additional ECoG stripes implanted. In addition to the signal from the subdural electrodes, 21 surface EEG electrodes, two to four electrooculography (EOG) electrodes, two electrocardiography (ECG) electrodes and several electromyography (EMG) electrodes were recorded. Signals from the ECoG electrode stripes, EEG, ECG and EMG electrodes were not analyzed in this study.

Recordings from all electrodes were digitized at 1024Hz sampling rate for S1, S2 and S3 (Brainbox EEG-1164 amplifier, Braintronics B. V., Almere, Netherlands) and at 2500Hz sampling rate for S4 and S5 (AC441-01 Neuvo amplifier, Compumedics Limited, Abotsford, Australia). Recordings for S1, S2 and S3 were made using a hardware high-pass filter with 0.032Hz cutoff frequency. Recordings for S4 and S5 were made without the hardware high-pass filter. Experiment control and paradigm presentation were performed using BMIsoft software package developed in the research group of Dr. Mehring. Subsequent data analysis was performed using MATLAB (MATLAB versions 7.4-7.11, Natick, Massachusetts: The MathWorks Inc., 2007-2011).

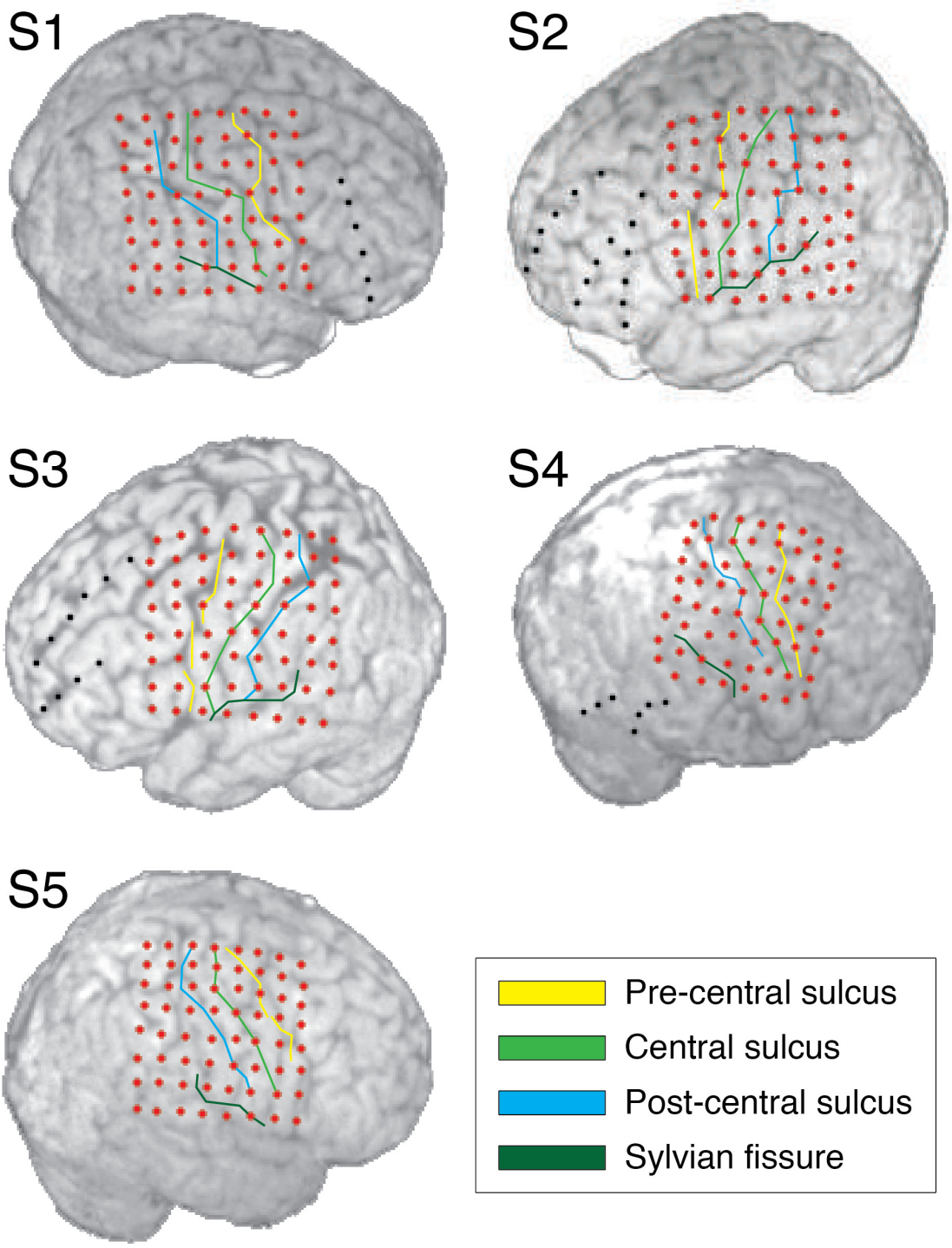

Figure 6 Position of the implants on the neocortex and in relation to the Sylvian fissure, precentral, central and postcentral sulci. Brain outlines were reconstructed from the pre-implantation MRI of the subjects. Electrodes (red and black dots) and sulci were reconstructed from the post-implantation MRI of the subjects. Note that, due to local pressure in the region of the implant, brain tissue can be partially compressed and the brain surface can be slightly deformed relative to the pre-implantation state. Therefore, a mismatch between the sulci on the pre-implantation MRI and sulci reconstructed from the post-implantation MRI is possible. I analyzed the signals from the electrode grid implants only (red dots).

Subject	Age	Sex	Handedness	Electrode location	Seizure focus
S1	33	M	R	Grid right fronto-central; Right fronto-lateral strip; 4 right inter-hemispheric strips	Right frontolateral; Right parietal; Right interhemispheric
S2	22	M	R	Grid left frontal; 3 left dorsolateral-prefrontal and frontal strips; 4 interhemispheric strips	Left frontal
S3	41	F	L	Grid left fronto-lateral; 2 left frontal strips 4 interhemispheric strips	Left precentral
S4	17	M	R	Grid right frontal; 2 depth electrodes to right insula and hippocampus; 2 right occipital and temporo-basal strips	Rest of gyrus temporalis superior (after resection); Right hippocampus; Right posterior insula; Right frontal lobe
S5	23	M	R	Grid right fronto-central; 5 interhemispheric strips; right parieto-occipital strip; 2 posterior parietal strips	Right frontal

Table 1 Clinical profiles of the subjects taking part in the experiment.

2.2.2. Task

Subjects interacted with an experimental paradigm shown on a computer screen (Figure 7). The experiment was carried out in sessions, defined as uninterrupted time epochs in which subjects continuously interacted with the paradigm. Each session consisted of 50 or 25 trials after which the subject stopped performing the task. Each trial consisted of a pause phase (1-2 sec, random, uniformly distributed) followed by a preparatory informative cue presentation (displayed for 1-2 sec, random, uniformly distributed), which informed the subject to prepare for moving a joystick to the left (purple rhomboid) or to the right (red rhomboid) using the hand contra-lateral to the implantation site. After a delay of 2-3 sec (random, uniformly distributed), a go cue (green dot) was presented and subjects had to initiate the movement during the next 1 second. During the movement, no visual feedback was given to the subject. After reaching the joystick end position, they had to keep it in this position for additional 2 seconds. If subjects did not follow this sequence correctly, the trial was stopped and not used. This was done to ensure stereotypical movements of the subjects after the go cue and no movements before the go cue. Subsequently, the cursor on the screen moved in the direction in which subjects moved the joystick (feedback phase).

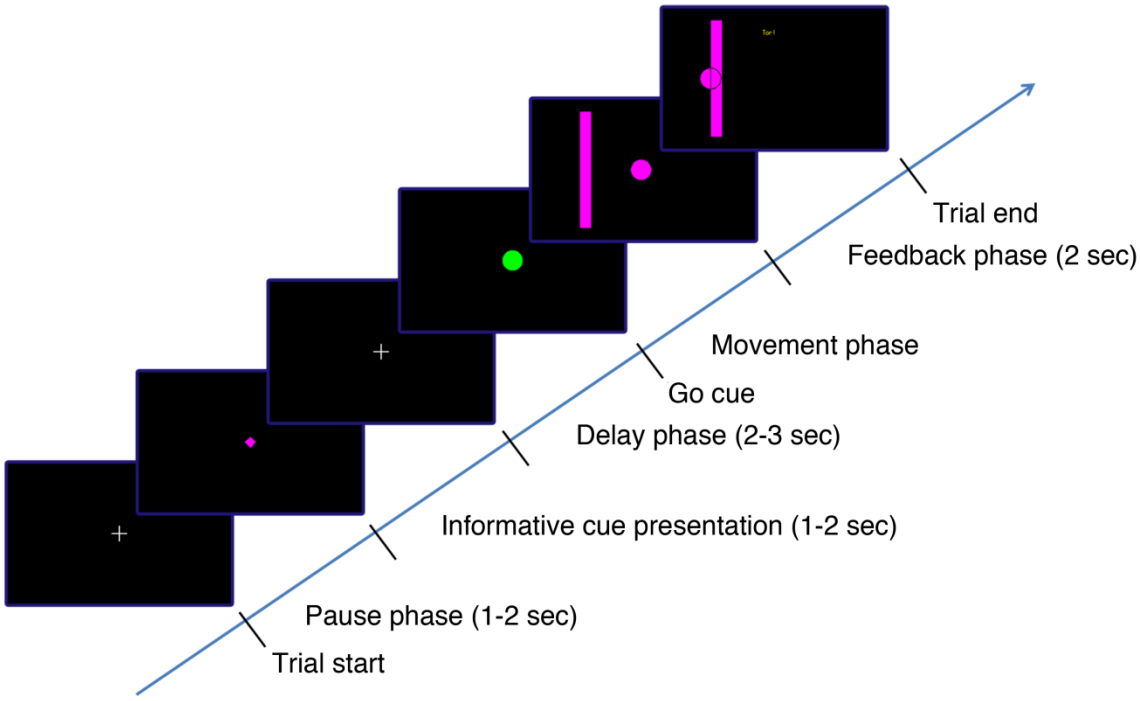

Figure 7 Subjects interacted with an experimental paradigm shown on a computer screen. One session consisted of 50 or 25 trials. Each trial consisted of a pause phase (1-2 sec, random, uniformly distributed), informative cue presentation (1-2 sec, random, uniformly distributed), a delay phase of (2-3 sec, random, uniformly distributed), a movement phase initiated by a go cue and a feedback phase. The screen showed a fixation cross during pause and delay phases, a coloured rhomboid (purple: movement to the left, red: movement to the right) during the informative cue presentation and a green dot during the movement phase, all in the centre of the screen. In the feedback phase the cursor changed to the colour of the informative cue, and was moved in the direction of the subjects' joystick movement. In addition, a thick line in the colour of the informative cue would appear in the path of the cursor. If the cursor crossed the line, the word "Tor" (German for "goal") would be written on the screen. If subjects did not perform stereotypic movements after the go cue or performed movements before the go cue, an error message would appear and the trial would be terminated. Subjects were then asked to resume the initial position and the next trial would start.

Each experiment started with an introduction session in which the subject was familiarized with the task. Subjects were encouraged to perform correct as well as incorrect trials, so that they would get used to the task and to the error messages written on the screen. Once the subject was familiar with the task, the introduction session was stopped and one or two training sessions followed. During the feedback phase of the training sessions, the cursor always moved over to the maximum distance from the centre in the correct direction. Once the training sessions were finished, a model was built from the collected data. One or more brain control sessions followed, identical to the training sessions, except for the feedback phase. In the brain control sessions, the distance travelled by the cursor was proportional to the posterior probability for the cued movement direction as decoded with the trained decoding model. A vertical line was positioned at the half of the maximum distance the cursor could travel, signifying posterior probability of 0.5. Every time the posterior probability was higher than 0.5, the cursor would cross the line and the word "Tor" (German for "goal") was written on the screen, providing positive feedback to the subject. After every brain control session

the model was re-built using one or more of the previous sessions as training data, sometimes with a change in the selection of electrodes. Table 2 summarizes the experiments for all subjects.

	Session	Number of trials			Model trained on	Number of electrodes	Electrodes used
		R	L	Tot			
S1	S1s1 – training	23	27	50			
	S1s2 – training	23	22	45			
	S1s3 – brain control	24	21	45	S1s1 & S1s2	16	ESM H&A motor
	S1s4 – brain control	23	22	45	S1s3	6	Visual inspection
	S1s5 – brain control	16	24	40	S1s4	6	Visual inspection
S2	S2s1 – training	24	20	44			
	S2s2 – brain control	18	23	41	S2s1	16	ESM H&A motor
	S2s3 – brain control	12	29	41	S2s1 & S2s2	16	ESM H&A motor
	S2s4 – brain control	24	22	46	S2s1, S2s2 & S2s3	16	ESM H&A motor
S3	S3s1 – training	24	23	47			
	S3s2 – brain control	20	27	47	S3s1	8	Visual inspection
	S3s3 – brain control	21	28	49	S3s1 & S3s2	2	Visual inspection
S4	S4s1 – training	26	20	46			
	S4s2 – brain control	13	9	22	S4s1	12	Visual inspection
S5	S5s1 – training	21	29	50			
	S5s2 – brain control	11	11	22	S5s1	19	ESM H&A motor

Table 2 Summary of the online closed loop experiment. Number of left (L), right (R) and total (Tot) number of correctly performed trials is shown for every session. Sessions, number of selected electrodes and electrode selection strategy (all ESM H&A motor electrodes, or selecting the electrodes by visual inspection of the neural responses) used for model building are listed for every brain control session.

2.2.3. Model building for decoding in brain control sessions

Data from relevant (Table 2) sessions was common average referenced using recordings from all electrodes on the 8x8 ECoG grid that did not have any defects or did not record epileptic activity.

First, I chose the strategy for selecting the electrodes to be used in model building. I either selected all electrodes that showed a hand or arm motor response during the electrical stimulation mapping (ESM; ESM H&A motor electrodes; Foerster, 1931; Uematsu et al., 1992) or chose the electrodes by visual inspection of the recorded ECoG amplitudes for each movement direction (Table 2).

Decoding model used in my study was based on several features of low-pass filtered ECoG signals (2nd order symetric Savitzky-Golay filter with window length optimized between 0.25 and 1 second; Savitzky and Golay, 1964; Steinier et al., 1972). Following filtering, features were taken at different time points with respect to the go cue. Model building consisted of testing different values of parameters defining the feature selection and the decoder used for classification. Feature selection consisted of selecting: (i) the window length of the Savitzky-Golay filter, (ii) the number of features from one electrode, (iii) the time of the first feature relative to the go cue, and (iv) the temporal distance between the first and the last feature. For decoding, I used regularized linear discriminant

analysis (RLDA; Friedman, 1989), which uses an additional parameter, the regularization coefficient (v), to improve generalization. ECoG recordings for S4 and S5 were not high-pass filtered by the recording system. Therefore, to remove low frequency potential drifts for S4 and S5, I subtracted the low-pass filtered ECoG signal that was obtained by filtering using a causal running average filter. In addition to other model parameters, for S4 and S5, I also selected between different values of (vi) the window length of the running average filter. For each of these parameters, I defined a set of values and tested every combination of these values using 5-fold cross validation. The set of parameter values which gave the highest estimated normalized decoding accuracy (DA) was used to build the model on the entire set of training data:

$$DA = \frac{1}{N_{class}} \sum_{i=1}^{N_{class}} \frac{c_i}{n_i} \tag{2.1}$$

where N_{class} is the number of classes (in this case 2; left and right movements), c_i is the number of correct trials for a given class and n_i is the total number of trials for a given class.

2.2.4. Offline data analysis

During the online experiment, the time for model building was limited. Therefore, the number of tested parameter values was reduced. In the offline analysis, I always used a more exhaustive range of parameter values: (i) Savitzky-Golay filter window length: ¼, ½, ¾ and 1 seconds; (ii) number of features from one electrode: 1, 2, 3, 4 and 6; (iii) temporal distance of the first feature relative to the go cue: from 0 till 1.4 seconds after the go cue in steps of 0.1 seconds; (iv) time interval between the first and the last feature: 1/16, 1/8, ¼, 3/8, ½, ¾ and 1 seconds; (v) regularization parameter: 0, 0.001, 0.1, 0.3, 0.5, 0.7, 0.9 and 0.99; (vi) window length of the running average filter: 5, 10 and 20 seconds (for S4 and S5 only).

2.2.5. Comparison of electrode selection strategies

To optimize decoding, electrode selection can be important (Demirer et al., 2009; Lal et al., 2004; Muller et al., 2000). In the case of patients recovering after intracranial surgery, an additional restriction is that the model has to be built in the short amount of time available for experiments and, hence, has to be based on only a small amount of training data. This restricts the number of possible electrode selections that can be tested. For this reason, before the brain control sessions, I selected the electrodes used for model building based either on ESM or on visual inspection of the neural responses, thereby not optimizing the electrode selection on the basis of DA.

Offline analysis was used to test whether selecting the electrodes in a different manner could have increased the DA. I restricted the electrode selection to the ESM H&A motor electrodes, trying to

avoid electrodes where information could be a result of some kind of artefact (e.g. eye movements) and minimizing the influence of sensory feedback induced by the subjects' movements. To further minimize the influence of sensory input, I also considered the subset of the ESM H&A motor electrodes that lay over the motor cortex according to the sulci reconstruction (ESM H&A motor + SR motor electrodes).

Thus, two electrode sets were considered for the offline electrode selection strategy: (a) all ESM H&A motor electrodes and (b) ESM H&A motor + SR motor electrodes. For each of these sets, I considered (i) single electrodes belonging to the electrode set (a or b), (ii) electrode pairs (vertical or horizontal) within the electrode set, (iii) three neighbouring electrodes within the electrode set, (iv) four neighbouring electrodes within the electrode set and (v) all electrodes together belonging to the electrode set. I evaluated the DA of all electrode subsets for all parameter values (see above) by 5-fold cross validation on the training data and selected the parameter values and electrode subset yielding the highest DA for (i), (ii), (iii), (iv) and (v) separately. These subsets and parameter values were then used to decode the brain control sessions offline. Sessions used for training and testing the model were chosen in the same way as in the online experiment (Table 2).

2.2.6. Significance testing of neural responses

To confirm that neural responses to left and right movements were significantly different from each other and from baseline activity, a Mann–Whitney–Wilcoxon test was applied between neural responses at every time point. Neural activity recordings were first low pass filtered with the Savitzky-Golay filter (symmetric, 2nd order, 0.5 seconds window length). Since the response had to be present within a limited time after the trigger, I tested the epoch of the neural activity from the go cue until 2 seconds after the go cue. Baseline neural activity was defined as all neural activity outside the epochs described above. To sample the baseline activity distribution properly, I removed the autocorrelation of the low-pass filtered activity arising from the filtering procedure by sampling the baseline activity only every 0.5 seconds (window length of the filter). To reduce the computation time of the significance testing, I tested significance of the neural responses every 31.25ms (corresponding to 32Hz), instead of testing for every recorded time point.

Due to the large number of statistical tests, correction for multiple testing was necessary to control the number of falsely rejected null hypotheses. I used the Benjamini-Hochberg procedure (Benjamini and Hochberg, 1995) with a correction for dependent statistics (Benjamini and Yekutieli, 2001) to set the false discovery rate for one subject at the level of 5% for all tests. A neural response to the go cue on a certain electrode was considered significant if there was at least one time point for which the neural response to the go cue for right movements was significantly different from baseline

neural activity or, alternatively, at least one time point for which the neural response to the go cue for left movements was significantly different from baseline neural activity. This condition needed to be satisfied after a correction for multiple testing was applied, taking into account all time-point-wise tests for both conditions. A neural response to the go cue was considered significantly different between left and right movements if there was at least one time point for which the neural response to the go cue for right movements was significantly different from the neural response to the go cue for left movements, after the correction for the multiple testing was made.

2.2.7. Movement onset versus go cue alignment

Since the neural signal epochs used for decoding were aligned to the go cue, differences in movement reaction times and, hence, in the onset times of neural responses time-locked to movement onset, could have quite different effects on DA, depending on whether they originate from trials of the same movement type (either left or right) or whether they stem from a systematic difference in reaction times for different movement types (left vs. right). In the latter case, the systematic difference in response onset by itself would allow for correct directional decoding, even for otherwise identical neural responses. Removing the systematic reaction time difference by aligning the neural signal epoch on movement onset instead of on go cue should then reduce the DA, or even eliminate it. On the other hand, differences in reaction times for trials of the same movement type would increase the variability of the neural responses of both movement types when aligned to go cue and, hence, lead to a reduction in DA. Removing the effect of reaction time variability by aligning the signal epochs on movement onset, instead of on go cue, would then be expected to result in an increase of DA.

To test which of these two scenarios were true, I realigned the neural responses to movement onset, thereby removing, or at least reducing, both response onset variability and systematic response onset latencies due to reaction times differences. I ran the whole experiment offline as if it was an online experiment, i.e. using the same sessions for training and testing (Table 2).

2.2.8. Electrical stimulation mapping (ESM) and neuroanatomical electrode assignment

Electrical cortical stimulation through the electrode grid was performed using an INOMED NS 60 stimulator (INOMED, Germany) as a part of the clinical procedure. Stimulation trains of 7s duration consisted of 50Hz pulses of alternating polarity square waves of 200μs each. The intensity of stimulation was gradually increased up to 15mA or to the induction of sensory and/or motor phenomena. Subjects were unaware of the timing of stimulation, unless these phenomena occurred. Phenomena were reported by the subject, specifying the limb of origin and the type of sensation

(motor or somatosensory). Consequently, ESM maps were created and used to select the electrodes used for online brain control (Figure 8).

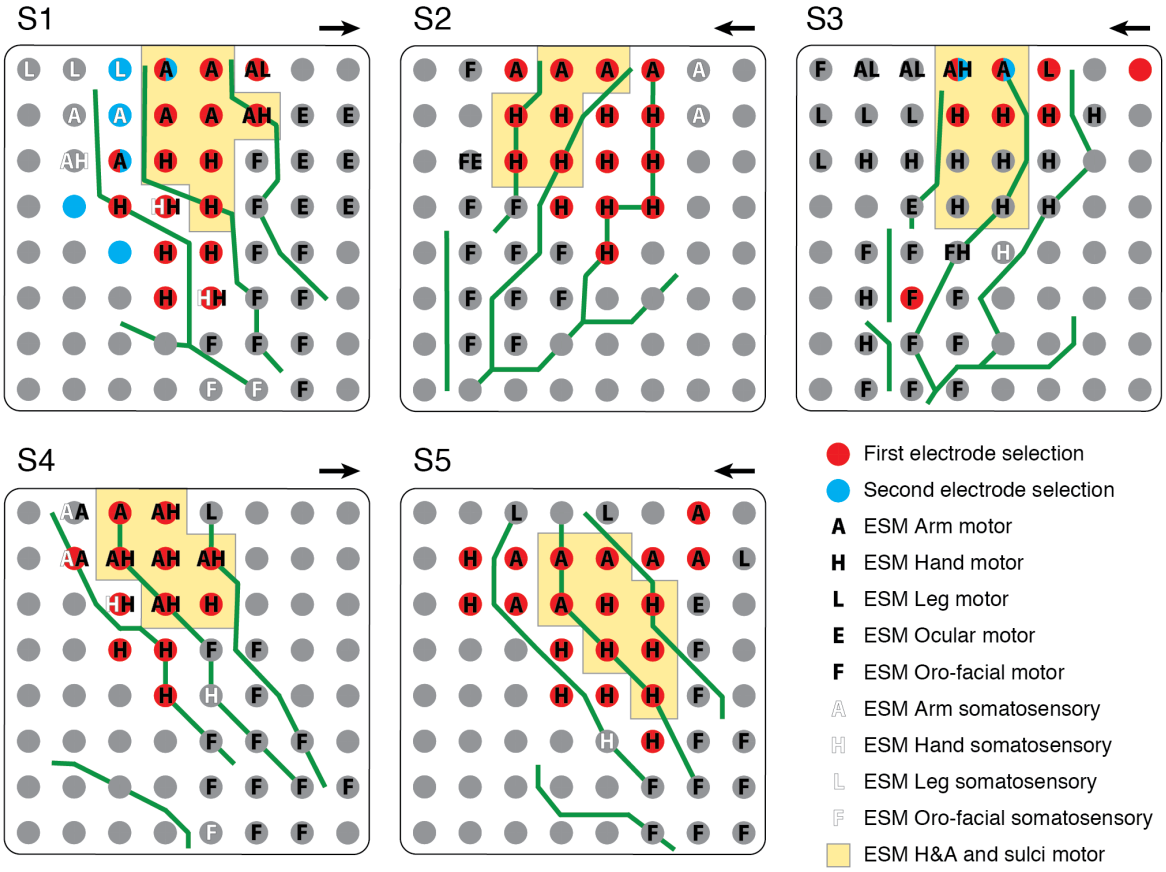

Figure 8. Overview of the electrode selection for the online brain control combined with ESM results and sulci reconstruction. For each subject, an 8x8 electrode grid (circles represent electrodes) is shown, oriented in the same manner as the grid in Figure 6. Arrows above the top right corner point in the frontal direction. Red circles mark the electrodes initially used for brain control, blue circles mark the electrodes used after the electrode selection was changed. Electrode selection was changed only once for S1 and only once for S3. Letters above the electrodes mark the type of the ESM response elicited: A: arm, H: hand, L: leg, E: eye and F: oro-facial responses. Black letters mark motor responses, white letters mark somatosensory responses. Solid green lines mark the Sylvian fissure, precentral, central and postcentral sulci reconstructions.

Data from post-implantation MRIs was used to reconstruct the positions of the Sylvian fissure, central sulcus, postcentral sulcus and precentral sulcus with respect to the electrodes (Figure 6 and Figure 8). The reconstruction was used to see if an electrode was lying over one of the reconstructed sulci or not. I defined the sulci reconstruction (SR) motor electrodes, as those electrodes laying over the central sulcus, over the precentral sulcus, or in-between the central and the precentral sulci according to the sulci reconstruction. Sulci reconstruction was available only after the online experiment had finished.

2.3. Results

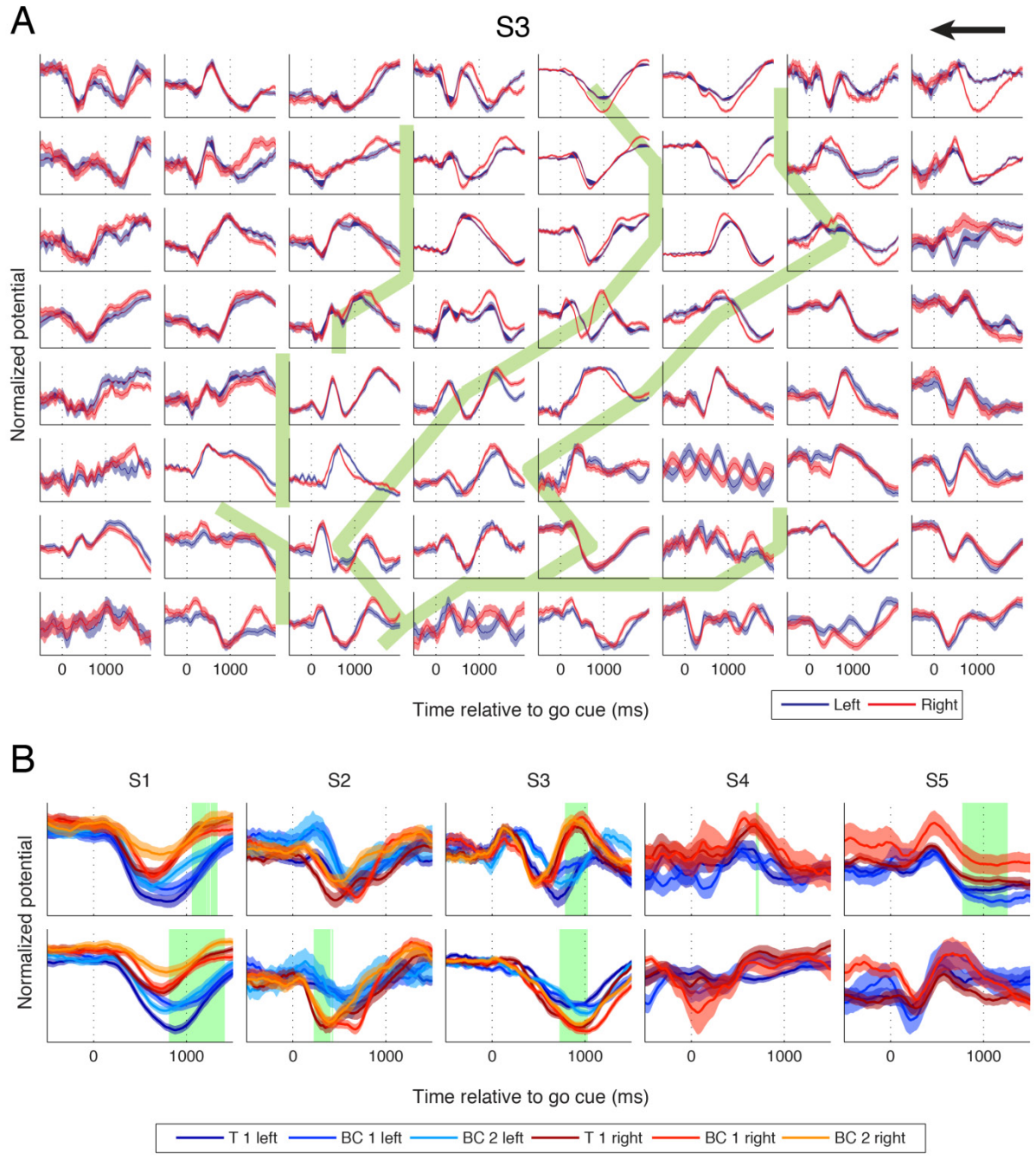

Figure 9 A: Mean ± standard error of the mean of the low-pass filtered neural activity (2nd order symmetric Savitzsky-Golay filter, 0.5 second length) for S3 for left (blue) and right (red) movements relative to the go cue (0 sec) over the electrode grid. Every subplot represents one electrode with the top left subplot corresponding to the top left grid electrode as shown in Figure 6. The arrow points in the frontal direction. Solid green lines in the background show sulci reconstructions. B: Low-pass filtered neural responses recorded from two selected electrodes for every subject (same filter as in A). 0 sec marks the go cue. For S1, S2 and S3 mean ± standard error of the mean of the neural response is shown for the first training session (T 1) and the first and the second brain control session (BC 1 and 2). For S4 and S5, only one brain control session was recorded. Therefore, only T 1 and BC 1 are shown. Green background marks the times when the neural response for left and right movements were significantly different from each other for all three sessions.

2.3.1. Neuronal responses

I found significant neural responses to go cue (Figure 9) on a large number of electrodes (47 out of 64 for S1, 37 out of 64 for S2, 52 out of 64 for S3, 19 out of 64 for S4 and 44 out of 64 for S5; 62% of the electrodes on average). In contrast, only a small number of electrodes showed significant differences between neural responses to left and right movements (8 electrodes for S1, 1 for S2, 7 for S3 and none for S4 and S5, 5% of the electrodes per subject on average). These results show that, even though the neural response to hand movements are widely distributed, only a small fraction of the responses contained directional information.

2.3.2. Decoding accuracy in online closed loop experiments

During the online experiment, I ran 2 training and 3 brain control sessions with subject S1, 1 training and 3 brain control sessions with S2, 1 training and 2 brain control sessions with S3 and 1 training and 1 brain control session with S4 and S5 each (Table 2). Table 3 shows the overview of the chosen parameter values during the model building phase for each of the brain control sessions.

Session	Filter window	Features per electrode	Time of the first feature	Time length	Regularization	High-pass filter
S1s3	1	2	1.4	1/4	0.7	x
S1s4	1	3	1	1/16	0.1	x
S1s5	1/2	2	0.9	3/8	0.01	x
S2s2	1/2	2	0.3	1/16	0.3	x
S2s3	3/4	1	0.4	x	0.01	x
S2s4	2/3	1	0.5	x	0.01	x
S3s2	1/3	1	1	x	0.1	x
S3s3	1/2	1	0.9	x	0.5	x
S4s2	1/2	1	1.3	x	0.3	5sec
S5s2	3/4	1	0.7	x	0	20sec

Table 3 Summary of the parameter values used for building the model before each of the brain control sessions during the online experiment. The high-pass filter, implemented by subtraction of the low-pass filtered signal using running average filter, was used for subjects S4 and S5 only.

I achieved significant ($p<0.01$, binomial test) directional decoding in online closed loop hand movement direction decoding in 4 out of 5 subjects and 8 out of 10 sessions (Figure 10a, Table 4) with average DA of 75%. I used two different strategies to select the electrodes used for model building. For the first brain control session for S1 and all brain control sessions for S2, S4 and S5, I used all ESM H&A motor electrodes (average DA 71%). For the other brain control sessions, I selected the electrodes which showed strongest tuning during training, not necessarily restricting myself to ESM H&A motor electrodes (average DA 80%). The difference in DA between these two strategies was significant ($p<0.05$, Fisher's exact test). On the other hand, I found no significant

difference (p=0.48, Fisher's exact test) between strategies of using only the last preceding session to train the model (average DA 77%) and using multiple sessions (average DA 74%).

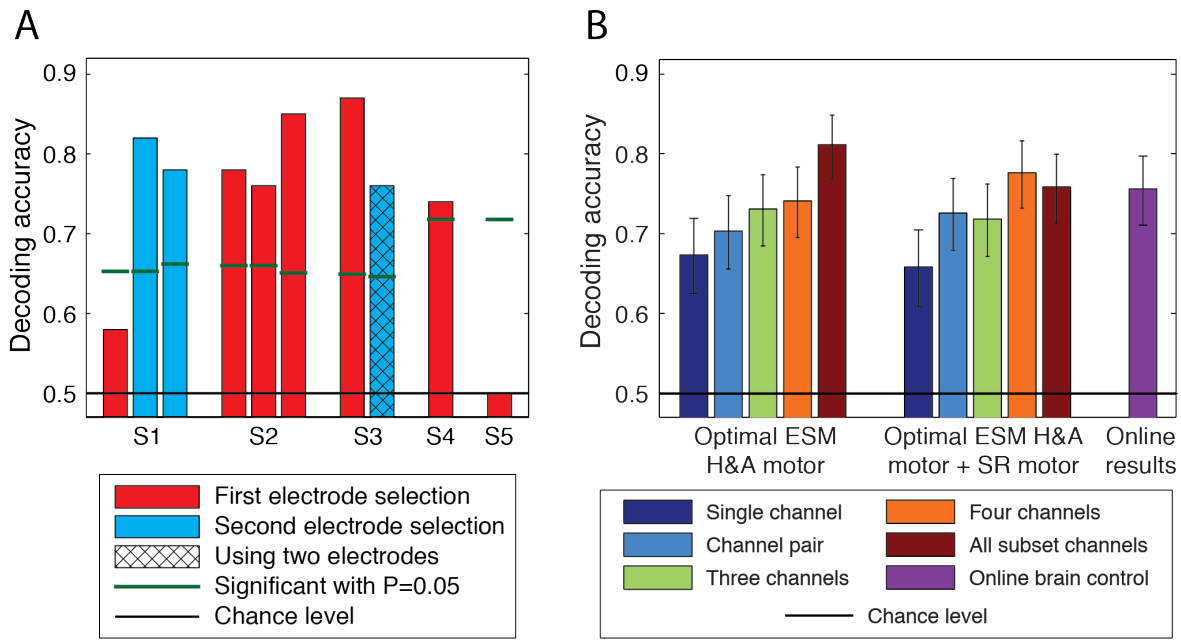

Figure 10. A: Overview of the DA in the online brain control experiment. B: Offline analysis of DA for different electrode sets (ESM H&A motor, ESM H&A motor + SR motor) and their subsets (single electrode, electrode pair, electrode quartet, all electrodes) and comparison to DA from the brain control sessions. For each or the electrode sets, the optimal electrode subset and the corresponding set of parameters were chosen by maximizing DA evaluated using 5-fold cross-validation on the sessions used for model building. Histograms show the average DA evaluated on the testing sessions with error bars showing 95% confidence intervals of the mean. Choice of sessions used for model building and testing sessions was identical to those used in the online experiment (Table 2).

In the second brain control session of S3, I used neural activity measured with only two neighbouring electrodes, 1cm apart, for decoding (Figure 10a, electrodes marked in Figure 8). The DA of 76% achieved by using only these two electrodes was not significantly different from the DA in the remaining sessions (mean DA=75%, p=1, Fisher's exact test).

Brain-control session	Successful trials		DA	P value
	R	L		
S1s3	15/24	11/21	0.58	0.12
S1s4	16/23	21/22	0.83	< 0.001
S1s5	9/16	22/24	0.74	< 0.001
S2s2	17/18	14/23	0.78	< 0.001
S2s3	8/12	23/29	0.76	< 0.001
S2s4	22/24	17/22	0.85	< 0.001
S3s2	18/20	23/27	0.87	< 0.001
S3s3	18/21	19/28	0.76	< 0.001
S4s2	9/13	7/9	0.74	0.009
S5s2	5/11	6/11	0.50	0.42

Table 4. Summary of DA in the online closed loop experiment. For every brain control session, I listed the number of left (L) and right (R) successful/total trials and significance level (p) testing a chance level decoder hypothesis using a binomial test.

2.3.3. Comparison of electrode selection strategies

I evaluated the DA from different electrode selection strategies and smaller electrode sets (Figure 10b). For ESM H&A motor + SR motor electrodes, the DA from four neighbouring electrodes (average DA 78%) was not significantly different from the DA from all subset electrodes (average DA 76%; p=0.61; Fisher's exact test) or the DA from the brain control sessions (average DA 76%; p=0.56; Fisher's exact test). This shows that most of the directional information was already present in the signals recorded from small sets of four neighbouring electrodes (contained within a 2cm x 2cm area). Additionally, ESM and SR give strong indication that all four of these electrodes recorded from the hand and arm area of the motor cortex.

Using all ESM H&A motor electrodes yielded the highest DA (average DA 81%), with a tendency to be higher than the DA from brain control sessions (p=0.07; Fisher's exact test) and the DA from using only all ESM H&A motor + SR motor electrodes (p=0.07; Fisher's exact test). Note that the 'all ESM H&A motor electrode set' can include electrodes that lay over pre-motor and somatosensory cortex according to the sulci reconstruction (see section 2.2.8).

2.3.4. DA topographies

Figure 11 shows the spatial distribution of DA over the electrode grid when electrode quartets were used for decoding. For all subjects, the maxima of the DA had at least one electrode in the quartet belonging to the ESM H&A motor electrode set, with other high DA quartets grouped around the locations of the maxima. This is expected for a task involving hand and arm movements and confirms that the neural responses used for decoding were not the product of artefacts.

2.3.5. Movement onset versus go cue alignment

Inspection of the joystick movements (Figure 12a) revealed that, apart from reaction time and movement direction, rightward and leftward movements were quite similar, both across movement types (left vs. right) and across trials within the same movement type (either left or right). Following the go cue, subjects initiated the movements (defined as crossing 15% of the maximum joystick deflection in horizontal direction) after 415±87ms (S1 304±12 ms; S2 156±12 ms; S3 439±13 ms; S4 661±33 ms; S5 513±16 ms). I observed a significant difference in reaction time between left and right movements ($p<0.05$; Mann–Whitney–Wilcoxon test) for some sessions of S2 and S4 (Figure 12b).

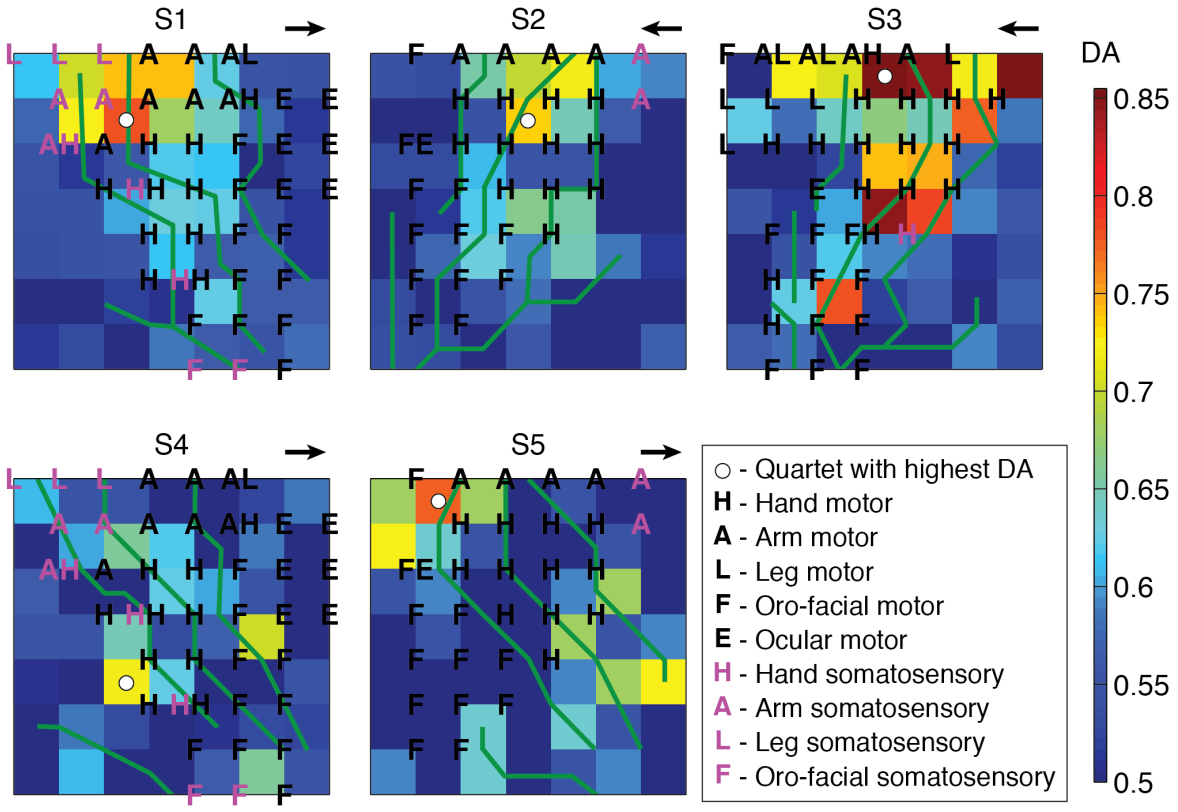

Figure 11 Topographies of DA, averaged over all brain control sessions, for all subjects with respect to the ESM responses (letters) and sulci reconstruction (solid green lines). The colour of each square indicates the DA achieved when using recordings from four electrodes located at the edges of the square. DA was calculated by selecting parameter values that gave the highest DA on the sessions used for model building (5 fold cross-validation), using these to build a model on the complete set of the same sessions and decoding using this model on the testing sessions. Choice of sessions used for model building and testing sessions was identical to those used in the online experiment (Table 2). White circle marks the electrode quartet with the highest DA. Arrows above the top right corner point in the frontal direction.

To test whether response onset variability has an effect on the DA, I re-aligned the neural responses to movement onset and re-ran the experiment using the same sessions for training and testing (Table 2). I found that, in all subjects, the resulting DA was higher after alignment to movement onset than during the brain control sessions where trials were aligned on the go cue (Figure 12c; DA increase 0.08±0.03%, $p<0.05$; signed Mann–Whitney–Wilcoxon test). This indicates that the selected neural responses were indeed coding for movement direction and that correct decoding was not due to systematic response latency differences for different movement types.

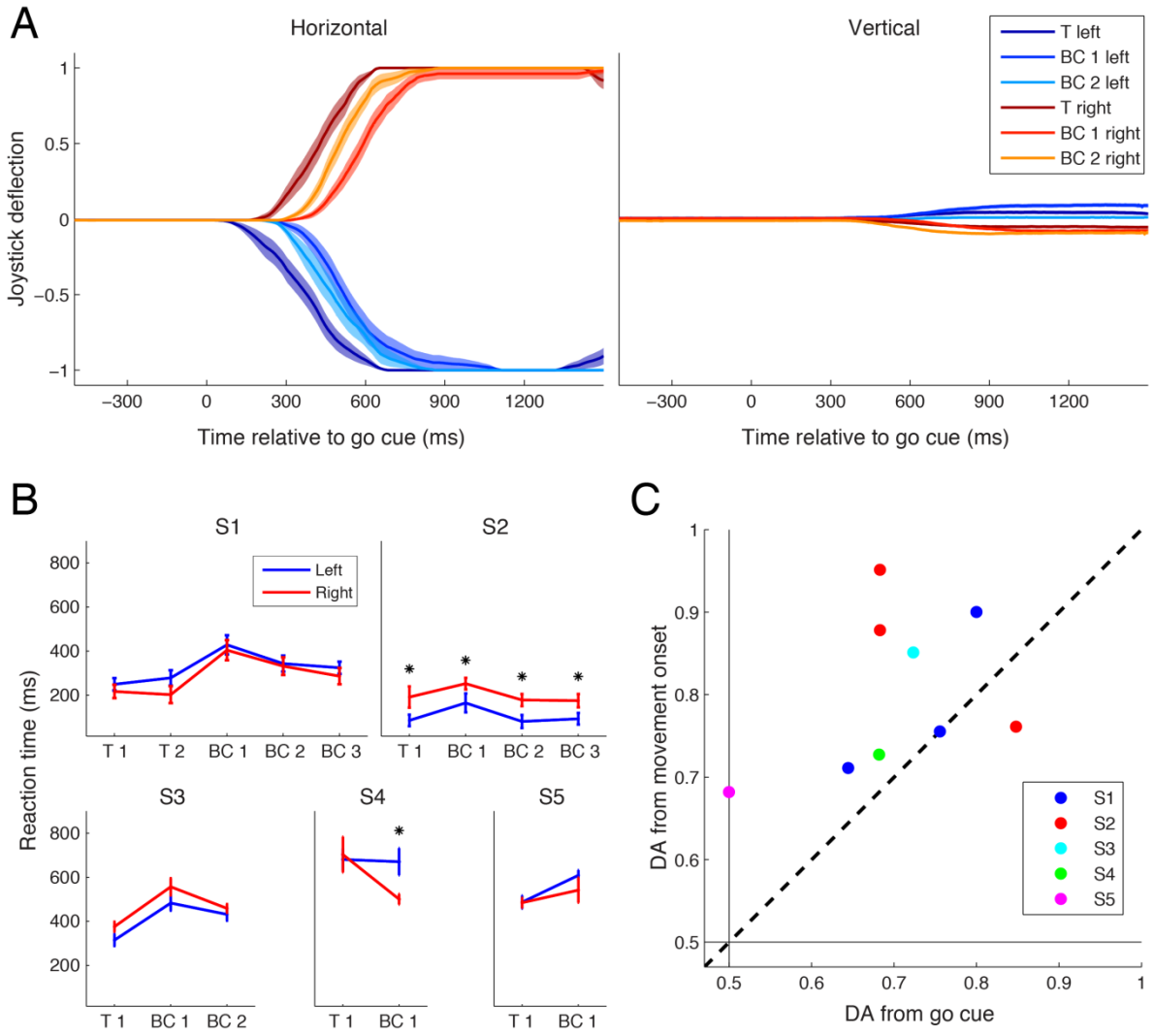

Figure 12. A: Horizontal and vertical joystick deflection for S3 (normalized to a range of -1 to +1). Movements are shown as average ± standard error of the mean. B: Average movement onset time (15% of joystick deflection) following the go cue for every subject and every training (T) and brain control (BC) session. Error bars show standard error of the mean. Stars mark significant differences (Mann–Whitney–Wilcoxon test) between left and right movement onset times. C: Comparison of DA from online brain control experiment and DA from trials realigned to movement onset. Thin black lines show DA chance level.

2.4. Discussion

Here I showed that it is possible to realize online brain-control using the directional tuning of human ECoG signals. Brain control was achieved for 4 out of 5 subjects. For the subject where no control was obtained (S5), I could run only one brain control session. Eventually, due to medical reasons, the experiments with S5 had to be stopped and no additional brain control sessions could be performed later on. For S1, the first brain control session was also unsuccessful. In the subsequent sessions for S1, I changed the electrode selection and achieved significant control. In case more experimental time had been available for S5, I would have employed the same strategy, hoping that it might have worked for S5 as well.

I also examined DA based on signals from a small subset of neighbouring electrodes. In the second brain control session of S3, I showed that brain control is possible using signals from only two neighbouring electrodes. DA obtained with these two electrodes was the same as the average DA from other online brain control sessions. Moreover, offline analysis revealed that, across all sessions and subjects, already four neighbouring electrodes provide almost all the available movement information. This supports the idea that most of the informative signals in the experiment presented in this Chapter can be recorded from area that is relatively small compared to the size of the entire ECoG grid. This is consistent with offline analyses of previous studies showing high DA from local ECoG electrode quartets (Ball et al., 2009b), thereby indicating the feasibility of using ECoG implants with small, possibly dense electrode grids for BMI applications.

One of the possible BMI applications is to control movements of hand and arm prosthesis. Such prosthesis might not provide proprioceptive feedback. Moreover, sources of the BMI control signals for the hand/arm prosthesis should not interfere with movements of other body parts. Thus, I focused on neural activity in the hand and arm area of the motor cortex. ESM was used as an indication which electrodes recorded neural activity predominantly related to hand and/or arm movements while sulci reconstruction was used to determine which of these electrodes were lying over the motor cortex (Figure 8). Here presented online experiment demonstrated that using all ESM H&A motor electrodes lead to a significant DA of 71% on average. When the identical experiment was repeated offline, now on all brain control sessions and with a complete search over all model parameters, DA increased to 81%. According to sulci reconstruction, some of the ESM H&A motor electrodes were lying over somatosensory cortex and some over the pre-frontal cortex. Thus, neural activity related to somatosensory feedback and cognitive processes may have contributed to decoding performance in the online control condition. To test whether this was the case, I used sulci reconstruction to determine a more restrictive set of electrodes by using only ESM H&A motor electrodes within the anatomically defined motor cortex. I demonstrated that one can still achieve a significant DA of 76% from this smaller electrode set. Even though neural activity related to visual and somatosensory feedback is present in motor cortex as well (Fetz et al., 1980; Merchant et al., 2001; Naito et al., 1999), neural activity in the motor cortex mainly codes for motor execution (Suminski et al., 2009). Therefore, this result suggests that BMI using decoding of movement kinematics from ECoG recordings in humans may be possible, even without somatosensory feedback.

In previous offline studies, higher DA was found when using low-pass filtered ECoG activity as compared to power in several frequency bands (Ball et al., 2009b; Pistohl et al., 2008; Schalk et al., 2007). Schalk et al. showed that using low-pass filtered ECoG signals greatly increases DA when

added to power modulations in different frequency bands. Pistohl et al. showed that decoding two dimensional arm movement trajectories from the low-pass filtered signal component (LFC) of the ECoG recordings provided greater accuracy than decoding from power in different frequency bands. However, it is not clear how conclusions from these offline studies would generalize to online experiments. Schalk et al. (Schalk et al., 2008) showed that online closed loop control is possible using power modulations in different frequency bands of the ECoG recordings. Here, I showed that online closed loop control is possible using the LFC of the ECoG recordings as well. Further studies are needed to reveal which feature of the ECoG recordings, LFC or power modulations in different frequency bands, provides a better signal for online closed loop control and weather these two features can be used together to improve accuracy.

In previous study by Ball et al. (Ball et al., 2009b), it was shown that it is possible to decode multiple directions of arm movement from ECoG recordings. While Ball et al. used offline decoding, here I demonstrate that it is possible to realize an online BMI based on decoding movement direction from ECoG signals. Schalk et al. (Schalk et al., 2008) realized an online cursor control using the human ECoG using either movement execution or movement imagery of different parts of the body. In the experiment presented in this Chapter, movements of a single limb (arm contralateral to the implantation site) were used to generate the neural control signals. Furthermore, recordings from a rather small area of the motor cortex were sufficient to extract most of the decoded movement information. Therefore, the size of a future electrode implant covering the relevant cortical area can likely be kept rather small as well. This is supported by the results of the second brain control session of S3, in which brain control was achieved using the recordings from only two neighbouring electrodes. The area covered by a hypothetical future implant with two electrodes, using the same design as in the implant used in this study, would be around $2cm^2$ only (the total area of the implants used in this study is approximately $64cm^2$). Further support comes from offline analysis which revealed that, across all sessions and subjects, recordings from four neighbouring electrodes (area of approximately $4cm^2$) already provided the maximum movement information.

When movements of different body parts are used, I expect that, due to a roughly somatotopic representation of the motor cortex, the required size of the implant to achieve BMI would be larger. Furthermore, in the approach used by Schalk et al., subjects have to learn how to transform movements of different body parts to the desired movements of a cursor, e.g. that tongue protrusion is mapped to the cursor going up. In the experiment presented in this Chapter, learning of such transformations is easier since the control is intuitive: movement of the arm to the left moved the cursor to the left and movement of the arm to the right moved the cursor to the right. Schalk et al. demonstrated a higher level of brain control compared to the level of brain control presented

here: subjects controlled computer cursors continuously in two dimensions, whereas here, subjects could only generate a binary control signal. However, the earlier study by Pistohl et al. (Pistohl et al., 2008) demonstrated that continuous decoding of two dimensional arm movement trajectories is possible using ECoG. Thus, the approach of using decoding of motor kinematics from ECoG might be extendable to continuous control and to more degrees of freedom. Findings presented in this chapter constitute a first step in this direction, confirming that online brain control using ECoG recordings with such approach is indeed possible. Future studies should reveal whether raising the level of brain control to continuous multidimensional control will be possible.

Experiment presented in this Chapter was performed using ECoG recordings aligned to the go cue. Offline analysis revealed that part of the decoding errors was a result of reaction time variability. When I reran the experiment offline, aligning the recordings to movement onset, DA increased significantly. This shows that signals used for decoding contained information about movement direction and not just information about the reaction time. In addition, it also suggests that DA could be substantially improved during online brain-control if movement onset triggers, rather than the go cue, were used for signal alignment. This could be implemented by tracking the joystick positions and using the moment where the joystick passed a certain threshold as a reference point for the decoder. Such movement onset detection could not be used in the case of movement imagery needed for the application for paralyzed patients. In that case, the neural response onset, a purely internal event, would need to be detected and used as a trigger.

Here presented results provide a proof of concept that BMI using directional tuning of ECoG recordings can be realized. I used recordings from an ECoG implant designed for epilepsy assessment, with electrode diameter of 0.4 cm and 1cm distance between electrodes. Recent studies recorded ECoG using high-resolution implants with electrode diameters and inter-electrode distances on the order of micrometers (µECoG), showing that epicortical potentials have spatial variability on a millimetre scale or less (Kim et al., 2007; Leuthardt et al., 2009; Slutzky et al., 2010). Therefore, due to the implant design used in the present study, it can be assumed that a large amount of informative signal was not recorded. Moreover, my findings indicate that most of the decoded movement information can already be obtained from a small area of the motor cortex. Thus, using high density µECoG implants over a small cortical area could potentially increase the accuracy of brain-control.

Studies using intracortical recording techniques showed better accuracy of brain control than predicted from respective offline studies. This increase can be attributed to neuronal plasticity which changes the neuronal representations of movements to improve BMI control (Ganguly and Carmena, 2009). These learning effects typically occur across days or weeks while, in hereby described

experiment, the available experimental time was limited to a few hours during one or two days. I expect that, with longer experimental time, the BMI accuracy would have significantly improved due to neuronal plasticity and learning.

Previous studies have shown that movements of individual fingers (Kubanek et al., 2009; Miller et al., 2009) as well as natural grasping movements (Pistohl et al., 2012) can also be decoded from ECoG. Future research will therefore reveal whether utilizing high-resolution recordings from µECoG implants together with subject training will increase the accuracy and the number of degrees of freedom of brain-control, so that the ECoG control of a dexterous hand and arm prosthesis becomes possible. If successful, such a BMI can be used to restore reaching and grasping function in paralyzed patients (e.g. after spinal cord injury or stroke) or amputees.

Chapter 3

Error related neuronal responses

Abstract. Brain-machine interface (BMI) devices make errors in decoding. Detecting these errors online from neuronal activity can improve BMI performance by modifying the decoding algorithm and by correcting the errors made. Here, I investigate the neuronal correlates of two different types of errors which can both be employed in BMI: (i) the execution error, due to inaccurate decoding of the subjects' movement intention; (ii) the outcome error, due to not achieving the goal of the movement. I demonstrate that, in electrocorticographic (ECoG) recordings from the surface of the human brain, strong error related neural responses (ERNR) for both types of errors can be observed. ERNRs were present in the low and high frequency components of the ECoG signals, with both signal components carrying partially independent information. Moreover, the observed ERNRs can be used to discriminate between error types, with high accuracy (≥83%) obtained already from single electrode signals. I found ERNRs in multiple cortical areas, including motor and somatosensory cortex. As the motor cortex is the primary target area for recording control signals for a BMI, an adaptive motor BMI utilizing these error signals may not require additional electrode implants in other brain areas.

3.1. Introduction

Current brain-machine interface (BMI) devices make errors in decoding. Decoding errors can be recognized by the subject and can evoke an error related neural response, ERNR. Such ERNRs could be utilized in two ways to improve the performance of a BMI: (1) to correct the error that was made and (2) to modify the decoding algorithm to decrease decoding errors in the future. The first strategy has already been applied in on-line BMI studies (Blankertz et al., 2003; Parra et al., 2003; Schalk et al., 2000), but thus far only in trial-based task designs. However, many powerful BMIs, such as the brain control of a prosthetic arm (Carmena et al., 2003; Hochberg et al., 2006; Velliste et al., 2008) and the brain control of a computer cursor (Serruya et al., 2002; Taylor et al., 2002; Hochberg et al., 2006) use continuous movement control of the effector. The principal feasibility of the second strategy has, thus far, only been demonstrated in computer simulations applying decoding algorithms which adapt using error signals (Blumberg et al., 2007; Rotermund et al., 2006).

Both strategies for improving the performance of BMIs require appropriate ERNRs. Most previous ERNR studies concentrated on trial-based tasks with human EEG. Several types of ERNRs were reported: response error related negativity (rERN) (Falkenstein et al., 1991; Gehring et al., 1993), feedback error related negativity (fERN) (Miltner et al., 1997), observation error potential (oErrP) (van Schie et al., 2004) and interaction error potential (iErrP) (Ferrez and del R Millan, 2008).

By contrast, only a small number of studies investigated ERNRs in continuous movement tasks. Again, different types of errors in continuous tasks were reported: target error in fMRI (Diedrichsen et al., 2005), execution error in fMRI (Diedrichsen et al., 2005), and outcome error in EEG (Krigolson et al., 2008). Target errors occur when the movement environment goes through unexpected changes, such as a target jump. Execution errors occur when the ongoing motor commands result in an unexpected movement, due to changes in the movement dynamics or kinematics. Such error occurs in BMI when, for example, the decoding algorithm decodes incorrect movements and, hence, the prosthesis does not perform the intended movement (Figure 13). If the difference between the intended and the decoded movement is large enough, it can be recognized by the subject and evoke an execution ERNR. Finally, an outcome error appears when the desired goal of a movement is not achieved. Such error would occur in BMI when the prosthesis reaches a wrong target.

Diedrichsen et al. (Diedrichsen et al., 2005) found fMRI correlates of execution errors and did not investigate outcome errors. Moreover, due to the low temporal resolution, fMRI would only allow for a rather slow BMI control. Krigolson et al. (Krigolson et al., 2008) observed EEG correlates of outcome errors but did not address the question of execution errors.

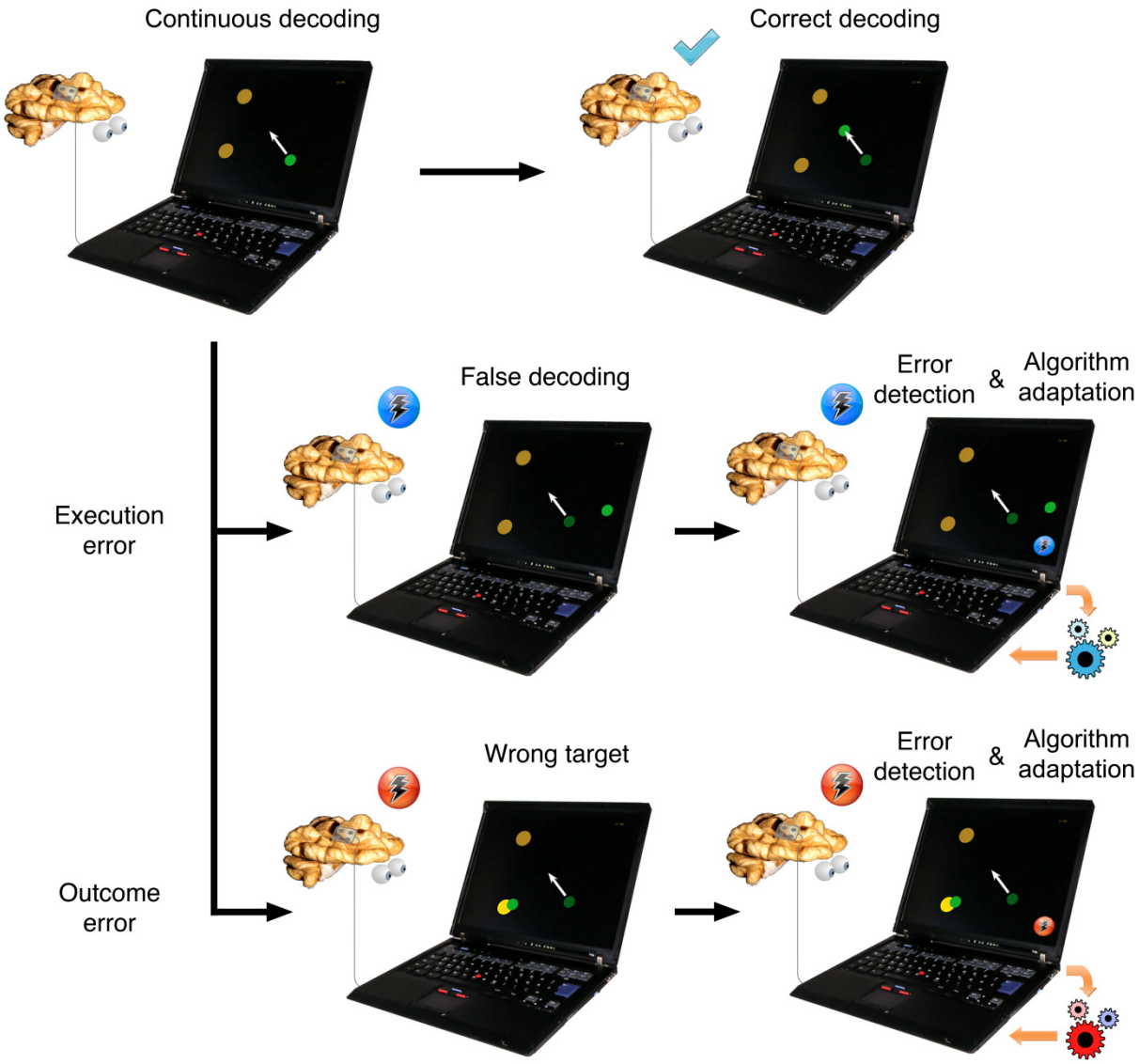

Figure 13 Application of neuronal error signals to improve the performance of a continuous BMI control. Subjects intend to move a cursor towards the top left target (white arrow). If the decoding is correct, the cursor performs the intended movement and no neuronal error signal is elicited in a subject. If there is a discrepancy between the intended and the decoded movement, an ERNR can be elicited. If the discrepancy is large enough, it can elicit an execution ERNR. If the execution error is detected by the BMI system, decoding algorithm can be adapted to reduce the number of errors in decoding in the future. If the unwanted movement causes the cursor to reach an unwanted target, an outcome ERNR might be evoked. If the outcome ERNR is detected by the BMI system, it can change the decoding algorithm as well, this time in a different way.

Here, I show that both execution and outcome ERNRs can be observed and differentiated in ECoG signals during a continuous movement task, similar to typical BMI control tasks. The semi-invasive ECoG is an attractive recording technique for BMIs as it does not require the implantation of electrodes into the cortex and offers a higher spatial and spectral resolution than the non-invasive EEG and MEG

I found ERNRs above different cortical areas, including motor cortex. Both low pass filtered ECoG signals and high gamma ECoG signals yielded execution and outcome ERNRs, with both signal

components carrying partially independent information. In addition, execution and outcome ERNRs can be differentiated with high decoding accuracy, even based on the responses from only one electrode.

3.2. Methods

3.2.1. Task

Subjects (S) played a simple video game in which they controlled a spaceship with a small analogue joystick on a gamepad (Logitech® Rumblepad™ 2, Logitech Europe S.A., Morges, Switzerland) in the horizontal dimension (left-right; Figure 14a). The task was to evade blocks dropping from the top of the screen at a constant speed. The game was challenging enough so that the spaceship collided with a block from time to time (collision event, Figure 14b, mean and standard error of the mean, sem, of time between events: S1: 26.25±1.80 s, S2: 38.57±3.11 s, S3: 47.62±4.80 s, S4: 15.83±0.96 s). After the collision event, the spaceship and all blocks stopped moving for 2 seconds, to allow subjects recognize the collision. Afterwards all blocks disappeared and the spaceship started to move again.

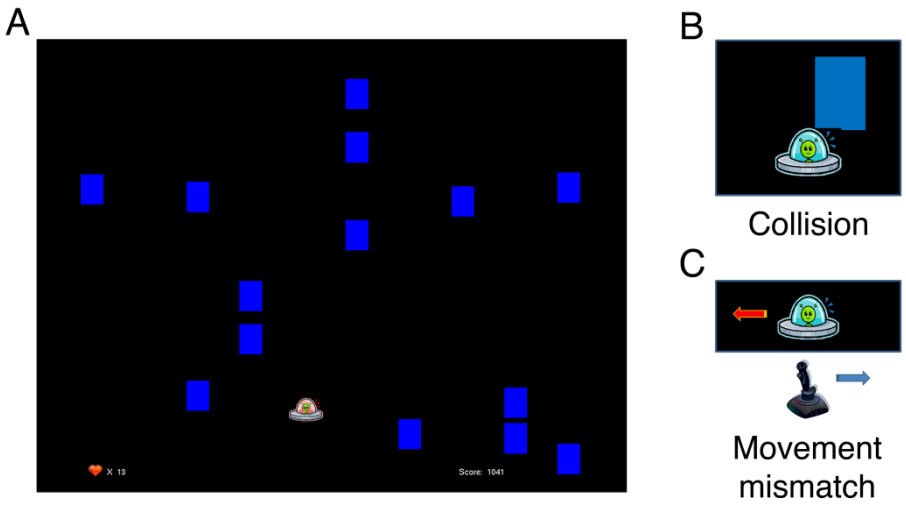

Figure 14 A: Picture of the paradigm as seen by the subjects. Subjects played a video game in which they moved a spaceship in the horizontal direction (left-right) to evade the blocks dropping from above. Every time the spaceship collided with a block (collision event; B) one life was lost. From time to time, the spaceship moved in the opposite direction of the joystick movement for 500ms (movement mismatch event; C). Performance of the subject was measured by a score shown in the bottom right of the screen. The number of remaining lives was shown in the bottom left corner. The game (and the experimental session) ended when all lives were lost.

Occasionally, the spaceship moved in the opposite direction to the joystick movement for the duration of 500ms (movement mismatch event, Figure 14c, mean and sem of time between events: S1: 18.46±1.08 s, S2: 13.17±0.49 s, S3: 30.36±2.52 s, S4: 24.79±2.33 s). Movement mismatch event was introduced to study neuronal responses to execution errors. To make these events noticeable

and to also make them look as part of the natural movement, they were triggered only when the following conditions were fulfilled: (i) the spaceship was not close to the paradigm borders, (ii) the joystick position was between 60% and 70% of the maximum deflection, (iii) the joystick velocity (first derivative of joystick deflection) was in the direction of the joystick deflection, and (iv) the blocks were not too close to the spaceship. Condition (iv) was introduced to minimize the chance of a block collision following an unexpected change in the spaceship movement direction due to the movement mismatch event. For the first two subjects, condition (iii) was not imposed and a movement mismatch event was triggered only during joystick movements to the right.

Points were awarded for moving the spaceship, and subjects were instructed to gather as many points as possible. The number of points increased linearly with the distance the spaceship travelled. To control the attention of the subjects the colour of the spaceship changed between red and blue at random instants, events which subjects were asked to orally report. Subjects correctly reported on colour changes except on a very few occasions. For the last two subjects, screen freeze events were added where, at a random instant (mean time between events: S3: 36.67±0.89 s, S4: 36.15±1.09 s), the spaceship and all blocks stopped moving for 2 seconds in the same manner as after a collision event. I added screen freeze events to serve as a visual and surprise control (see section 3.2.2. for detailed description).

To avoid mixing between neuronal responses to different events, all triggered events (movement mismatch, screen freeze and colour change) were triggered at least 2 seconds away from the last preceding event of any kind (movement mismatch, screen freeze, colour change, collision, paradigm restart after collision and end of screen freeze event). This procedure was not enough to remove the mixing completely, since the timing of the collision events could not be controlled. Therefore, events were classified after the experiment as “clean” if no other event was closer than 2 seconds.

Subjects	Sessions	Collision events		Mismatch events		Color ch. events		Freeze events	
		All	Clean	All	Clean	All	Clean	All	Clean
S1	8	160	120	195	155	101	63	0	0
S2	4	80	38	227	185	125	85	0	0
S3	4	80	51	121	92	139	134	109	109
S4	6	120	87	71	38	71	62	62	62

Table 5 Number of recorded sessions and events for each of the subjects. For subjects S1 and S2 freeze event was not implemented in the experiment.

Subjects started the game with 20 “lives”. Each time the spaceship collided with a block, the number of “lives” was reduced by one. When the number of “lives” reached 0, the game, together with the recording session, ended. Recording sessions of all subject lasted between 5 and 24 minutes. There

were no auditory stimuli presented during the experiment. Summary of the number of recorded sessions and the number of recorded events is given in Table 5.

3.2.2. Error and control events

To play the game as long as possible and, thereby, earn more points, subjects needed to evade hitting the blocks falling down from the top. Therefore, every collision event that occurred presented a clear disadvantage in reaching the goal of the game. Thus, collision events reflect outcome errors. During the movement mismatch event, the ongoing motor command resulted in an unexpected movement due to the change in movement kinematics. Thus, movement mismatch events reflect execution errors.

Neuronal responses triggered on collision or movement mismatch events might also, partly or entirely, be the result of specific behaviours and/or visual inputs related to the error event, rather than only the neuronal response to the errors themselves. Hence, to identify ERNRs, the responses to collision or movement mismatch events need to be compared to the neuronal responses during behaviour and visual stimuli specific to the collision or movement mismatch events, but without the error context. Any significant deviation between the two responses may then be assumed to present an ERNR. I considered the following controls:

(1) Movement control: All subjects in this study had implants over the motor and the somatosensory related areas. Therefore, neuronal responses to collision or movement mismatch events can be movement related. To minimize the influence of movement related neuronal responses (MRNR), subjects were asked to relax and perform a minimum amount of movement. The only movements they had to perform were thumb movements to move the joystick. Thumb movements were always carried out with the thumb contra-lateral to the brain hemisphere where the electrode grid was located. Subjects occasionally made eye movements to observe what was happening on the screen. To remove the influence of the eye and thumb movements from the recorded neuronal signals, MRNR were removed using the subtraction method described in section 3.2.4.

(2) Visual control: Specific visual feedback provided by the paradigm can generate part of the neuronal response triggered by collision or movement mismatch events. Screen freeze events presented identical visual stimuli as collision events, the only difference being that, in the screen freeze event, the spaceship did not touch one of the blue blocks on the screen. Therefore, screen freeze events were used as a visual control for the collision events. This visual control was implemented for S3 and S4 only.

(3) Surprise control: Great care was taken to make movement mismatch events look as part of the undisturbed spaceship movement, unrecognizable from watching the paradigm only. Therefore, no

visual stimulus was specific to the movement mismatch events. On the other hand, movement mismatch events could not be predicted by the subject and, hence, could trigger a surprise related neuronal response. Therefore, I used freeze events, which could also not be predicted by the subject, as a control event for the movement mismatch events. This surprise control was implemented for S3 and S4 only.

3.2.3. Subjects and recordings

Four subjects (3 male, 1 female) suffering from intractable pharmaco-resistant epilepsy voluntarily participated in the study after having given their informed consent. The study was approved by the University Hospital's Ethics Committee.

For pre-neurosurgical epilepsy diagnosis, the subjects were implanted with an 8 x 8 grid of subdural surface electrodes covering parts of the primary and pre-motor cortex (Figure 15). In addition, S1, S2 and S3 had the following implanted electrodes: S1 had two strips, with 6 electrodes each, implanted subdurally over the prefrontal cortex and 4 strips, with 4 electrodes each, implanted subdurally in the interhemisphere region touching the left hemisphere. S2 had two strips, with 6 electrodes each, implanted subdurally over the bottom of the cerebellum and 4 strips, with 4 electrodes each, implanted subdurally over the temporal and prefrontal cortices. S3 had two strips, with 4 electrodes each, implanted subdurally over the prefrontal cortex. The sites of all electrode implantations were exclusively based on the requirements of the clinical evaluation. In S2, the signals from the top row of electrodes in the grid implant and from one of the strips over the bottom of the cerebellum (TBd) were not recorded from due to the limited number (128) of available channels in the recording system. In addition to the subdural surface electrodes electrodes, additional intracortical electrodes were implanted and signals from 22 EEG electrodes, two to four EOG electrodes, two ECG and two EMG electrodes were recorded simultaneously. Signals from the intracortical, EEG, ECG and EMG electrodes were not analyzed in this study.

Recordings from all electrodes were digitized at 256 Hz sampling rate for S1 and S2 and at 1024 Hz sampling rate for S3 and S4, in all cases using a clinical AC amplifier (Brainbox EEG-1164 amplifier, Braintronics B. V., Almere, Netherlands). No analogue filters were used during the data acquisition. Power line frequency was 50Hz. Experiment control and paradigm presentation was performed using in house laboratory software. Subsequent data analysis was performed using MATLAB (MATLAB version 7.4-7.11, Natick, Massachusetts: The MathWorks Inc., 2007-2011).

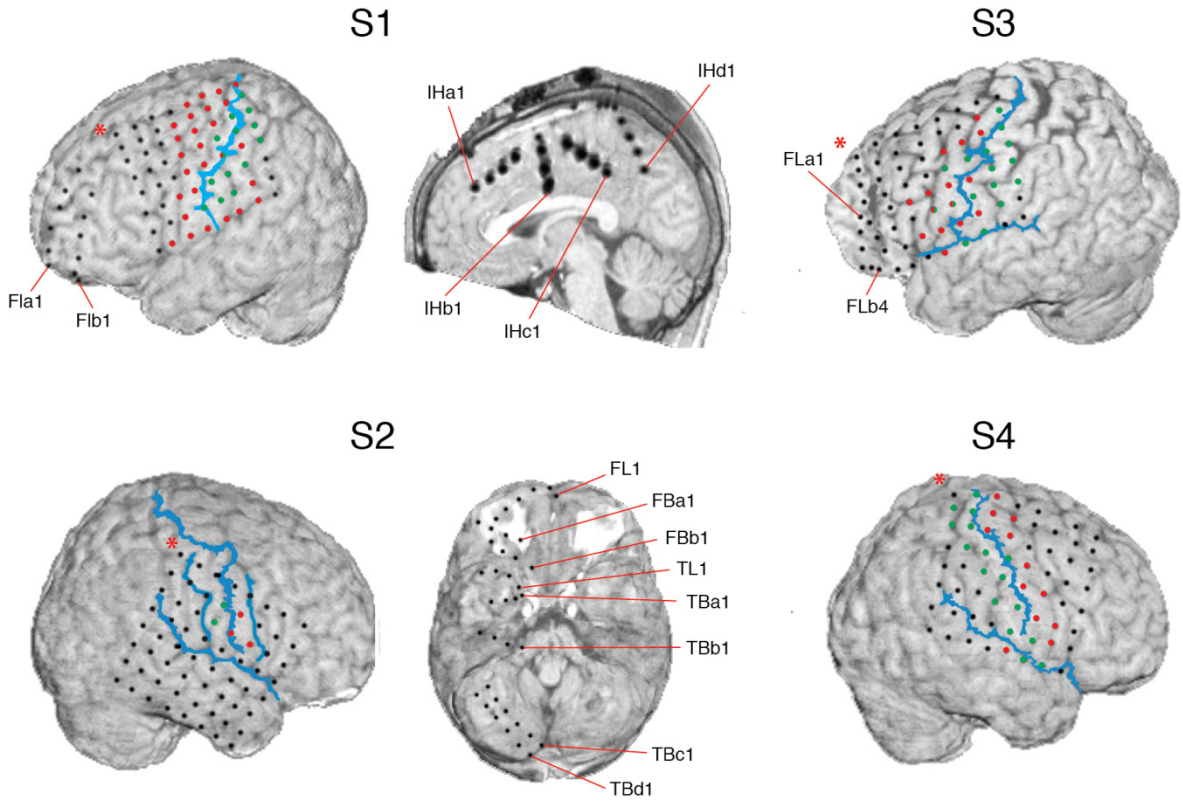

Figure 15 Locations of implanted electrodes (red, green and black circles). Electrode positions were reconstructed from the post-implantation MRI scan and positioned over the pre-implantation MRI scan (Kovalev et al., 2005). For S1, S3 and S4 red (green) circles represent electrodes that showed motor (somatosensory) response from electrical stimulation mapping (ESM). For S2 motor and somatosensory electrodes were determined from sulci reconstruction. Central sulci, Sylvian fissures and, for S2 only, pre and post central sulcus are shown as blue lines. These were drawn by hand to resemble sulci reconstruction from the post-implantation MRI scan. S1 was implanted with an 8 x 8 ECoG grid over the parts of frontal and parietal lobe, two 6 electrode ECoG strips over the frontal lobe (FLa and FLb) and four 4 electrode ECoG strips inter-hemispherically (IHa, IHb, IHc and IHd). S2 was implanted with an 8 x 8 ECoG grid over parts of temporal, parietal and frontal lobe, two 6 and three 4 electrode ECoG strips on the basal temporal cortex (TL, TBa, TBb, TBc and TBd) and two 4 electrode and one 6 electrode ECoG strips on the basal frontal lobe (FL, FBa and FBb). In S2 no recordings were made from the top row of the 8 x 8 electrode grid and from the TBd ECoG strip. S3 was implanted with 8 x 8 ECoG grid over the parts of frontal and parietal lobe and two 4 electrode ECoG strips (FBa and FBb) over the frontal lobe. S4 was implanted with an 8 x 8 ECoG grid over parts of parietal and frontal lobe. In all pictures the red star marks the edge of the electrode grid corresponding to the top left corner in the spatial distribution pictures shown in Figure 19, Figure 25, Figure 26, Figure 27.

3.2.4. Data analysis

Preprocessing

Common-average referencing for grid electrodes was made using all grid electrodes that showed no artefacts (one electrode for both S3 and S4 had to be excluded). Electrode strips above frontal cortex of S1 were re-referenced using all electrodes on those two strips. Inter-hemisphere electrodes for S1 were re-referenced using all electrodes on those four strips. For S2, electrode strips above the bottom of the cerebellum, temporal and frontal areas were re-referenced together. For S3, electrode recordings from two strips above frontal areas were re-referenced together. To correct for

changes in channel offsets between sessions, the mean voltage over the entire session was subtracted for every session and for every channel after re-referencing.

Low frequency signal component

I extracted low and high frequency components of the recorded ECoG signals. To analyze the low frequency component of the signal, the preprocessed ECoG signals were smoothed using a symmetric Savitzky-Golay filter (Savitzky and Golay, 1964; Steinier et al., 1972). The Savitzky-Golay filter is not a filter designed with a specific cut-off frequency. It is a smoothing filter that performs least-square fitting of a polynomial of the certain order (2nd order in the case of this study) to the signal in a certain time window (250ms of recorded data points in the case of this study). Even though the frequency domain properties of a Savitzky Golay filter do not resemble that of a typical low-pass filter (Schafer, 2011) a nominal 3dB cut off frequency can be determined and was, in the case of this study, 7.85Hz for S1 and S2 and 7.59Hz for S3 and S4.

To show that the chosen filter was suitable for extracting ERNRs contained in the low frequency signal, I compared the SNR of ERNRs gained from using the chosen filter with the SNR of ERNRs gained by other low and band pass filters. Recordings were filtered with low and band pass 8th order Butterworth filters with low and high cuttoff frequencies taking all possible combinations of values from 0Hz to 127Hz in steps of 1Hz. To measure the ERNR strength, I calculated the SNR of the filtered neural responses to collision and to mismatch events against the baseline activity. Collision and movement mismatch SNR was pooled over subjects and then averaged across channels, for all tested Butterworth filters and for the chosen Savitzky-Golay filter (Figure 16). For both collision and mismatch SNR, the low pass Butterworth filter had a higher average SNR than any bandpass Butterworth filter. The difference between maximum SNR for Butterworth filter (average collision SNR: 0.34, cutoff frequency of 6Hz; average mismatch SNR: 0.202, cutoff frequency 10Hz) and the SNR for the chosen Savitzky-Golay filter (collision: 0.35; mismatch: 0.199) was not significant ($p<0.05$; Wilcoxon signed-rank test). Therefore, I conclude that here used Savitzky-Golay filter was a good choice for extracting the low frequency component (LFC) of the ERNRs.

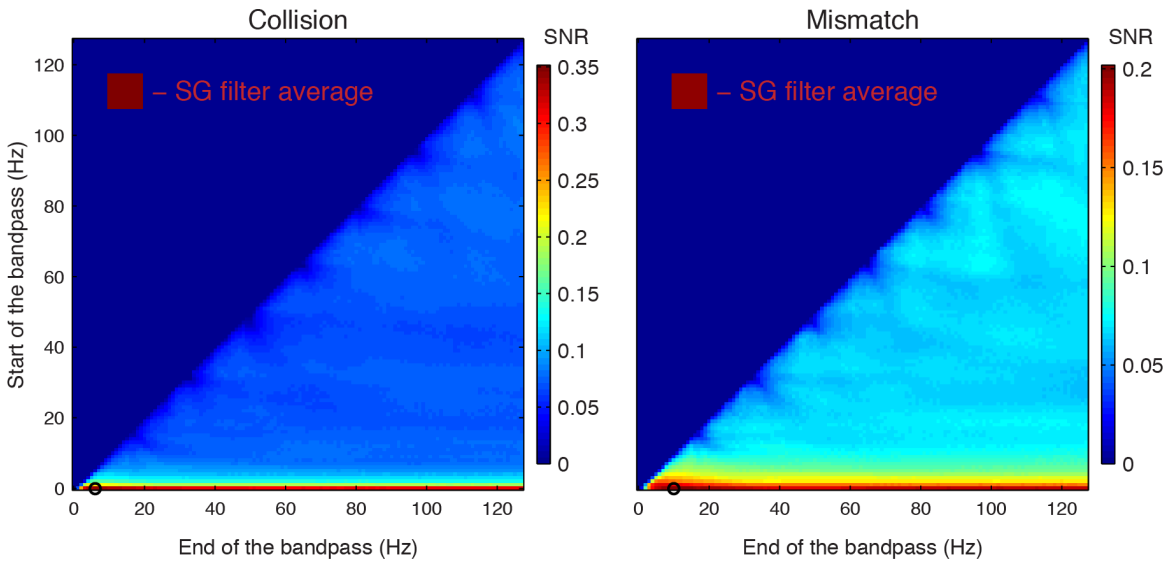

Figure 16 Average collision (left) and movement mismatch (right) SNR for low and band pass filtered signals. SNRs were pooled over subjects and averaged across electrodes and are shown for all possible choices of bottom and top cutoff frequency of the Butterworth filter used to filter the signal. Cutoff frequencies that provided the highest average SNR are shown with black circle. Inset square shows the average SNR gained by using the Savitzky-Golay filter used for defining the low frequency component of the ERNRs in my study.

High frequency signal component

To analyze the high frequency component of the signal, time-resolved Fourier transformation (TRFT) using a Hamming window (333ms window width, shifted in steps of 31ms) was applied to the preprocessed signals, and the amplitudes were used for further analysis. To investigate event induced changes in amplitudes and to account for the general decrease in amplitude with increasing frequency, the amplitudes of every frequency bin were normalized by dividing them by the average baseline amplitude of the same frequency bin in the respective session. Afterwards, the average amplitude across a frequency range was computed for further analysis.

I defined a window around each event (movement mismatch, screen freeze, colour change, collision), starting 3 seconds before each event and lasting until 3 seconds after each event. The signals outside all of these windows were used as baseline activity. To enable a clear comparison to baseline, the average baseline activity was subtracted from the average amplitudes in each session for each channel. The resulting signal was defined as the high frequency component (HFC) of the signal.

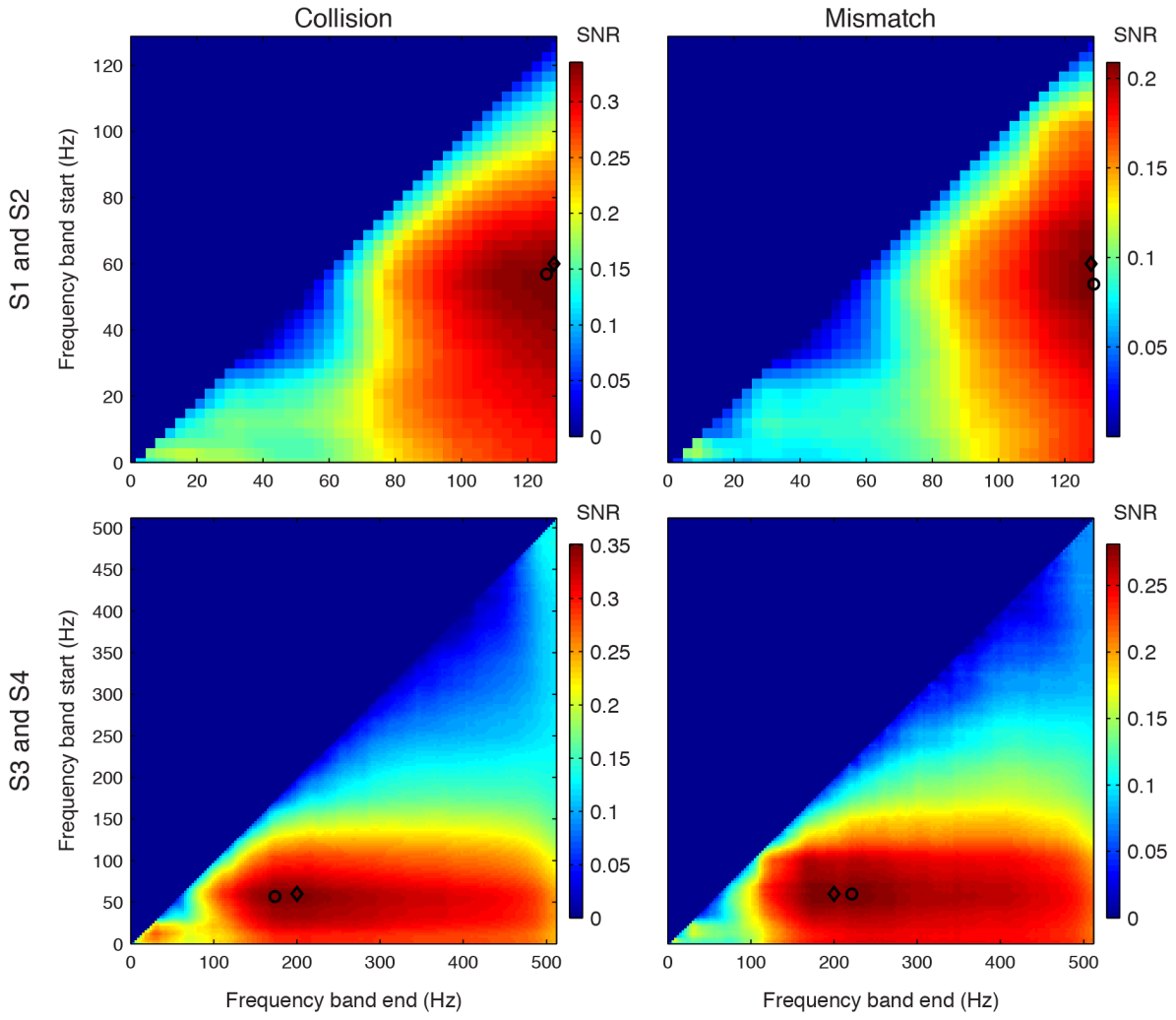

Figure 17 Average collision (left) and movement mismatch (right) SNRs for the amplitudes of different frequency bands. SNRs were pooled over subjects and averaged across electrodes and for all possible choices of bottom and top frequencies of the frequency band used to construct the signal. Recordings for S1 and S2 were made at sampling frequency of 256Hz, and recordings for S3 and S4 were made at 1024. Therefore, I averaged SNR for S1 and S2 (top row) independently from the averaging for S3 and S4 (bottom row). Frequency bands were tested until the respective Nyquist frequency (128Hz for S1 and S2; 512Hz for S3 and S4). I marked the band with the highest average SNR (black circle) and the band used in this study for the high frequency component of the neural response (black rhomboid).

I computed the SNR (event vs. baseline) of the amplitudes in different frequency bands for collision and mismatch events. Collision and movement mismatch SNRs were pooled over subjects and then averaged across channels (Figure 17). For S1 and S2, where the Nyquist frequency was 128Hz, the average collision SNR peaked at the band starting at 51Hz and ending at 117Hz (average SNR: 0.35), while the average movement mismatch SNR peaked at the band staring at 54Hz and ending at 126Hz (average SNR: 0.172). For S3 and S4, where the Nyquist frequency was 512Hz, the average collision SNR peaked at the band starting at 60Hz and ending at 174Hz (average SNR:0.351), while the average movement mismatch SNR peaked at the band staring at 60Hz and ending at 226Hz (average SNR:0.281). For all subjects and both events, SNR peaks were rather broad and small changes of the

upper and lower bounds of the frequency bands did not affect the SNR considerably. Given the lower Nyquist frequency in S1 and S2, it is not surprising that the upper bound of the optimal frequency band in these subjects is lower than in S3 and S4. Indeed the optimal upper bound for S1 and S2 is close to the Nyquist frequency in S1 and S2.

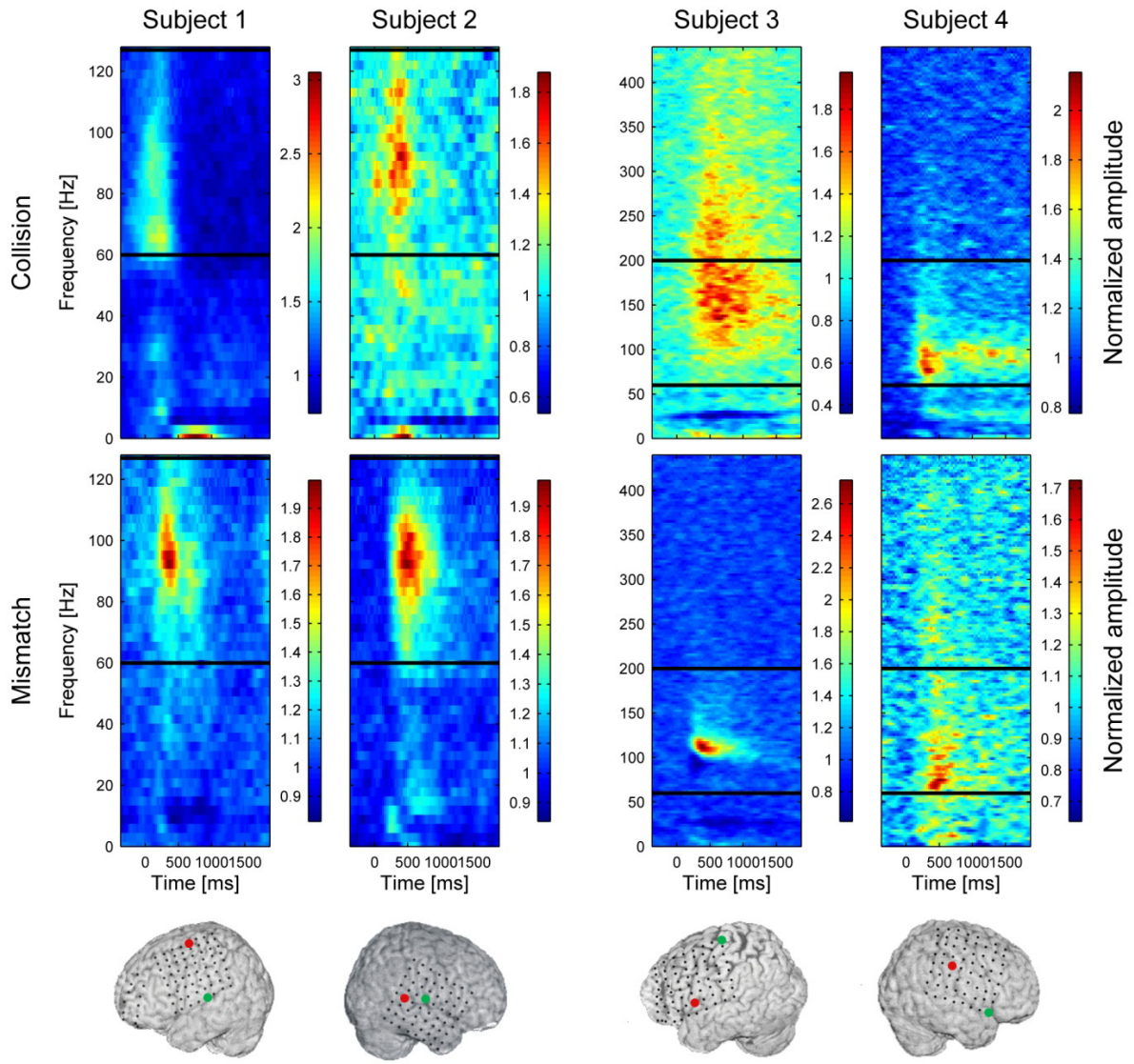

Figure 18 Examples of the averaged normalized spectrograms to collision and to mismatch events for one electrode for each of the subjects. Channels used as examples are marked in red for collision and green for mismatch events on the small depictions of the subjects' brains below the spectrograms. Black horizontal lines indicate the bottom and top frequencies of the band used for the high frequency component of the signal. In S1 and S2 the upper boundary of this band was at the Nyquist frequency.

To choose a common band for both events and a band which has the same lower border for all subjects, I decided to use the band 60Hz-200Hz in S3 and S4 and the band 60Hz-128Hz in S1 and S2 (Figure 18). For S1 and S2, collision and mismatch SNR was not significantly different between the peak frequency band and the band that I chose to use (band spans from 60Hz to 128Hz; average collision SNR: 0.33; average mismatch SNR: 0.169; $p<0.001$; Wilcoxon signed-rank test). For S3 and

S4, collision and mismatch SNR was significantly different between the peak frequency band and the band that I chose to use (band spans from 60Hz to 200Hz; average collision SNR: 0.348; average mismatch SNR: 0.279; p<0.19; Wilcoxon signed-rank test), but the differences between the average collision and mismatch SNR for the optimal band and the band I chose is below 1% of the average collision and mismatch SNR for the optimal band.

MRNRs were then subtracted from both signal components as described in the following.

MRNR subtraction

As described above, I considered that thumb and eye movements might be correlated with error events. If so, parts of the neuronal responses correlated to error events, might not be evoked by error events but by accompanying eye and thumb movements.

To remove the movement related component of the neuronal response following a mismatch or a collision event, I derived a model relating the signals to the movements using only non-event data (i.e. all data which was at least 1s before and 3s after any event) and then subtracted the signals predicted by this model for the movements during the events from the recorded event-related signals. The required thumb movements were tracked indirectly through the joystick movements, while the required eye movements were tracked through the horizontal and vertical EOG.

Two types of models were considered, linear and non-linear models. Linear models assumed a linear relationship between the neuronal response at time t, $Y_{CH}(t)$, and the joystick position X, the absolute joystick position $|X|$, the joystick velocity V, the absolute joystick velocity $|V|$, the horizontal EOG $heog$ and the vertical EOG $veog$ at different time points around t:

$$\Delta t_i = \begin{cases} 0 & \text{for } N = 1 \\ \left(\frac{i-1}{N-1} - \frac{1}{2} \right) * \mathrm{L} & \text{for } N > 1 \end{cases} \tag{3.1}$$

$$\begin{aligned} Y_{CH}(t) = a_0^{CH} + \sum_{i=1}^{N} b_i^{CH} X\left(t+\Delta t_i\right) + \sum_{i=1}^{N} c_i^{CH} \left|X\left(t+\Delta t_i\right)\right| + \sum_{i=1}^{N} d_i^{CH} V\left(t+\Delta t_i\right) \\ + \sum_{i=1}^{N} e_i^{CH} \left|V\left(t+\Delta t_i\right)\right| + \sum_{i=1}^{N} f_i^{CH} heog\left(t+\Delta t_i\right) + \sum_{i=1}^{N} g_i^{CH} veog\left(t+\Delta t_i\right) \end{aligned} \tag{3.2}$$

where N is the number of used data points for each movement parameter, L is the length of the movement information provided to the decoder, a_0^{CH}, b_1^{CH},..., b_N^{CH}, c_1^{CH},..., c_N^{CH}, e_1^{CH},..., e_N^{CH}, f_1^{CH},..., f_N^{CH}, g_1^{CH},..., g_N^{CH} are the model coefficients and Δt_i are the time lags relative to the neuronal response. Time lags Δt_i were such that the times of the N movement data points entering the model were spread equidistantly on a time stretch of length L centred on the time t.

Non-linear models try to address a possibly non-linear relationship between the neuronal response at time *t, $Y_{CH}(t)$,* and the joystick position X, the joystick velocity V, the horizontal EOG $heog$ and the vertical EOG $veog$ at different time points around t:

$$Y_{CH}(t) = F\left(X\left(t+\Delta t_i\right),...,V\left(t+\Delta t_i\right),...,heog\left(t+\Delta t_i\right),...,veog\left(t+\Delta t_i\right),...\right) \quad (3.3)$$

Time lags Δt_i were the same as used in the linear model. Absolute position and absolute velocity were not used since non-linear modelling is able to account for the non-linear absolute value transformation. In the case of the linear models, for a certain value of L and N, the model coefficients can be fitted by linear least-squares regression. For non-linear models more complex algorithms have to be used. Here, I used the epsilon-SVR algorithm, part of the LIBSVM library (Fan et al., 2005).

Optimal values of L and N are not known a priori: if many time lags are used (high value of N), the model might overfit the data and, therefore, the model predictions might poorly generalize due to inaccurate model coefficients. If only few time lags are used (low value of N), the model predictions might also generalize poorly as not all available information for predicting the movement related neuronal responses is incorporated into the model. Similarly, if the time stretch (L) is too small, the information contained in points further away in time would not be used, whereas nearby points might contain redundant information. Using large time stretches, on the other hand, might result in a miss of information contained between two time lags. Therefore, I needed to determine the values of L and N which yield optimal model prediction. To this end, I split the non-event data into two halves: the first half was used to estimate the model coefficients for certain values of L and N. These model coefficients were then used to predict the signals of the second half of the data. To determine the performance of the model, I computed r^2 values between the model predictions and the real neuronal responses in the second half of the data:

$$r^2 = 1 - \frac{V\left(Y(t) - Y_{MODEL}(t)\right)}{V\left(Y(t)\right)}$$

This measure was computed for different values of L (62.5ms, 109.4ms, 156.2ms, 203.1ms, 250ms, 375ms, 500ms, 750ms, 1000ms, 1250ms, 1500ms, 1750ms and 2000ms) and N (1, 2, 3, 4, 6, 10, 14, 18 and 22) for both linear and non-linear models and the one yielding the highest r^2 values was then used for the MRNR subtraction. These optimal values were determined for each channel individually (Figure 19). Channels yielding an r^2 below 0.01 were considered as being not movement related; for these channels nothing was subtracted from the event-related signals.

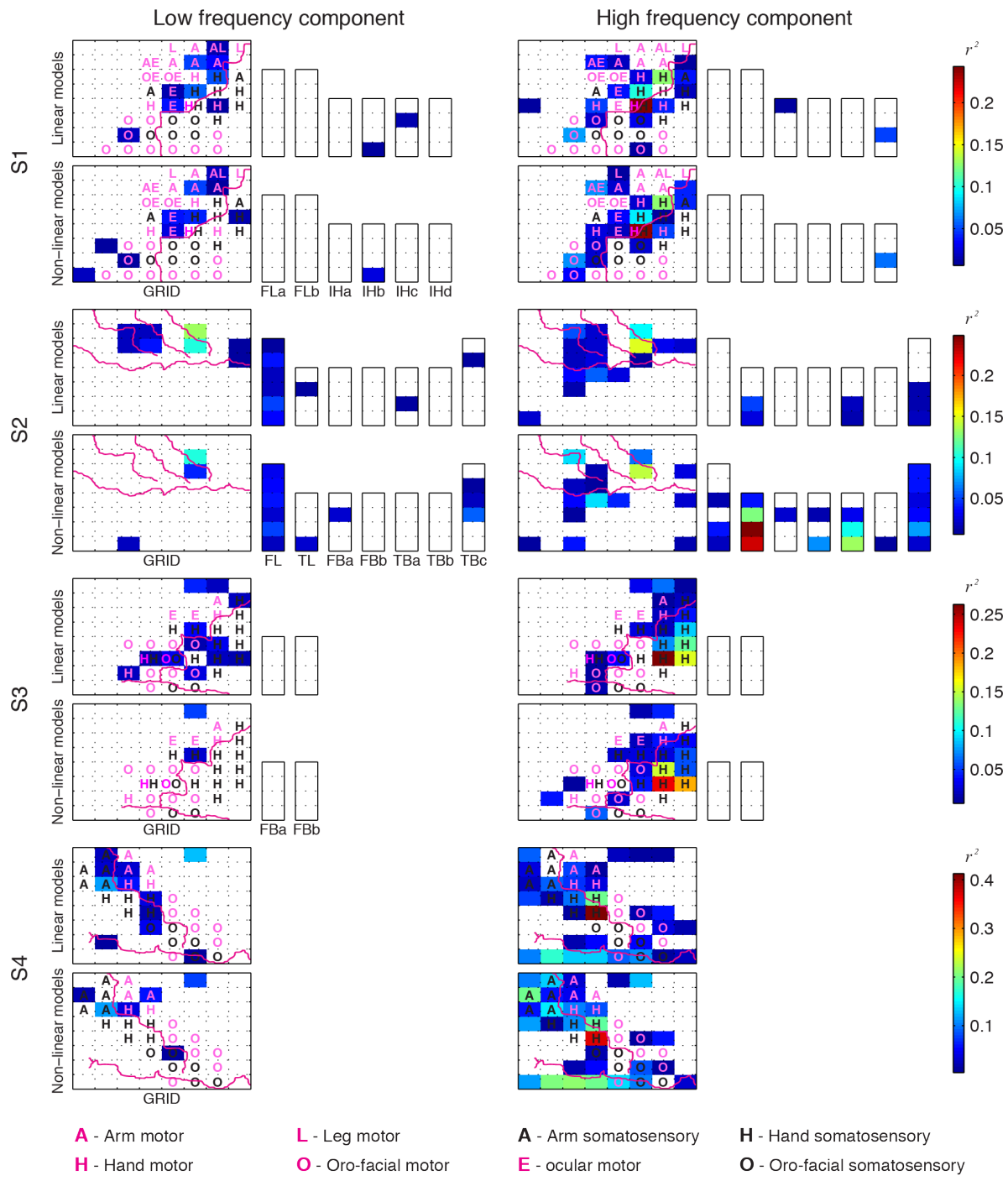

Figure 19 Spatial distribution of r^2 values for each subject, signal component, model type and electrode in relation to the individual anatomy of the subject. Purple lines depict the central sulcus, the Sylvian fissure and, for S2 only, the pre and post central sulci. Letters in the squares mark the functional subarea (A – arm, H – hand, L – leg, E – ocular, O – oro-facial) in motor (purple) and somatosensory (black) cortex as determined by ESM. Every small square represents one electrode. As no recordings were made from the top row of grid electrodes for S2, this row is shown as white. TBd ECoG strip from S2 was also not recorded from and is, therefore, not shown. The top left square in the ECoG grids correspond to the electrode closest to the red star in Figure 15. In the case of the ECoG strips, the bottom square corresponds to the first electrode of the strip. Colours of the squares depict the highest r^2 value over number of used data points (N) and length of the movement information (L); white squares represent channels with highest r^2 values below 0.01.

Error related neuronal responses

To avoid mixing of neuronal responses to different events only epochs from clean events (see section 3.2.1.) were used for subsequent analysis. After the MRNR subtraction, the remaining signal should predominantly contain the neuronal responses to errors. Therefore, the neuronal responses to collision and mismatch events are called outcome and execution ERNRs after MRNR subtraction.

Signal to noise ratio analysis

To compare the event triggered neuronal response Φ_{EVENT} to the baseline activity $\Phi_{BASELINE}$ or to the event triggered neuronal response of another event Φ_{EVENT2}, the signal to noise ratio (SNR) was used. Let n be the event index, t the time within the event epoch, m the index of the baseline measurement, E the expectation operator, and std the standard deviation operator. I defined the SNR as follows:

$$\begin{aligned} \mu_{EVENT}(t) &= E\left(\Phi_{EVENT}(n,t),n\right) & \sigma_{EVENT}(t) &= std\left(\Phi_{EVENT}(n,t),n\right) \\ \mu_{BASELINE} &= E\left(\Phi_{BASELINE}(m),m\right) & \sigma_{BASELINE} &= std\left(\Phi_{BASELINE}(m),m\right) \end{aligned} \tag{3.4}$$

$$SNR(t)_{\substack{EVENT\ vs.\\ BASELINE}} = \frac{\left|\mu_{EVENT}(t) - \mu_{BASELINE}\right|}{\sigma_{EVENT}(t) + \sigma_{BASELINE}} \tag{3.5}$$

$$SNR(t)_{\substack{EVENT1\ vs.\\ EVENT2}} = \frac{\left|\mu_{EVENT1}(t) - \mu_{EVENT2}(t)\right|}{\sigma_{EVENT1}(t) + \sigma_{EVENT2}(t)} \tag{3.6}$$

For limited numbers of trials, the SNR is positively biased (Mehring et al., 2003). To correct for this, I used a bootstrap bias correction (Efron and Tibshirani, 1993), with 1000 times re-sampling of the event data to remove this bias.

The above computations yielded, for each type of ERNR, an SNR against baseline and an SNR against the control event. Since, to detect ERNRs, I needed to differentiate them from baseline and control events, I quantified the SNR of an ERNR by the minimum among these two SNR values. This yielded one SNR value for each point in time. To describe the strength of the ERNR by a single number, I introduced the outcome SNR and the execution SNR as the maximum of these SNR values between 100ms and 800ms after the trigger.

To be able to differentiate between outcome and execution error events, outcome ERNRs have to be different from the execution ERNRs. Since outcome and execution ERNR may have different delays with respect to the trigger, these two signals cannot be directly compared. Therefore, I computed the outcome vs. execution SNR as follows:

$$SNR_{MAX} = \frac{\left|\mu_O\left(t_{O\max}\right) - \mu_E\left(t_{E\max}\right)\right|}{\sigma_O\left(t_{O\max}\right) + \sigma_E\left(t_{E\max}\right)}; \quad \begin{vmatrix} t_{O\max} = \max\limits_t \arg\left(\mu_O\left(t\right)\right) \\ t_{E\max} = \max\limits_t \arg\left(\mu_E\left(t\right)\right) \end{vmatrix} \tag{3.7}$$

$$SNR_{MIN} = \frac{\left|\mu_O\left(t_{O\min}\right) - \mu_E\left(t_{E\min}\right)\right|}{\sigma_O\left(t_{O\min}\right) + \sigma_E\left(t_{E\min}\right)}; \quad \begin{vmatrix} t_{O\min} = \min\limits_t \arg\left(\mu_O\left(t\right)\right) \\ t_{E\min} = \min\limits_t \arg\left(\mu_E\left(t\right)\right) \end{vmatrix} \tag{3.8}$$

$$SNR_{\substack{OUTCOME \text{ vs.} \\ EXECUTION}} = \max\left(SNR_{MAX}, SNR_{MIN}\right) \tag{3.9}$$

where t runs from 100ms to 800ms after the trigger, μ_O is the average outcome ERNR, μ_E is the average execution ERNR, σ_O is the standard deviation of the outcome ERNR across trials, and σ_E is the standard deviation of the execution ERNR across trials.

Classification analysis

To see how well ERNRs can be differentiated from baseline activity on a single-trial basis, I performed a binary classification analysis of outcome or execution ERNRs vs. baseline activity using regularized linear discriminant analysis (RLDA) (Friedman, 1989). The class representing baseline activity contained all baseline activity recordings. The other class representing either outcome or execution ERNR was composed of outcome (execution) ERNRs at the time of the average outcome (execution) ERNR peak. Only single signal components from single channels were used as inputs to the RLDA. Trials were shuffled and divided into a training set, which contained 2/3 of the data, and a test set, which contained the remaining 1/3 of the data. The training set was used to train the RLDA model which was then used to classify the test set. The decoding accuracy (DA) was computed as described in equation (2.1). The regularization parameter of the RLDA was optimized on the training data by five times five-fold cross validation.

Additionally, I classified outcome vs. execution ERNR using the same classification procedure as above. Instead of using only one time point to differentiate between two signals, I allowed for 1-4 points cantered around the time of the ERNR peak. The number of time points and the temporal distance between the first and the last time point (between 31ms and 281ms) together with the regularization parameter of the RLDA were optimized on the training set using five times five-fold cross validation.

Significance testing of neural responses

To confirm that ERNRs were significantly different from neural responses during baseline and to freeze events the Mann–Whitney–Wilcoxon test was applied between an ERNR in every time point and the baseline activity. To avoid the autocorrelation of the low frequency component arising from

the filtering procedure, I sampled low frequency component baseline activity every 250ms and high frequency component baseline activity every 333ms. To confirm that ERNRs were significantly different from freeze events the Mann–Whitney–Wilcoxon test was applied between an ERNR and the neuronal response to freeze event in every time point after the event trigger. Since ERNR had to be present within a limited time after the trigger, I tested the epoch of the neural response from 100ms till 800ms after the event trigger. To reduce the calculation time of the significance testing, I tested significance of the neural responses every 31ms (roughly 32Hz) instead of testing for every recorded time point .

Due to the large number of statistical tests, correction for multiple testing was necessary to control the number of falsely rejected null hypotheses. I used the Benjamini-Hochberg procedure (Benjamini and Hochberg, 1995) with a correction for dependent statistics (Benjamini and Yekutieli, 2001) to set the false discovery rate for one subject at the level of 5% for all tests. A neuronal response from a single channel/frequency component was declared significant if there was at least one time point for which the ERNR was significantly different from the baseline and significantly different from the freeze neuronal response after the correction for multiple testing was made.

To test whether the used statistical test for the significant event responses was not detecting large number of false positives, I made 100 repetitions of the procedure for significance testing. In each repetition, I assigned random time to every event (collision, movement mismatch, freeze and colour change), respecting the rule that all paradigm triggered events (movement mismatch, freeze and colour change) have to come at least 20 seconds after any event (movement mismatch, screen freeze, colour change, collision, paradigm restart after collision and end of screen freeze event). To remove the MRNR, I used the same models that were used in the analysis of data using non-shuffled triggers.

3.2.5. Neuroanatomical analysis

To determine whether the motor or the somatosensory cortex played a more distinctive role in generating ERNR, I classified electrodes into motor cortex electrodes, somatosensory cortex electrodes, and other electrodes. Classification was performed combining the results of sulci identification on the post-implantation MRI scans with the results of direct cortical electrical stimulation mapping (ESM) (Foerster, 1931; Uematsu et al., 1992).

Electrical cortical stimulation through the electrode grid was performed using an INOMED NS 60 stimulator (INOMED, Germany). Trains of 7 s duration consisted of 50 Hz pulses of alternating polarity square waves of 200μs each. The intensity of stimulation was gradually increased up to 15

mA or to the induction of sensory and/or motor phenomena. The patients were unaware of the timing of stimulation unless motor symptoms or somatosensory sensations occurred.

Electrical stimulation of by-passing paths may indeed lead to functional responses that are not directly related to the cortex under a given electrode contact. To reduce such effects, electrical stimulation was carried out against different reference electrodes, such as directly neighbouring ones or electrodes with a large distance to the stimulated ones. As stimulation against difference reference electrodes will cause different current distributions, such effects may be reduced, albeit not completely excluded, in this manner. Only effects that were consistently observed, independently of the choice of the reference electrode, were used to generate the maps shown in the manuscript.

Data from post-implantation MRIs was used to reconstruct the positions of central sulcus and Sylvian fissure with respect to the electrodes. The central sulcus was used to generate a border between motor and somatosensory cortex, while the Sylvian fissure was used to generate a border between the temporal lobe and the frontal and parietal lobe, containing motor and somatosensory cortex, respectively. Results of ESM were used to define a border between motor cortex and the remainder of the frontal lobe on the one hand, and somatosensory cortex and the rest of the parietal lobe on the other hand. S2 did not go through the ESM. Therefore, in that case, I used the pre and postcentral sulci, as derived from post-implantation MRI, to define the borders of the motor and the somatosensory cortex.

In addition, I used the ESM results to further classify motor and somatosensory electrodes into hand, arm, leg, ocular and oro-facial subgroups. This classification was performed solely on the basis of ESM results. S2 was excluded from this analysis since ESM was not carried out for this subject. Leg motor electrodes only existed in S1 and, for the other three subjects where ESM was performed, ocular and leg somatosensory electrodes were not found.

3.3. Results

I present my results in the following order. First, I show that significant outcome and execution ERNR can be found in all subjects and that these ERNRs are widespread over the part of the cortex that I recorded from. Second, temporal distribution of ERNR peaks is presented and the reason for my choice of the time analysis window, from 100ms after the event until 800ms after the event is shown to be plausible. Third, I provide the evidence that, for every subject, ERNRs can be differentiated from baseline and between each other. Next, I show the spatial distribution of the ERNRs and look whether there is a clear focus of outcome or execution ERNRs over motor or somatosensory cortex.

Finally, I present the results of the classification analysis, showing that both outcome and execution ERNRs can be classified from baseline and between each other with high DA.

3.3.1. Widespread ERNRs

For the outcome error, 63% (397 out of 632; S1: 161 out of 184, S2: 92 out of 176, S3: 72 out of 144, S4: 72 out of 128) and for the execution error, 41% (259 out of 632; S1: 117out of 184, S2: 73 out of 176, S3: 53 out of 144, S4: 16 out of 128) of channels/signal components had significant ERNR. When using shuffled times of the events, none of the channels were found significant for any of the errors and any of the signals components in all shuffles for S1 and S2. For S3 and S4, 0.03 and 0.0025 channels were found significant for any error/signal component on average. This shows that out statistical test is highly conservative and that the expected number of falsely detected ERNRs is very low.

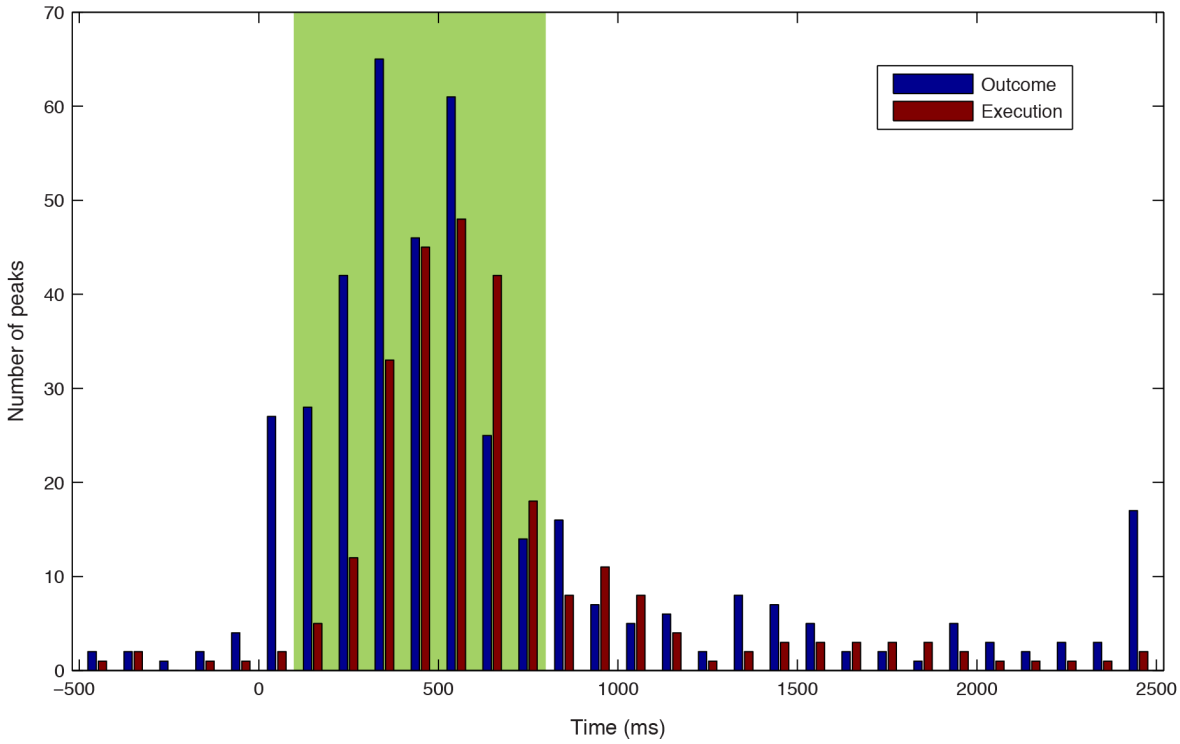

Figure 20 Temporal distribution of the ERNR peaks of channels/signal components with significant response when significance was check on a window between 500ms before till 1500ms after the error event. Number of the outcome ERNR peaks is shown in blue, while the number of the execution ERNR peaks is shown in red. Green background depicts the time interval (100ms after the error event until 800ms after the error event) used to calculate the outcome and execution SNR.

3.3.2. ERNRs latencies

To quantify the response strength, I computed the SNR at the peak of the outcome or execution ERNR within the time window from 100ms to 800ms after the error event. To verify that this window captured the majority of the responses I calculated the temporal distribution of the peaks of the

ERNRs (Figure 20). This distribution clearly peaks within the time window chosen for the ERNR analysis in my study (100-800ms). Furthermore, 90% of all ERNRs significant between 500ms before and 1500ms after the event were also significant within the chosen time window. Thus, the chosen time window captured essentially all ERNRs.

3.3.3. Differentiating ERNRs from baseline and between each other

Every channel and signal component can either have a strong response to both error types (outcome and execution), a strong response to either one of the errors and a weak or no response to the other one, or a weak or no response to both errors. If a signal is strongly responsive to both errors, the outcome vs. execution SNR shows whether the response to both errors is similar or dissimilar. To fully utilize all information from the ERNR, one needs to find a combination of channels/ signal components for every subject that can be used to detect execution and outcome ERNRs and to differentiate between the two. This would be possible if one of the following three conditions is met: (1) separate signals with strong outcome ERNR and weak execution ERNR and with strong execution ERNR and weak outcome ERNR co-exist in the same subject, (2) one or more signals with strong but dissimilar ERNRs to execution and outcome errors co-exist in the same subject, (3) one or more signals with strong and similar ERNRs for both error events co-exist in the same subject with at least one other signal with a strong ERNR for only one of the error events.

For all subjects at least one of the required conditions was met, even when a very high threshold of SNR>=0.5 was applied. Condition 1 was met for S3 only, condition 2 was met for all of the subjects and condition 3 was met for all subjects except S1 (see Figure 21 and Figure 22 for examples).

To be able to detect and differentiate outcome and execution errors from only one channel/signal component, high outcome SNR and high execution SNR is required simultaneously with highly different responses to both errors. Figure 23a shows the outcome vs. execution SNR against the minimum between outcome SNR and execution SNR for all channels and signal components for each of the subjects. Points far from the origin with regard to both axes indicate channels that can be used to detect and differentiate ERNRs. For each subject such channels/signal components were found.

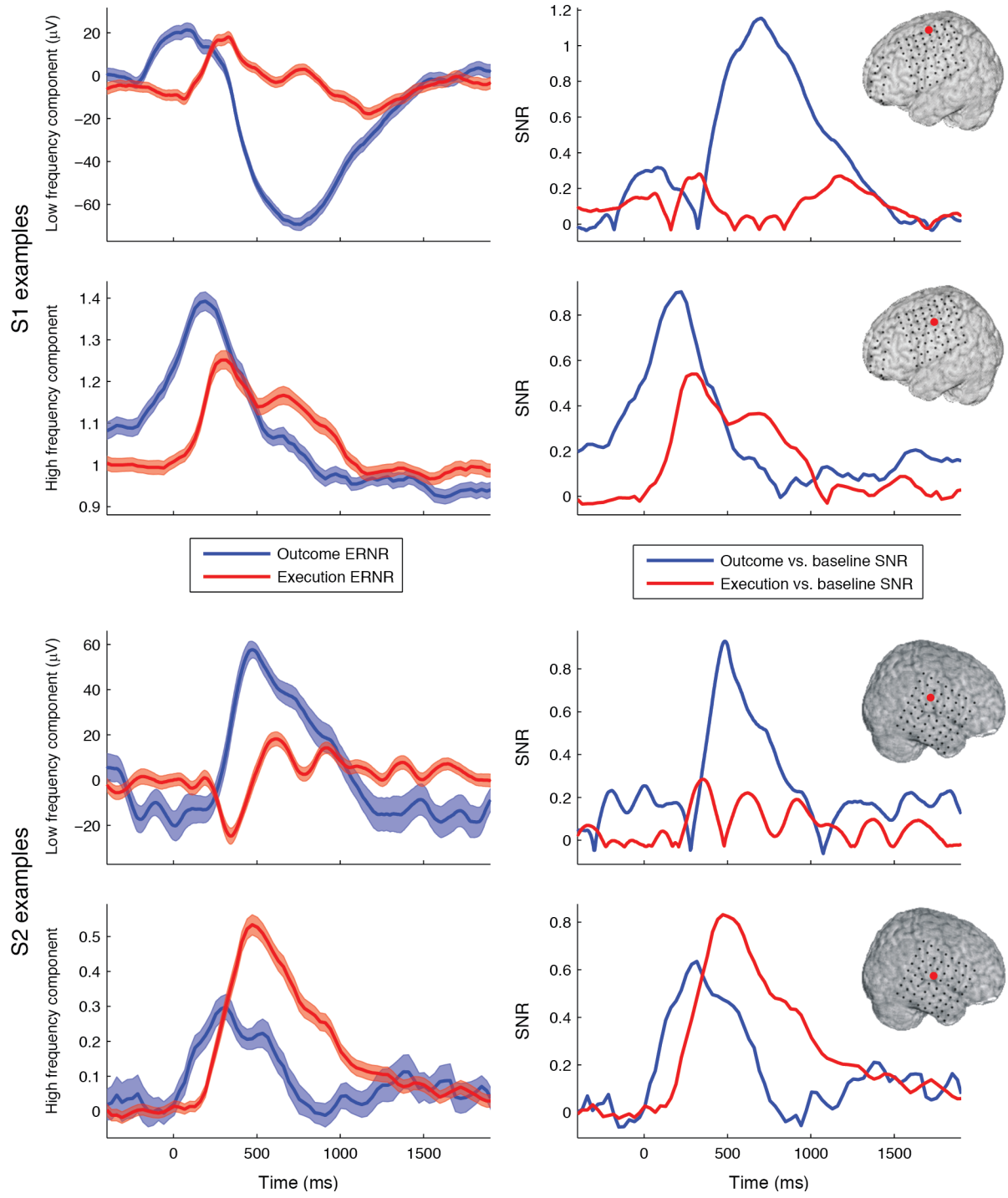

Figure 21 Example of two channels for S1 and two channels for S2 that could be used to detect both execution and outcome errors and differentiate between them. Channels selected as examples are shown as red dots on the small depictions of subjects' brains on the right side. Left panels show outcome ERNR (blue) and execution ERNR (red) as mean ± sem. Right panels show outcome vs. baseline SNR (blue) and execution vs. baseline SNR (red) for both channels. For both subjects the channel shown in the top panel exhibited a strong outcome ERNR, while the channel in the bottom panel exhibited a strong outcome ERNR and a strong execution ERNR.

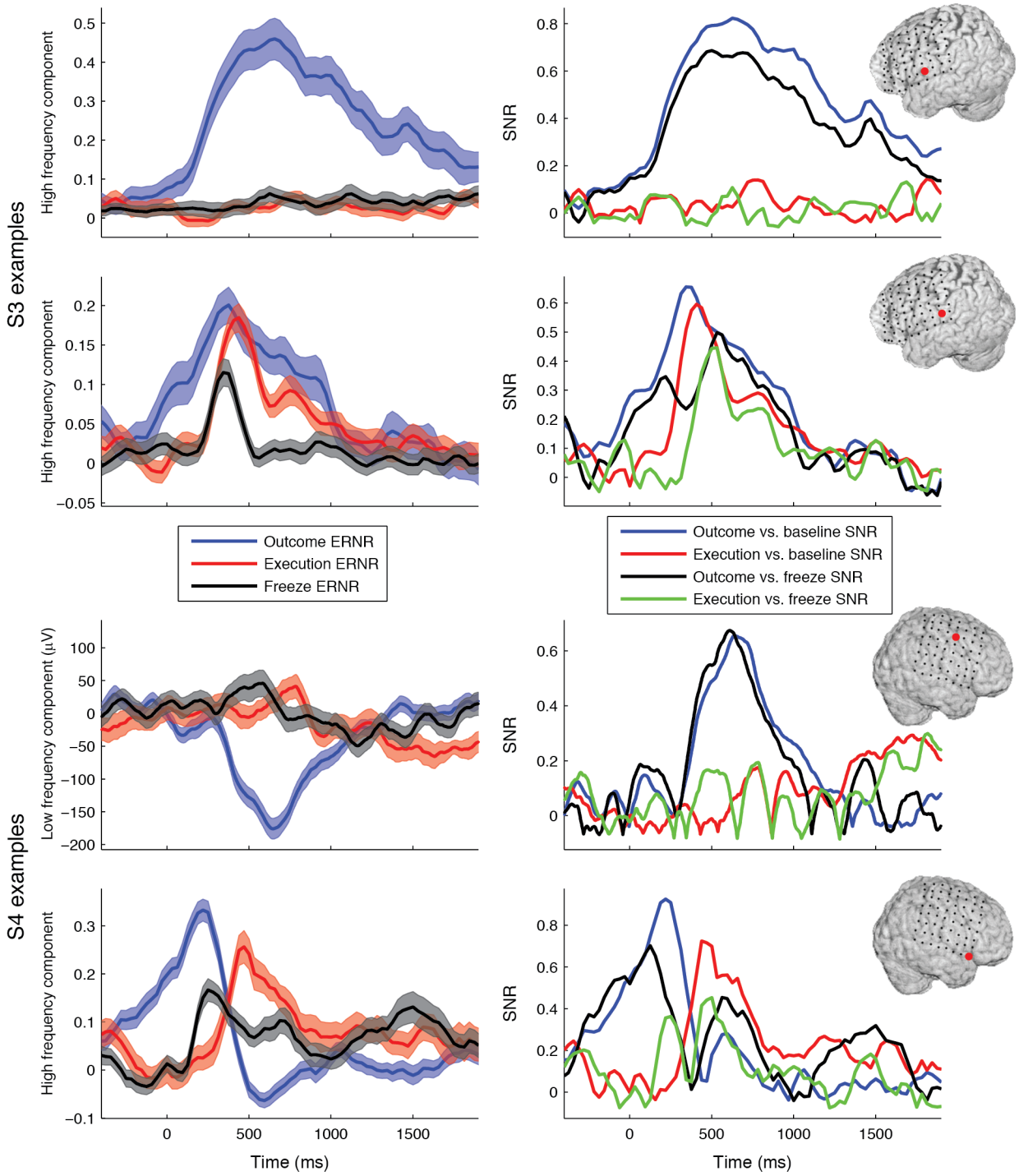

Figure 22 Example of two channels for S3 and two channels for S4 that could be used to detect both execution and outcome errors and differentiate between them. Channels selected as examples are shown as red dots on the depictions of the subjects' brains on the right side. Left panels show outcome ERNR (blue), execution ERNR (red) and freeze neuronal response (black) as mean ± sem. Right panels show outcome vs. baseline SNR (blue), execution vs. baseline SNR (red), outcome vs. freeze SNR (black) and execution vs. freeze SNR (green). For S3 the channel shown in the top panel exhibited a strong outcome ERNR, while the channel in the bottom panel exhibited a strong outcome ERNR and a strong execution ERNR. In the case of S4 the channel in the top panel exhibited a strong outcome ERNR, while the channel in the bottom panels exhibited a strong outcome ERNR and a strong execution ERNR.

In addition, information from multiple channels and signal components can be used to improve the detection of outcome and execution errors and the discrimination between the two. Figure 23b

shows the distribution of the execution SNR against the outcome SNR of all channels/signal components for each of the subjects. Note that each of the subjects had several channels/signal components with both strong outcome SNR and strong execution SNR. On average, the outcome SNR was significantly higher than execution SNR for all subjects, except for S4 (S1 $p<10^{-17}$, S2 $p<10^{-18}$, S3 $p<10^{-3}$, S4 p=0.94, all subjects pooled $p<10^{-38}$, Mann–Whitney–Wilcoxon test). For every subject, at least one channel could be found with outcome SNR of 0.93 or higher (highest SNRs: S1: 1.26, S2: 1.18, S3: 1.02, S4: 0.93) and with execution SNR of 0.50 or higher (highest SNRs: S1: 0.54, S2: 0.84, S3: 0.63, S4: 0.50). Importantly, for each subject a large number of electrodes with high execution SNRs and/or high outcome SNRs could be found: on average, 68% of channels exhibited a significant ERNR for at least one signal component (average calculated over subjects and signal components). Interestingly, I found strong ERNRs in the low as well as in the high frequency component. For the outcome error, SNR of the low frequency component (0.36±0.01) had a tendency to be higher than the SNR of the high frequency component (0.35±0.01; p=0.054, Mann–Whitney–Wilcoxon test). In the case of the execution error, SNR of the low frequency component (0.207±0.005) was significantly higher than the SNR of the high frequency component (0.206±0.007; p<0.05, Mann–Whitney–Wilcoxon test).

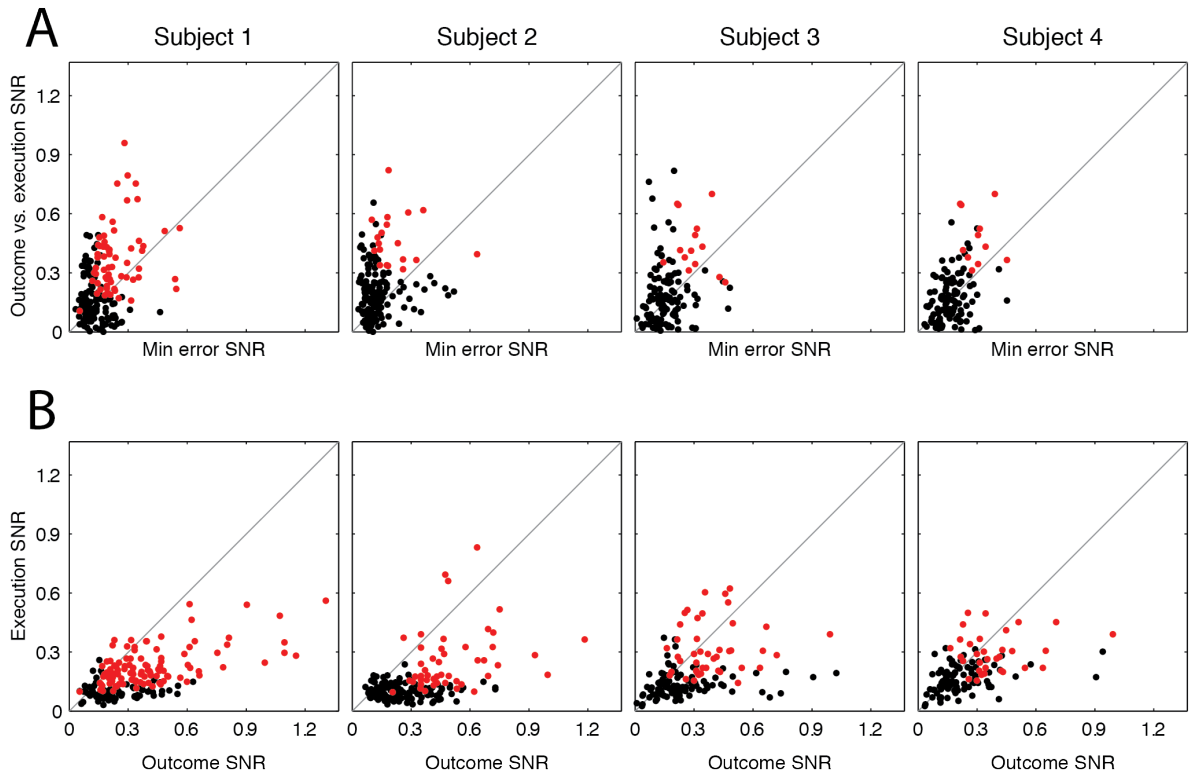

Figure 23 A, Scatter plot showing outcome vs. execution SNR against the minimum between outcome SNR and execution SNR (min error SNR). One dot represents one signal component of one channel. Red dots depict channels/signal components with a significant outcome, execution and outcome vs. execution SNR. B, Scatter plot showing execution SNR against outcome SNR. Red dots depict channels/signal components that had both significant outcome ERNR and execution ERNR.

Differences between outcome and execution ERNRs on the single channel and signal component were investigated by looking at the outcome vs. execution SNR. For every subject I found at least one channel and signal component that showed outcome vs. execution SNR of 0.70 or higher (maximum outcome vs. execution SNR: S1: 1.05, S2: 0.83, S3: 0.81, S4: 0.70).

I also investigated whether low and high frequency components from the same electrode contained independent information about errors. Figure 24 shows scatter plots of the low frequency component SNR vs. the high frequency components SNR of the same channel. For every subject one can find channels that are far from the diagonal, indicating that low and high frequency components can be used as partially independent sources of information for the purpose of ERNR detection and differentiation.

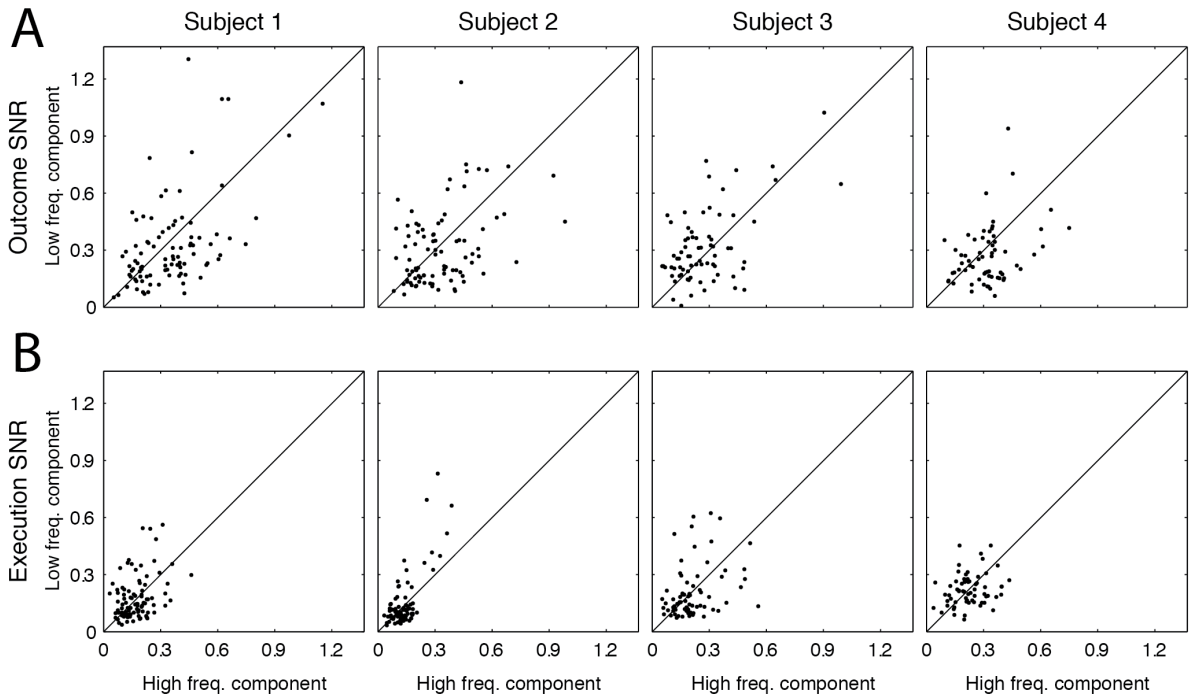

Figure 24 Scatter plot showing the low frequency component SNR against the high frequency component SNR. Results are shown separately for outcome ERNR (A) and for execution ERNR (B). One dot represents one channel.

3.3.4. Spatial distribution of ERNRs

Next, I investigated in which cortical areas ERNRs could be found (Figure 25). Electrodes were classified as motor, somatosensory or other using the ESM (described in Methods). For outcome error, 70% of the motor, 70% of the somatosensory and 60% of the electrodes from other areas showed a significant ERNR (Table 6). For execution errors, the proportions were: 50% for motor, 44% for somatosensory and 38% for other areas (Table 7). There were no significant differences in the proportions of the electrodes with significant ERNR between the motor and somatosensory areas for both error types ($p>0.47$, Fisher's exact test) and between somatosensory and other areas

(p>0.07, Fisher's exact test). Proportion of electrodes with significant ERNR was significantly higher for motor area compared to other areas for both error types (p<0.05, Fisher's exact test). For both error types, the average SNRs of electrodes showing significant responses (outcome error: motor SNR 0.46±0.02, somatosensory SNR 0.46±0.03, SNR of other areas 0.40±0.01; execution error: motor SNR 0.29±0.02, somatosensory SNR 0.28±0.02, SNR of other areas 0.24±0.01) was not significantly different (p>0.81, Mann–Whitney–Wilcoxon test) between motor and somatosensory areas for both error typesand was significantly higher for motor compared to other areas (p<0.05, Mann–Whitney–Wilcoxon test) and for somatosensory compared to other areas (p<0.05, Mann–Whitney–Wilcoxon test).

	Motor		Somatosensory		Other	
S1	93%	(41/44)	89%	(32/36)	85%	(88/104)
S2	50%	(3/6)	50%	(2/4)	52%	(87/166)
S3	61%	(22/36)	55%	(12/22)	44%	(38/86)
S4	45%	(10/22)	61%	(17/28)	58%	(45/78)
Pooled	70%	(76/108)	70%	(63/90)	59%	(258/434)

Table 6 Number and proportion of electrodes with significant outcome ERNR (see Methods for details of significance criteria). For each of the subjects, electrodes were pooled across two signal components (low and high frequency bands). In the bottom row, electrodes were additionally pooled across subjects.

	Motor		Somatosensory		Other	
S1	68%	(30/44)	72%	(26/36)	59%	(61/104)
S2	50%	(3/6)	50%	(2/4)	41%	(68/166)
S3	50%	(18/36)	41%	(9/22)	30%	(26/86)
S4	14%	(3/22)	11%	(3/28)	13%	(10/78)
Pooled	50%	(54/108)	44%	(40/90)	38%	(165/434)

Table 7 Number and proportion of electrodes with significant execution ERNR. See legend of Table 6 for details.

In motor (somatosensory) cortex outcome SNR was above 0.62 (0.65) while execution SNR was above 0.18 (0.18) for at least one electrode in each subject. S2 had a poor coverage of motor cortex with only 3 electrodes recording from that area (see Figure 15). Disregarding this subject increased the minimum SNR values to 0.62 (0.73) for outcome error and 0.40 (0.41) for execution error. Therefore, it was always possible to find electrodes with significant ERNR with SNR above 0.40 in motor cortex for both outcome and execution error if the electrode grid had a good coverage of the motor cortex.

In addition, I found outcome vs. execution SNR of 0.53 or higher for at least one channel and signal component in the motor cortex (S1: 1.05, S2: 0.65, S3:0.76, S4: 0.54) and 0.50 or higher for at least one channel and signal component in the somatosensory cortex (S1: 0.81, S2: 0.54, S3: 0.81, S4: 0.50) for every subject. Therefore, outcome and execution ERNRs in the motor cortex are not only

different from baseline, but one can also find electrodes where these ERNRs are different between each other.

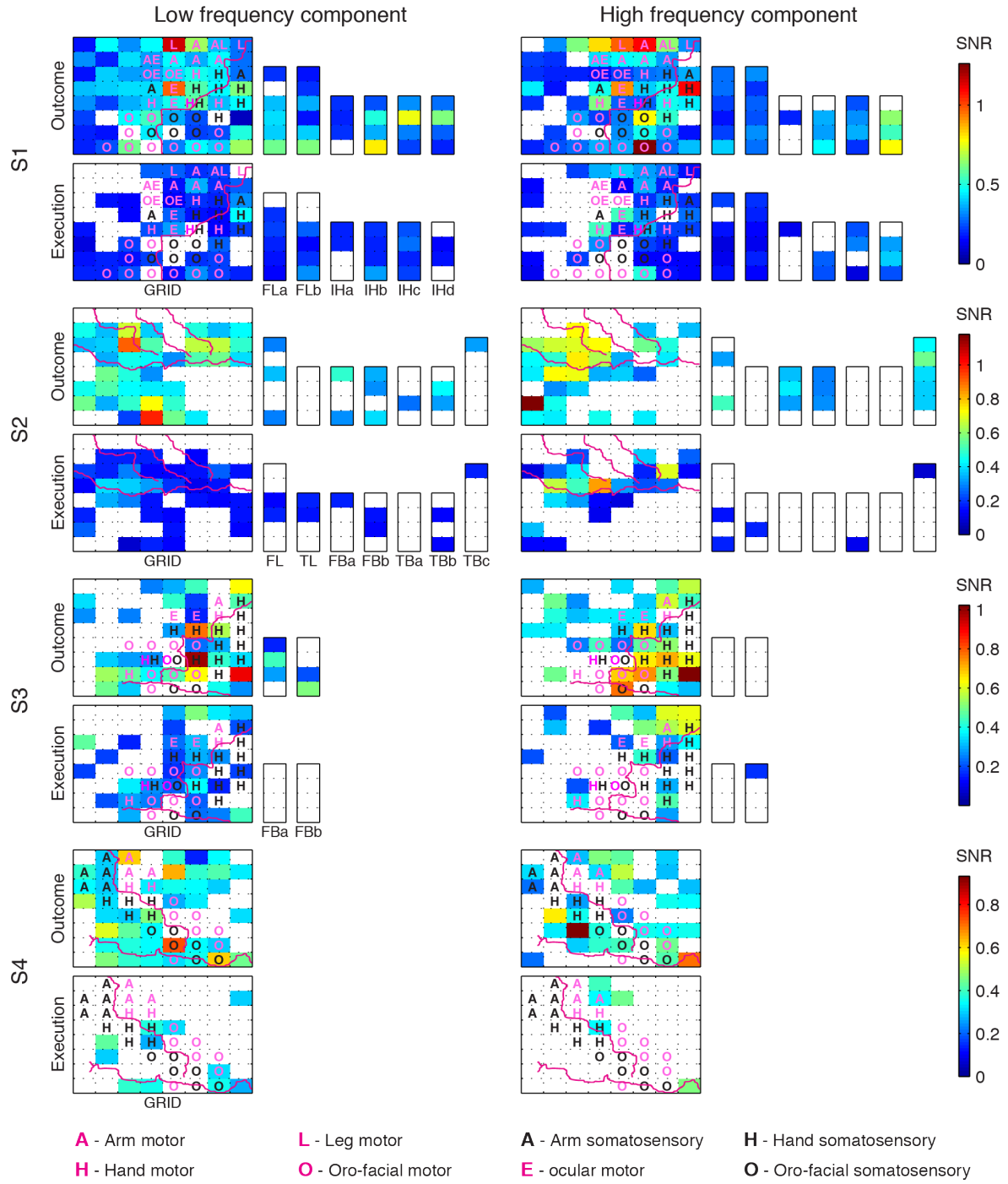

Figure 25 Spatial distribution of outcome SNR and execution SNR for low and high frequency components in relation to the individual anatomy of the subject (see caption of Figure 19 for details). Colours of the squares depict the SNR according to the colour bar; white squares represent channels/signal components that did not show a significant response.

I also compared the ERNR strength of different functional subareas of the motor and somatosensory cortex. To this end, the percentage of electrodes exhibiting a significant ERNR and the average SNRs of these electrodes were computed for the different subareas (Table 8 and Table 9). Responses were pooled over frequency components. Therefore, each electrode was counted twice. For motor and somatosensory cortex no significant differences in the SNRs or in the electrode proportions between the subareas were found; neither for outcome nor for execution error (Fisher's exact test to compare proportions; Mann–Whitney–Wilcoxon test to compare SNRs) after the correction for the multiple testing (Benjamini-Hochberg procedure with false discovery rate of 5%).

	Outcome error			Execution error		
	Percent	Count	SNR	Percent	Count	SNR
Hand	61%	(11/18)	0.42±0.12	61%	(11/18)	0.29±0.11
Arm	80%	(16/20)	0.50±0.19	60%	(12/20)	0.28±0.12
Ocular	93%	(13/14)	0.42±0.25	57%	(8/14)	0.29±0.12
Oro-facial	68%	(38/56)	0.40±0.20	38%	(21/56)	0.26±0.09
Leg	100%	(6/6)	0.63±0.36	83%	(5/6)	0.27±0.09

Table 8 Number, percentage and SNR (average ± standard deviation) of electrodes with significant responses, separately for electrodes recording from different subareas of motor cortex (see Methods for details of significance criteria). Anatomical information was gained from ESM (see Methods for details). Electrodes were pooled over subjects and frequency components.

	Outcome error			Execution error		
	Percent	Count	SNR	Percent	Count	SNR
Hand	72%	(36/50)	0.49±0.19	58%	(29/50)	0.33±0.13
Arm	79%	(11/14)	0.37±0.06	14%	(2/14)	0.27±0.08
Oro-facial	61%	(17/28)	0.44±0.18	25%	(7/28)	0.24±0.06

Table 9 Number, percentage and SNR (average ± standard deviation) of electrodes with significant responses, separately for electrodes recording from different subareas of somatosensory cortex. See legend of Table 8 for details.

3.3.5. Classification analysis

I investigated how well outcome or execution ERNRs can be differentiated from baseline activity on a single trial basis (see section 3.2.4. for methodological details). Signals from single electrodes were already information-rich enough to obtain high classification accuracies (Figure 26). For each subject and both errors at least one electrode existed which yielded an accuracy of 80% or higher (outcome error: S1: 0.85, S2: 0.91, S3:0.85, S4: 0.80; execution error: S1: 0.88, S2: 0.86, S3: 0.83, S4: 0.88; Figure 26). When signals from all motor electrodes were used, decoding accuracy remained high, 77% or higher, except for execution ERNRs for S2 (outcome error: S1: 0.97, S2: 0.79, S3:0.79, S4: 0.86; execution error: S1: 0.77, S2: 0.60, S3: 0.92, S4: 0.80).

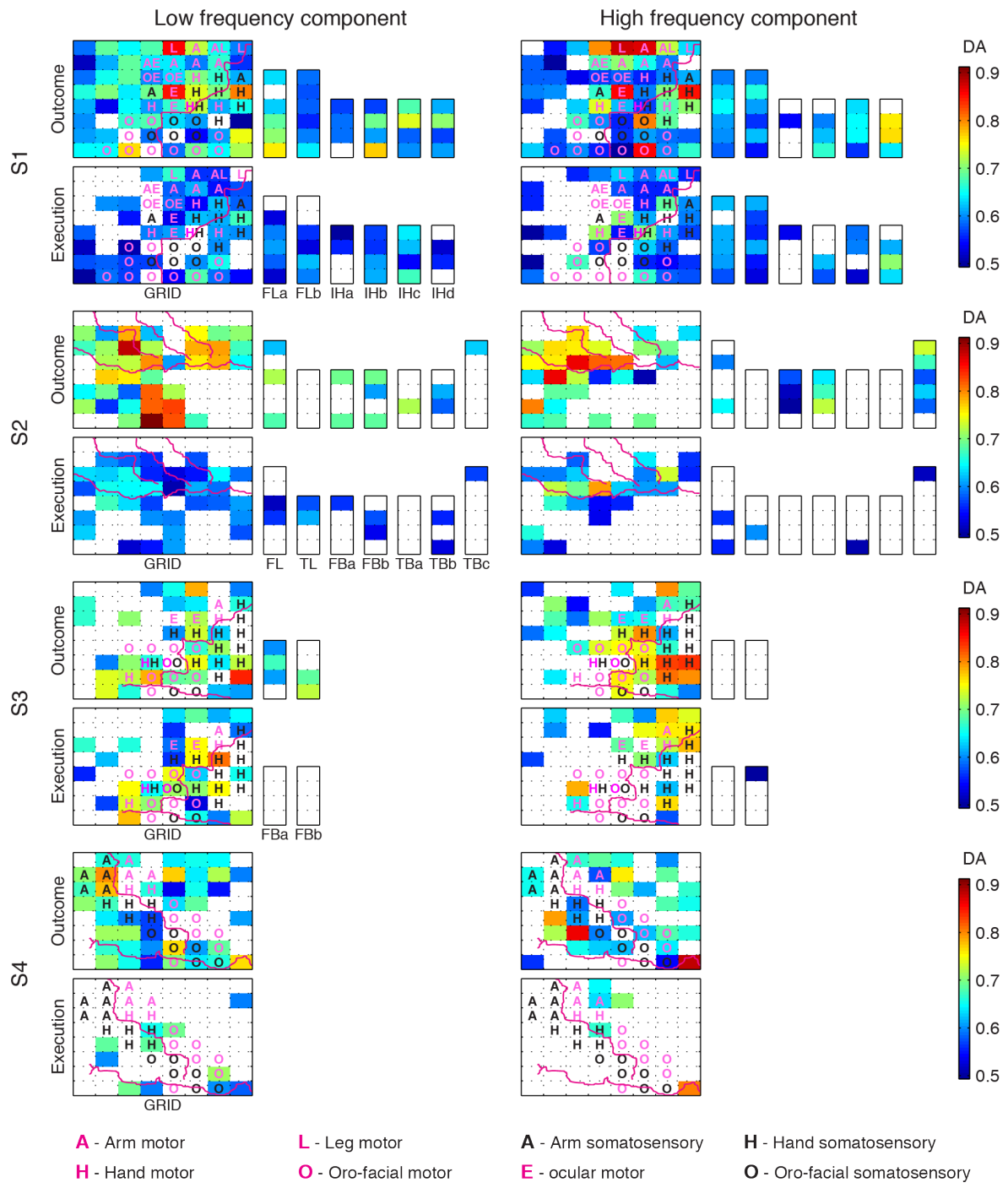

Figure 26 Spatial distribution of DA of classifying outcome SNR against baseline and execution SNR against baseline for low and high frequency components in relation to the individual anatomy of the subject (see caption of Figure 19 for details). Colours of the squares depict the DA according to the colour bar.

Next, I classified outcome vs. execution ERNR on a single-trial basis (see section 3.2.4. for methodological details). Again, high classification accuracies could be obtained with signals from single electrodes (Figure 27), where for each subject at least one electrode yielded an accuracy of 83% or higher (S1: 0.87, S2: 0.88, S3:0.83, S4: 0.85; Figure 27). When signals from all motor

electrodes were used, decoding accuracy remained high, at 76% or higher (S1: 0.97, S2: 0.76, S3:0.83, S4: 0.80).

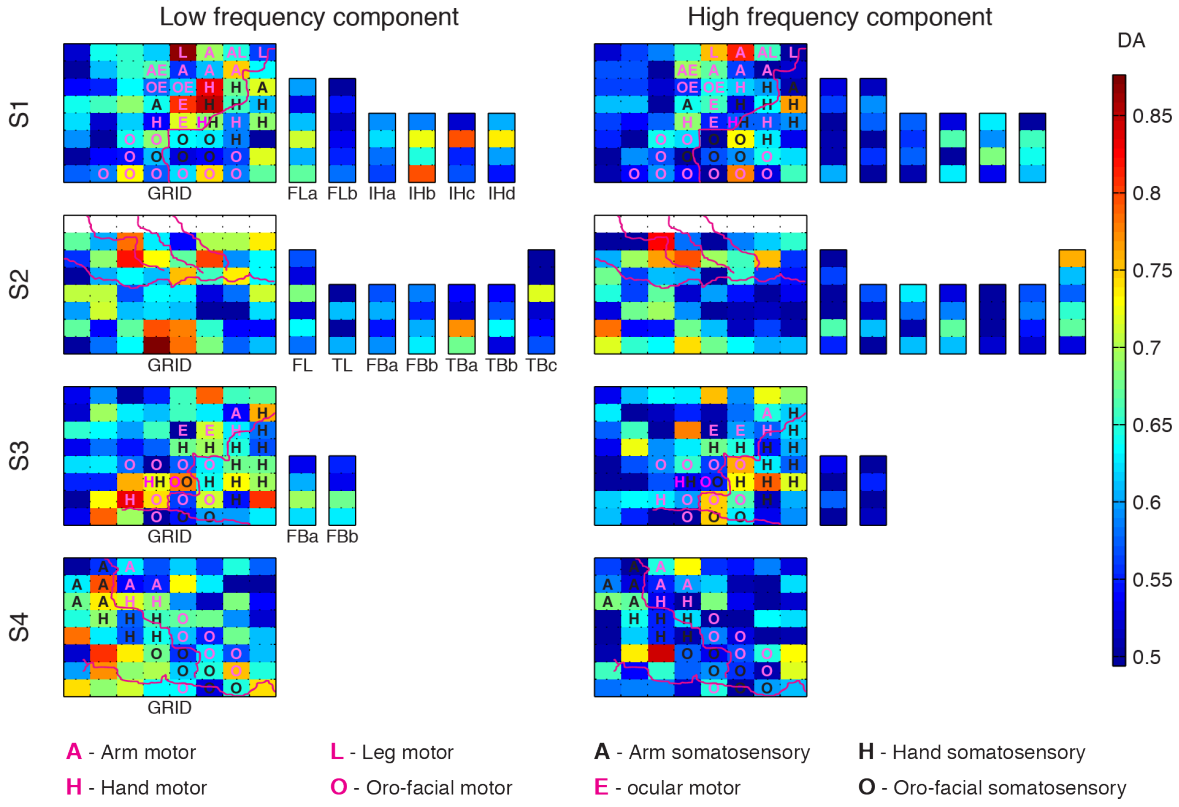

Figure 27 Spatial distribution of DA of classifying outcome SNR against execution SNR for low and high frequency components in relation to the individual anatomy of the subject (see caption of Figure 19 for details). Colours of the squares depict the DA according to the colour bar.

3.4. Discussion

In this chapter, I showed that neural correlates of outcome and execution errors can be found in ECoG recordings from the motor, somatosensory, parietal, temporal and pre-frontal cortex. For each subject, I found electrodes whose signals can be used to differentiate outcome and execution errors from the baseline activity and to differentiate between the two error types.

I observed neuronal responses to errors both in the low pass filtered ECoG signal and in the high gamma activity. ERNRs in low pass filtered signals have been found before in a large number of EEG (for review see Bechtereva et al., 2005; Jocham and Ullsperger, 2009; van Veen and Carter, 2006) and MEG (Koelewijn et al., 2008) studies. Jung et al. (Jung et al., 2010) discovered ERNRs in high frequency activity. In that study intracortical stereoencephalography (SEEG) was used, method that measures field potentials in the cortex, in contrast to the recording method used here (ECoG) which records field potentials from the cortical surface.

In addition, I showed that the low and high frequency signal components of the same electrode can carry partially independent information about the errors, as for many electrodes only one of the components showed a strong response to one of the errors, while the other component did not. Therefore, low and high frequency components of the ERNR might be used in conjunction for error detection and discrimination. Moreover, I observed a wide distribution of error response strength across different cortical areas. For both error types, there was at least one electrode per subject yielding a high SNR (0.93 or higher for outcome error and 0.50 or higher for execution error) and more than half of the recorded electrodes exhibited a significant ERNR. In addition, decoding analysis revealed that, based on signals from single electrodes, one can decode outcome or execution ERNR from the baseline activity at the level of 80% or higher. This implies widespread neuronal responses to error events. However, not all responses were specific to only one type of error. Reconstruction of the electrode locations demonstrated that, for every subject and for both error types, at least one electrode exhibited a strong (SNR>0.40) ERNR over the motor cortex. Furthermore, decoding outcome or execution ERNR from the baseline activity, using only channels over the motor cortex, was possible with DA of 77%. An exception was the execution error for S2 where, due to the placement of the implant and more conservative electrode selection criteria, only 3 electrodes were located over the motor cortex and a DA of only 60% was reached. An implant position similar to those of other subjects would have provided more electrodes over the motor cortex and, thus, might have provided recordings of more informative signals.

I also investigated the differences between outcome and execution ERNRs. For every subject, it was possible to find an electrode with outcome vs. execution SNR of 0.53 or higher. In addition, for every subject, outcome and execution ERNRs could be decoded with DA of at least 76%. If S2, who had a poor coverage of motor cortex, is excluded, each subject had a channel with DA of 80% or above. These results show that it is possible to decode outcome and execution ERNRs between each other and against baseline activity.

Screen freeze events were used as a control for specific visual stimuli in the case of outcome ERNR and as a control for the surprise in the case of execution ERNR. This control was not present for the first two subjects. Thus, one might speculate that outcome and execution average SNR for the first two subjects would not be as high, had the freeze event been included as a control event, as it was for the last two subjects. This was, however, not the case: for the outcome error no significant differences were found between the average SNRs (first two subjects: average SNR 0.48 ± 0.04, last two subjects: average SNR 0.43 ± 0.03, $p=0.41$, Mann–Whitney–Wilcoxon test). In the case of execution error the average SNR of the last two subjects was even significantly higher than for the first two subjects (first two subjects: average SNR 0.26 ± 0.02, last two subjects: average SNR

0.34±0.03, p<0.01, Mann–Whitney–Wilcoxon test). Therefore, I conclude that (1) including the freeze event control improved the sensitivity of ERNR detection and (2) that the SNRs of outcome and execution error of the first two subjects were representative as well, even though the freeze control was missing.

3.4.1. Spectro-temporal characteristics of neuronal error responses

Following an error event, one can observe stereotypical spectral responses in which the amplitude in very low frequencies (0-4 Hz) and in high gamma frequencies (above 40Hz) is increased in relation to the baseline (Figure 18). I found that changes in the low frequencies can better be described using the low pass filtered signal, since in that case phase information is included as well. The high gamma response was present in a wide frequency band where amplitudes changed across many frequencies homogeneously. Therefore, computing the average amplitudes over these frequencies yields a less noisy response. I chose a frequency band from 60 Hz to 200 Hz because this band exhibited a common behaviour across subjects, channels and error events (Figure 17). For subjects S1 and S2 the upper boundary of the high frequency band was limited to 128 Hz due to the sampling frequency of the recording amplifier.

Jung et al. (Jung et al., 2010) studied intracortical SEEG signals in a reaction time task where negative feedback was given if timing requirements were not met. They reported high gamma neuronal responses with spectro-temporal characteristics similar to the ones I found in response to outcome and execution errors during my continuous control task. Even though task and recording method were both different, neuronal responses are, in essence, error event neuronal responses and could, therefore, be related.

On the other hand, neuronal responses to non-error events can also exhibit similar spectro-temporal characteristics: onset of arm movements (Ball et al., 2009b), self paced individual finger movements (Kubanek et al., 2009; Miller et al., 2009; Wang et al., 2009), thumb button press (Crone et al., 2006), hand movements (Leuthardt et al., 2004; Wisneski et al., 2008), tongue, fist and foot isometric contraction (Crone et al., 1998a; Crone et al., 1998b), onset of auditory stimuli (Boatman-Reich et al., 2010; Crone et al., 2001; Ray et al., 2008), tactile stimulus (Ray et al., 2008), face recognition (Lachaux et al., 2003), attention and short term memory (Jensen et al., 2007), mental calculation (Vansteensel et al., 2010) and word recognition (Jerbi et al., 2009). To test how well ERNRs can be differentiated from all such non-error events, further ECoG experiments with freely behaving subjects, where ERNRs can be compared to neuronal responses to other events, have to eventually be conducted. Such differentiation may be possible as ERNRs could be evoked on different electrodes and exhibit different time courses compared to neural responses to non-error events.

This is supported by my finding of different ERNRs to different types of errors (outcome and execution) and by different responses to different non-error events in some of the before mentioned studies (Ball et al., 2009b; Boatman-Reich et al., 2010; Wang et al., 2009).

3.4.2. Comparison to previous ERNR studies and widespread ERNR

ERNR have previously been reported over motor cortex in the low frequency range (0-4Hz; van Schie et al., 2004) using EEG recordings and in the beta (15-23Hz) range (Koelewijn et al., 2008) using MEG recordings. In addition, increased brain activation correlated to execution errors has been reported in the motor cortex using fMRI (Diedrichsen et al., 2005). In line with these studies, I found strong outcome and execution ERNR in both low and high frequency components of the signal. To the best of my knowledge, this study is the first showing high gamma ERNRs in the motor cortex.

Increased fMRI activation correlated to execution errors has also been reported in the somatosensory cortex (Diedrichsen et al., 2005). I showed that correlates of execution errors and, moreover, outcome errors are present in electrophysiological signals from somatosensory cortex both in low and high frequency signal components.

Besides in motor and somatosensory cortex, I also found widespread ERNRs to outcome and execution errors in other brain areas, including frontal, parietal and temporal cortex. This is consistent with previous studies. Increased fMRI activation in response to negative feedback was found in dorsolateral pre-frontal cortex (Jung et al., 2010; Zanolie et al., 2008), medial pre-frontal cortex (Ullsperger and von Cramon, 2003; Zanolie et al., 2008), orbito-frontal cortex (Jung et al., 2010; Walton et al., 2004; Zanolie et al., 2008), pre-suplementary motor area (Jung et al., 2010) and insula (Jung et al., 2010; Zanolie et al., 2008). Diedrichsen et al. (Diedrichsen et al., 2005) found fMRI activations in response to execution errors in multiple parietal areas. In the lateral temporal cortex, responses to errors in identification and memory tasks were found in single-unit activity (Ojemann, 2003; Ojemann et al., 2004). Task used in my study did not have any identification or memory component but it is possible that there are areas in the temporal lobe responsive to errors in general.

Most of the earlier ERNR studies concentrated on the activation of anterior cingulate cortex (ACC) and its functional meaning (for review see Bechtereva et al., 2005; Jocham and Ullsperger, 2009; van Veen and Carter, 2006). In only one of out of four subjects, 2 electrodes were implanted in the vicinity of the ACC. Therefore, I did not investigate the activation of ACC. Involvement of ACC in error processing during continuous tasks deserves further clarification by future studies.

I measured the strength of ERNRs of different cortical areas (motor, somatosensory and pooled data from all other areas) by computing the proportion of electrodes exhibiting significant ERNR and the

average SNR of these electrodes. My results show that, for both error types, the proportion of channels with a significant ERNRs and their response strength (as quantified by SNR) is not different between motor and somatosensory cortex. Compared to all other cortical areas that were investigated, the response strength of motor cortical ERNRs is significantly higher. By further evaluating ERNRs in different functional subareas of the motor and the somatosensory cortex, I showed that significant ERNRs were present in different functional subareas that I recorded from (hand, arm, ocular, oro-facial). I also found significant ERNRs in the leg area of the motor cortex. As the leg electrodes were in immediate vicinity of arm electrodes this finding might be explained by ERNRs originating in the arm area and being also picked up on leg electrodes due to spatial spread of the electrical signals. Furthermore, ERNRs on leg motor electrodes were found only in one subject. This makes the statistics of the ERNR activity in the leg motor area much more unreliable than the statistics for the other subareas, where electrodes were available from several patients. Within motor cortex, all functional subareas exhibited the same response strength to outcome errors. For execution errors the response strength was also not different among different motor cortical subareas. The same result was found for the functional subareas of the somatosensory cortex.

One might suspect that some of these ERNRs were caused by movements correlated with error events and, thus, did not directly reflect error-related neuronal responses. To distinguish ERNRs from movement-related responses, I subtracted responses evoked by eye and thumb movements using the best out of linear and non-linear models relating ECoG signals to these movements (see Methods). Therefore, I conclude that these movements cannot explain the ERNRs I observed.

On the other hand, due to technical and clinical limitations, movements of other parts of the body or the respective muscle activations could not be tracked. Even though such movements did not play a role for the task and, thus, there is no a priori reason to expect these movements to be correlated with error events, I cannot completely disprove that parts of the observed neuronal error signals were confounded by such movements.

3.4.3. Relevance for brain machine interfaces

One motivation for this study was to investigate whether ERNRs can be used to improve the performance of continuous movement BMIs (Carmena et al., 2003; Hochberg et al., 2006; Kim et al., 2008; McFarland and Wolpaw, 2005; Serruya et al., 2002; Taylor et al., 2002; Velliste et al., 2008). Study presented in this Chapter provides a significant first step in this direction, showing that strong error-related neuronal responses could be found in ECoG recordings during a continuous control paradigm which mimicked a continuous BMI control task. In addition, I demonstrated that it is possible to differentiate between execution (Diedrichsen et al., 2005) and outcome (Krigolson et al.,

2008) errors. These two types of errors provide independent sources of information. Moreover, both of them can be used to improve the performance of the BMI in different ways. An outcome error can be used to correct an error after it has been made (Blankertz et al., 2003; Buttfield et al., 2006; Ferrez and del R Millan, 2008; Parra et al., 2003) and as a critic for a reinforcement learning adaptive algorithm (DiGiovanna et al., 2009). An execution error, on the other hand, can be used as a direct indicator of when the decoded trajectory was decoded improperly, thereby providing useful information for adaptive decoding algorithms (Rotermund et al., 2006).

Motor cortex is one of the primary target areas for the implantation of electrodes for invasive BMIs. I showed that strong ERNRs for both error types can be found in motor cortical signals. Therefore, movement decoding and error detection may be implemented using the same electrode implants. Consequently, no additional implants over other cortical areas would be required for BMIs employing such neuronal error signals. This would substantially reduce the burden of implantation for such BMIs.

Chapter 4

Detection of ERNRs recorded by ECoG in humans during continuous movements

Summary. Brain-machine interfaces (BMIs) can translate user's movement intentions into movements of an artificial effector, using user's neuronal activity only. In spite of continuous advancement of BMI systems, errors in movement decoding are still present. If the difference between decoded and intended movements becomes noticeable, it leads to execution error. Outcome errors, where subjects fail to perform a certain movement goal, are also present during online BMI operation. Detecting such errors can be beneficial for BMI operation: (i) errors can be corrected online after being made and (ii) BMI decoding algorithm can be updated to make less errors in the future. Here, I show that error events can be detected from human ECoG during continuous tasks with high precision, given a temporal tolerance of 300-400 milliseconds. I quantified the detection accuracy and showed that, using only a small set of 2x2 ECoG electrodes, 82% of detection information for outcome error and 74% of detection information for execution error available from all ECoG electrodes can be retained. Using a smaller electrode implant for detection could significantly reduce the medical risk of implantation.

4.1. Introduction

Even though the control of prosthetic devices using brain-machine interfaces (BMIs) has highly improved during the last several years (Kim et al., 2008; Koyama et al., 2010; Velliste et al., 2008), such devices are still prone to decoding errors. Decoding errors can elicit error related neuronal responses (ERNRs). Detecting these errors can be beneficial for the BMI performance. If detected, errors can be subsequently corrected, recognizing that a certain effector movement was not intended. This strategy has already been implemented in on-line BMI studies (Blankertz et al., 2003; Parra et al., 2003; Schalk et al., 2000), but only in externally paced BMIs. However, many powerful BMIs are used to continuously decode and control the movements of the effector. Most prominent examples are the BMI control of a prosthetic arm (Serruya et al., 2002; Taylor et al., 2002; Hochberg et al., 2006) and the brain control of a computer cursor (Carmena et al., 2003; Hochberg et al., 2006; Velliste et al., 2008).

Error detection can also be used to modify the decoding algorithm to make less decoding errors in the future. This approach is far more suitable for BMIs decoding continuous movements, since subjects correct for movement discrepancy by producing corrective movements, thereby making subsequent error correction outdated. Feasibility of this strategy has been demonstrated only by computer simulations (Blumberg et al., 2007; Rotermund et al., 2006).

To apply error detection to continuous BMI control, it is necessary to show that errors are indeed elicited during such tasks. A number of studies looked at errors during continuous movement tasks, identifying neuronal activity elicited to three different error types: (i) target error (Diedrichsen et al., 2005), elicited when task environment goes through unexpected changes such as target jumps, (ii) execution error (Diedrichsen et al., 2005), elicited when the ongoing motor commands result in an unexpected movement, and (iii) outcome error (Krigolson et al., 2008), elicited when the desired goal of a movement is not achieved. Outcome and execution errors are of special interest for BMI application, since both error events can occur during the online BMI control. For example, execution error can occur when the decoding algorithm decodes incorrect movements, thereby moving the cursor or the prosthesis in an undesirable direction (Figure 13). If the difference of intended and executed movements is large enough, it can evoke an execution ERNR. If the incorrectly decoded movement causes the effector to reach an unintended goal or perform an unintended function, this can elicit an outcome ERNR (Figure 13).

In recent years, electrocorticography (ECoG) emerged as a possible alternative to intracortical recordings as a recording technique that can be used for a continuous BMI (Moran, 2010; Schalk, 2010; Schalk and Leuthardt, 2011). Continuous BMI controlling two degrees of freedom has already

been realized using ECoG (Schalk et al., 2008). Other recent studies shown that many other movements primitives can be decoded offline from ECoG signals, such as 7 degrees of freedom of the arm movements (Chao et al., 2010), individual finger movements (Kubanek et al., 2009) and natural grasps (Pistohl et al., 2012). Therefore, ECoG is a suitable platform for implementing a continuous BMI.

To use error signals in a ECoG based BMI, one needs to show that ERNRs can be detected from the ECoG signal with sufficient reliability. In Chapter 3, I showed that both outcome and execution ERNR are present in human ECoG recordings during a continuous task. In this Chapter, I show that times of the events that elicited these ERNR can indeed be detected with high accuracy.

4.2. Methods

Experimental task, recording technique, properties of the recoded data, movement related neuronal response subtraction method and neuroanatomical procedures used to divide ECoG electrodes into anatomical subsets are described in details in Chapter 3. In this Chapter, I analyzed the recordings from the 8 x 8 grid of subdural surface electrodes only.

4.2.1. Measures of detection accuracy

One can imagine a process where a subject is actively observing and, when a given stimulus appears, a neuronal response is elicited. Neuronal activity is continuously recorded and a detection algorithm is continuously estimating whether a stimulus appeared, given the neuronal activity. Efficiency of a detector can then be measured by comparing two point processes, set of time points when the stimulus was presented and a set of time points when the detector detected the stimulus from the neuronal recordings.

Due to the internal processes in the brain and other sources of noise, even the perfect decoder will have a temporal noise in the detected times of events. On the other hand, detected event will still be useful if the times of detections are not perfectly aligned to the times of the events. For some applications, high temporal precision is not necessary. I describe this requirement on a detector as temporal tolerance.

If detected events are tolerated within the time Δt from the real events, than any detection within this time window will be counted as a true positive detection. Every event window in which there are no detected events will be counted as false negative detection. To measuring the detection accuracy, it is also necessary to know the ability of the detector at predicting non-events. To get a fair estimate of such ability, the area between the event time windows has to be divided in the windows of the same size, $2\Delta t$. Every non-event time window in which there are no detected events

will be counted as a true negative detection and every non-event time window in which there is a detected event will be counted as false positive detection.

Sensitivity and specificity of a detector

Accuracy of a detector can be described by measuring how well it performs in two different tasks: (i) detecting events when events are present and (ii) not detecting events when events are not present. One way to describe the first property is by measuring the sensitivity of the detector by calculating the true positive ratio (TPR; Solis-Escalante et al., 2008) as a number of true positive detections (N_{TP}) divided by the total number of real events. Since the total number of real events is given by the sum of true positive detections and false negative detections (N_{FN}), true positive ratio is given by:

$$TPR = \frac{N_{TP}}{N_{TP} + N_{FN}} \tag{4.1}$$

The second property can be described by measuring the specificity of the decoder by calculating the false positive ratio (FPR; Solis-Escalante et al., 2008) as the ratio of false positive detections (N_{FP}) divided by the number of all detections. Since the total number of all detections is given by the sum of true positive detections and false positive detections (N_{FP}), false positive ratio is given by:

$$FPR = \frac{N_{FP}}{N_{TP} + N_{FP}} \tag{4.2}$$

Disadvantage of measuring the detection accuracy by TPR and FPR is that one cannot directly compare two different detectors where both TPR and FPR of one detector is higher than the TPR and FPR of another detector. Therefore, a metric incorporating both sensitivity and specificity of the detector is needed. One such metric is the mutual information.

Mutual information of a detector

One way to measure the performance of a detector is to calculate the mutual information between a dataset containing times of real events and a dataset containing times of detected events. Mutual information is given by:

$$I(X,Y) = -\sum_{X}\sum_{Y} p(x,y)\log_2\left(\frac{p(x,y)}{p(x)\,p(y)}\right) \tag{4.3}$$

where X and Y are the sets of all possible states of the real and detected events datasets and x and y are specific states from those sets, $p(x)$ and $p(y)$ are the probabilities of specific states and $p(x,y)$ is the joint probability that states x and y happen at the same instance. In my case, set of real event states consists of "real event" (*re*) and "real non-event" (*rne*), while the set of detected events

consists of “detected event” (*de*) and “detected non-event” (*dne*). Joint and marginal probabilities used to calculate the mutual information are given by:

$$\begin{aligned} p(re,de) &= \frac{N_{TP}}{N} \qquad p(re,dne) = \frac{N_{FN}}{N} \qquad p(re) = \frac{N_{TP}+N_{FN}}{N} \\ p(rne,de) &= \frac{N_{FP}}{N} \qquad p(rne,dne) = \frac{N_{TN}}{N} \qquad p(rne) = \frac{N_{FP}+N_{TN}}{N} \\ p(de) &= \frac{N_{TP}+N_{FP}}{N} \qquad p(dne) = \frac{N_{FN}+N_{TN}}{N} \end{aligned} \tag{4.4}$$

Given a certain dataset of real event times and certain tolerance, maximum value of the mutual information is obtained when detected event times perfectly match real event times. This value is identical to the entropy of real event times $H(X)$:

$$H(X) = -\sum_{X} p(x)\log_2\left(p(x)\right) \tag{4.5}$$

To compare the mutual information over different tolerances, I calculated the normalized mutual information, C_{YX}:

$$C_{YX} = \frac{I(X,Y)}{H(X)} \tag{4.6}$$

Calculating mutual information and entropy from a recorded dataset will give a good estimate of their true values, as long as the calculated probabilities are good estimates of the real probabilities. However, recorded datasets have a finite length, which will make the estimated probabilities fluctuate around their real values. Using the estimated probabilities to calculate the mutual information and entropy leads to a bias in the estimation (Treves and Panzeri, 1995). To remove the bias of the mutual information, I used the first and the second order of the mutual information bias expansion derived in the study by Treves and Panzeri (Treves and Panzeri, 1995):

$$I(X,Y) = I_N(X,Y) - I_1^C - I_2^C \tag{4.7}$$

$$I_1^C = \frac{1}{2N\ln 2} \tag{4.8}$$

$$I_2^C = \frac{1}{12N^2\ln 2}\left[\sum_X\sum_Y\left(\frac{1}{p(x,y)}-\frac{1}{p(x)}\right)-\sum_Y\frac{1}{p(y)}+1\right] \tag{4.9}$$

where $I_N(X,Y)$ is the mutual information estimated from a dataset of length N. Here, the values of joint and marginal distributions have also been estimated from the same dataset. To remove the bias of the entropy, I used the first and the second order of the entropy bias expansion derived in the study by Victor (Victor, 2000):

$$H(X) = H_N(X) + H_1^C + H_2^C \tag{4.10}$$

$$H_1^C = \frac{1}{2N\ln 2} \tag{4.11}$$

$$H_2^C = \frac{1}{12N(N+1)\ln 2}\left(\sum_X \frac{1}{p(x)} - 1\right) \tag{4.12}$$

Therefore, the bias corrected value of the normalized mutual information was calculated as:

$$C_{YX} = \frac{I_N(X,Y) - I_1^C - I_2^C}{H_N(X) + H_1^C + H_2^C} \tag{4.13}$$

4.2.2. Signal components

I analyzed the low and high frequency components of the recorded ECoG signals. Low frequency component was extracted by smoothing the preprocessed ECoG signals using a symmetric 2nd order Savitzky-Golay filter (Savitzky and Golay, 1964; Steinier et al., 1972) with a time window of 250ms (nominal 3dB cut off frequency: 7.85Hz for S1 and S2, 7.59Hz for S3 and S4; estimated using table from Schafer, 2011). I defined a window around each event of any kind, starting 3 seconds before each event and lasting until 3 seconds after each event. The signals outside all of these windows were used as baseline activity. To enable a clear comparison to baseline, the average baseline activity was subtracted from the filtered recordings in each session for each electrode. The resulting signal was defined as the low frequency component of the signal (LFC).

To analyze the high frequency component of the signal, time-resolved Fourier transformation using a Hamming window (333ms window width, shifted in steps of 31ms) was applied to the preprocessed signals, and the amplitudes were used for further analysis. To account for the general decrease in amplitude with increasing frequency, the amplitudes of every frequency bin were normalized by dividing them by the average baseline amplitude of the same frequency bin in the respective session. I then extracted the average amplitude across a frequency band from 60Hz to 128Hz for S1 and S2 (Nyquist frequency 128Hz) and from 60Hz to 200Hz for S3 and S4 (Nyquist frequency 512Hz). Amplitudes calculated from ECoG signals recorded at least 3 seconds from any event were labelled as baseline. To enable a clear comparison to baseline, the average baseline activity was subtracted from the extracted amplitudes in each session for each electrode. The resulting signal was defined as the high frequency component of the signal (HFC).

Due to different scaling, when LFC and HFC were used together for detection, I normalized every electrode and signal component to zero mean and unit variance.

4.2.3. Detection algorithm

To detect error events from the neural activity, I derived a set of models that tried to capture the features of the ERNRs. To be sure that these features are captured from ERNRs that are not mixed with neural responses to other events, I used ERNRs elicited by "clean" events only. Each model could be described by an array of time points (t_1, ..., t_n) in relation to the collision or movement mismatch events. Array of time points was defined by a set of parameters: (i) a time of the first feature in relation to the error event, t_1, (ii) a number of features, n and (iii) a time distance between the first and the last feature, t_n-t_1. Therefore, neuronal response in every trial and every electrode in one of the signal components was represented by a vector of features. I labelled the extracted feature vectors as "positive" class. All the features vectors extracted using the same array of time points, but this time shifted in time, were labelled as "negative" class.

$$\begin{aligned} P_{class} &= \left\{ \left(signal_{ch(1)}\left(t_{E_i}+t_1\right),...,signal_{ch(m)}\left(t_{E_i}+t_n\right)\right), i \in 1:N \right\} \\ N_{class} &= \left\{ \left(signal_{ch(1)}\left(t_{E_i}+t_1+k\cdot\delta t\right),...,signal_{ch(m)}\left(t_{E_i}+t_n+k\cdot\delta t\right)\right), i \in 1:N, k \neq 0 \right\} \end{aligned} \tag{4.14}$$

where δt is the time resolution of the signal component (LFC: 4ms for S1 and S2, 1ms for S3 and S4; 31ms when HFC or both components were used) and *ch(1), ..., ch(m)* is a list of electrodes/frequency components used in the feature extraction. These classes were used to build either a regularized linear discriminant analysis (rLDA) model or a regularized quadratic discriminant analysis (rQDA) model (Friedman, 1989). QDA model is built by fitting a Gaussian distribution to each of the classes and gives the probability to belong to one of the classes for any arbitrary point in the feature space. Each Gaussian is represented by a class mean and a covariance matrix. LDA is a simplification of QDA, where only fitted Gaussian distributions share a common covariance matrix. Regularization is implemented by modifying the covariance matrix of the fitted Gaussian distributions and has the purpose to improve the accuracy of the discriminant analyses on a new, independent set of data. I used the regularization of the form:

$$C_R = \left(1-\gamma\right)C + \gamma \cdot \left\langle diag\left(C\right)\right\rangle \cdot I \tag{4.15}$$

where C is the covariance matrix of the fitted Gaussian distribution, C_R is the regularized covariance matrix, γ is the covariance coefficient and I is the identity matrix of the same size as C. In the case of rQDA, the number of vectors in the negative class is much higher than the number of vectors in the positive class. Therefore, I regularized the covariance matrix of the Gaussian fitted to the positive class only. Model was then used to calculate the probability of every feature vector F in the testing dataset to belong to the positive class.

$$F\left(t_F\right)=\left\{\left(signal_{ch(1)}\left(t_F+t_1\right),...,signal_{ch(m)}\left(t_F+t_n\right)\right),\frac{t_F}{\delta t}\in\mathbb{Z}:-t_1\le t_F\le t_{end}-t_n\right\} \quad (4.16)$$

where t_F is time point corresponding to the calculated probability and t_{end} is the time length of the tested dataset. I then extracted all local maxima of the probabilities and assigned a '*dne*' state to remaining points. Threshold value was then selected and I assigned a '*dne*' state to all time points for which the value of the maxima was below the threshold. Finally, I assigned a '*dne*' state to all remaining maxima points for which there was a higher maximum point within the neighbourhood of 1 second. I assigned a '*de*' state to all remaining maxima. Since the model should be able to detect error events whose ERNRs are only slightly mixed with neuronal responses to other events, I calculated the detection measures between the times of detected events and the times of all real events within the testing dataset, instead of just using the "clean" events.

To properly validate the models, I divided the recorded data into three similarly long parts by splitting each session into three parts, each containing one third of the "clean" events. First, I chose a set of parameter values consisting of: (i) a time of the first feature in relation to the error event, t_1, (ii) a number of features, n and (iii) a time distance between the first and the last feature, t_n-t_1, (iv) regularization coefficient, γ, and (v) probability threshold. rLDA or rQDA model was then built using the first part of the dataset. Using the build model, I detected the events on the second part of the data and calculated the C_{YX}. Values of the parameters were then changed and the process was repeated, until all parameter values from the parameter grid were tested. I used a following grid of parameter values: (i) t_1: from -667ms to 667ms in steps of 56ms; (ii) n: 1, 3, 4, 5 and 8 when using single electrodes and electrode quartets for detection and 1, 2 and 3 when using anatomical electrode subsets or all grid electrodes for detection; (iii) t_n-t_1: 100ms, 125ms, 250ms, 500ms, 750ms and 1000ms; (iv) γ: 0, 0.01, 0.1, 0.3, 0.5, 0.7, 0.9, 0.99 and 1; and (v) probability threshold: from 0.5 to 1 in steps of 0.17. Model that gave the maximum C_{YX} on the second part of the dataset was used to detect the events on the third part of the dataset and TPR, FPR and C_{YX} were then calculated from this detection. The same process was repeated, now using third part of the dataset for testing the grid of parameter values and second part of the dataset for model testing. Average of the final TPR, FPR and C_{YX} was then reported as the measured detection accuracy.

Different tolerance values were used to bin the experiment time into non-overlapping time bins, as described in section 4.2.1. Tolerance value directly determines the length of the dataset and, for used tolerance values, Table 10 gives the corresponding dataset lengths.

		Tolerance									
		50ms	155ms	261ms	366ms	472ms	577ms	683ms	788ms	894ms	1s
Dataset length	LFC	34 253	10 898	6 233	4 347	3 326	2 724	2 274	1 947	1 701	1 503
	HFC	31 041	9 892	5 665	3 953	3 030	2 482	2 076	1 780	1 557	1 381
	LCF & HFC	31 041	9 892	5 665	3 953	3 030	2 482	2 076	1 780	1 557	1 381

Table 10. Total dataset length for different temporal tolerances.

4.2.4. MRNR subtraction

To remove the movement related neuronal responses (MRNRs) following a mismatch or a collision event, I used the MRNR subtraction method described in Chapter 3. MRNR were identified by deriving and testing a set of models relating the signals from one electrode to the movements using only non-event data (i.e. all data which was at least 1s before and 3s after any event). The most predictive model was selected and used to predict the MRNR for the whole recording, this time including the event data. MRNR signals were then subtracted from the initial signal, and result was termed MRNR-free signals. All reported results were achieved by using MRNR-free signal for detection, unless specified otherwise.

4.2.5. Neuroanatomical analysis

To determine whether the motor or the somatosensory cortex played a more distinctive role in generating ERNR, I classified electrodes into motor cortex electrodes, somatosensory cortex electrodes, and other electrodes (Figure 15) in the same way as done in Chapter 3.

4.3. Results

4.3.1. Detection of error related neuronal responses

To quantify how well outcome and execution events can be detected, I used signals from all ECoG grid electrodes and in both signal components as an input for my detection algorithm (Figure 28). When detecting outcome error with tolerance of 366ms and across all four subjects, average C_{YX} was 0.65 with average TPR of 0.83 and average FPR of 0.30 (for individual subject values see Table 11). For detection of execution error with the same tolerance, average C_{YX} was 0.35 with average TPR of 0.61 and average FPR of 0.59 (for individual subject values see Table 11). Over all tolerance values, outcome error C_{YX} values were higher than execution error C_{YX} when both frequency components were used (C_{YX} difference: S1: 0.50±0.05, S2: 0.12±0.01, S3: 0.11±0.03, S4: 0.33±0.01, $p<0.05$; signed Mann–Whitney–Wilcoxon test). These results show that detection of outcome errors works better than the detection of execution errors.

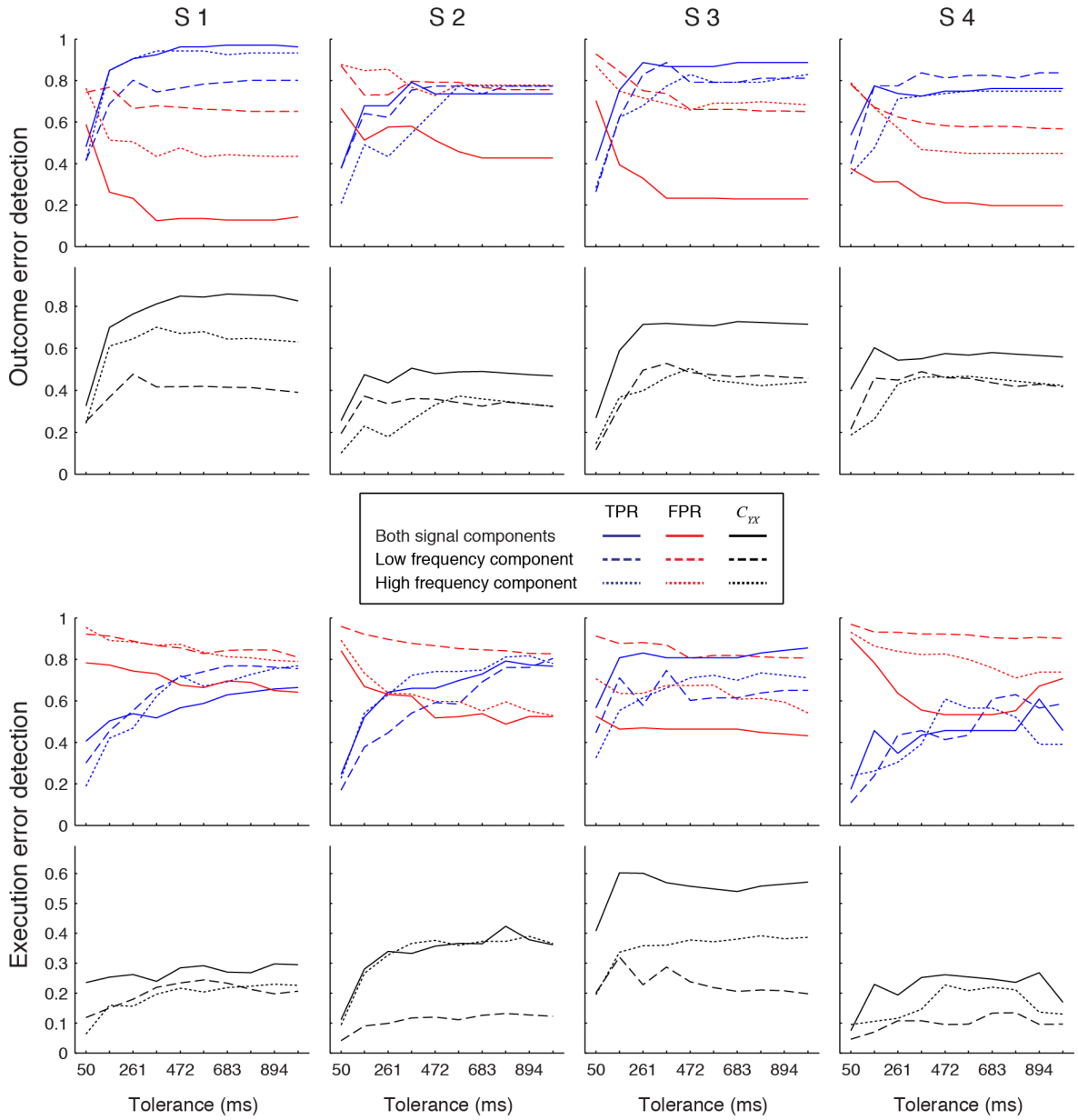

Figure 28. Overview of detection results when signal from all ECoG electrodes are used for detection of outcome (A) or execution (B) errors. For detection, I used low frequency component (dashed line), high frequency component (dotted line) or both frequency components together (full line). Top row of panels show the *TPR* (blue lines) and *FPR* (red lines), while the bottom row of panels show the normalized mutual information C_{YX} (black lines). Different columns show results for different subjects.

	Outcome error				Execution error			
	S1	S2	S3	S4	S1	S2	S3	S4
C_{YX}	0.82	0.50	0.72	0.55	0.24	0.33	0.57	0.25
TPR	0.92	0.79	0.87	0.73	0.52	0.66	0.81	0.43
FPR	0.13	0.58	0.23	0.24	0.73	0.62	0.46	0.56

Table 11. Detection accuracy when both LFC and HCF signals from all ECoG electrodes are used for detection using rLDA.

Using both signal components gives higher C_{YX} then when using either one of the components (C_{YX} difference: outcome error: LFC & HFC vs. LFC: 0.22±0.02; LFC & HFC vs. HFC: 0.18±0.01; execution

error: LFC & HFC vs. LFC: 0.18±0.02; LFC & HFC vs. HFC: 0.08±0.01; p<0.05; signed Mann–Whitney–Wilcoxon test). Using HCF gives higher C_{YX} than when LFC is used, although difference is statistically significant for execution error only (C_{YX} difference: outcome error: 0.03±0.02, p=0.41; execution error: 0.10±0.02; p<0.05; signed Mann–Whitney–Wilcoxon test).

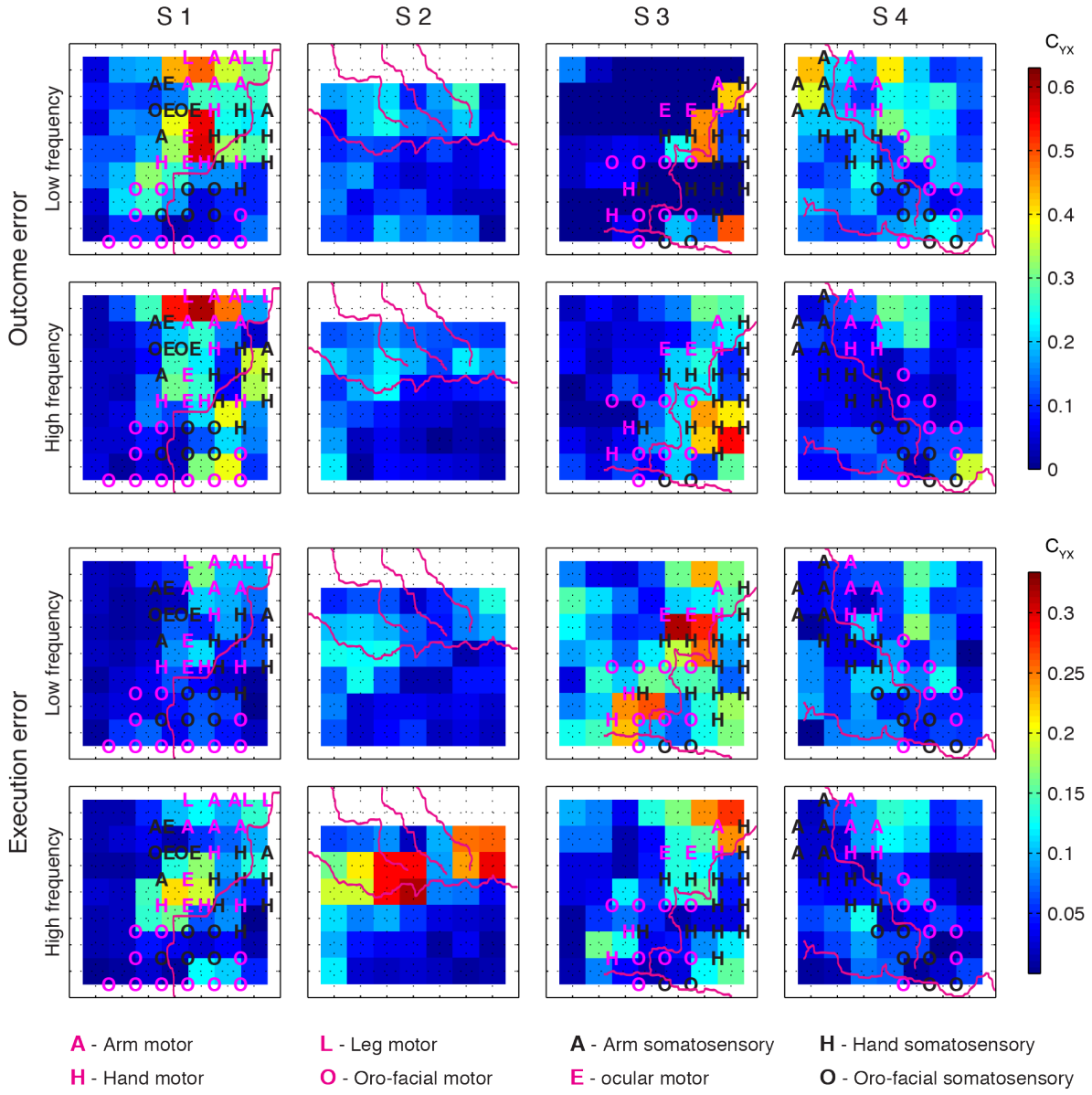

Figure 29. Spatial distribution of normalized mutual information of outcome and execution error events for low and high frequency components in relation to the individual anatomy of the subject. Purple lines depict the central sulcus, the Sylvian fissure and, for S2 only, the pre and post central sulci. Letters in the squares mark the functional subarea (A – arm, H – hand, L – leg, E – ocular, O – oro-facial) in motor (purple) and somatosensory (black) cortex as determined by ESM. Every coloured square represents one quartet of electrodes with the electrodes at the corners of the square. Colours of the squares depict the normalized mutual information according to the colour bar. Since no recordings were made from the top row of grid electrodes for S2, I show the top row of quartets as white. The top left square in the ECoG grids correspond to the electrode closest to the red star in Figure 15.

4.3.2. Topographical distribution of informative signals for error detection

To find out the topographical distribution of signals that are informative for the error detection, I performed detection using signals recorded from electrode quartets (Figure 29). For most of the subjects, several isolated, often quite distant peaks of C_{YX} could be found over the cortical regions I recorded from. Locations of these peaks often differed for different errors and different signal components. Thus, no topographical location was systematically beneficial for detection of either outcome or execution errors.

4.3.3. Error detection using signals from motor or somatosensory areas

I also wanted to see if recordings from motor or somatosensory areas provided enough information for high accuracy of error detection. To this end, I divided the ECoG grid electrodes into sets of motor, somatosensory and other electrodes. Detection was then performed using both signal components with rLDA models (Figure 30). For all subjects and tolerance levels, C_{YX} using all ECoG grid electrodes was higher than the C_{YX} of the best anatomical subsets (C_{YX} difference: outcome: 0.06±0.01; execution: 0.04±0.01; p<0.05; signed Mann–Whitney–Wilcoxon test).

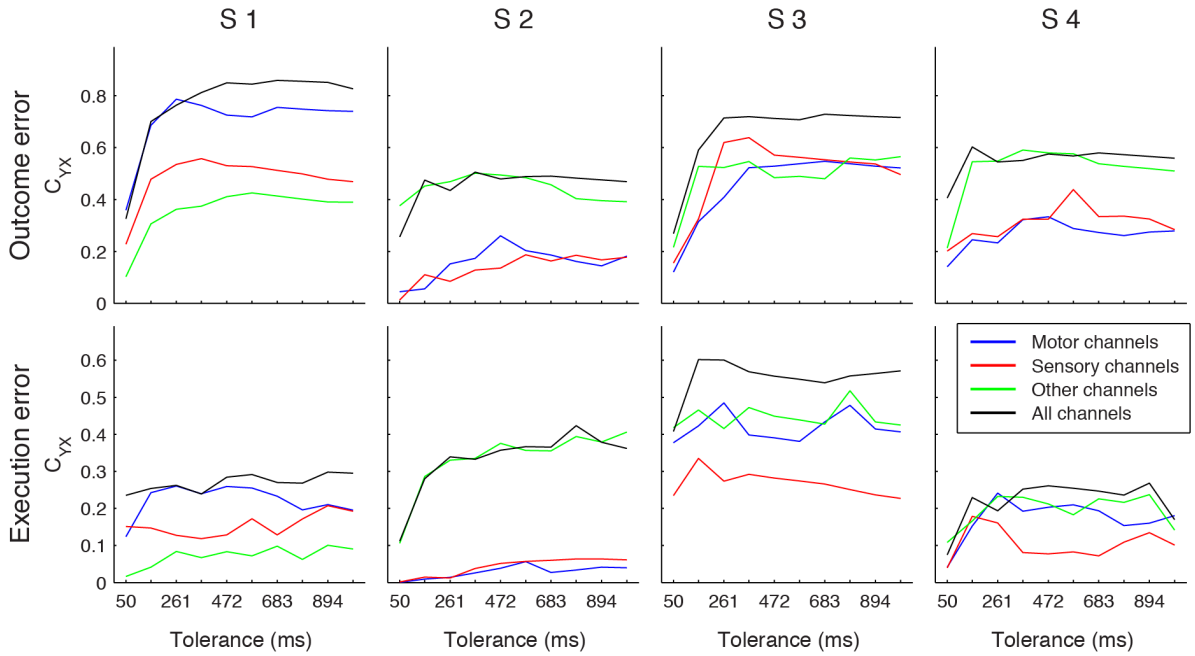

Figure 30. C_{YX} for outcome and execution error events using signals recorded from electrode sets containing all electrodes over motor cortical areas (blue), somatosensory cortical areas (red) and all remaining electrodes (green).

For S2, there are only 3 electrodes assigned to the motor set and only 2 electrodes assigned to the somatosensory set (Table 12). Therefore, I considered C_{YX} values for S2 not representative and removed them from comparison of C_{YX} for different anatomical regions. When taking the remaining three subjects, the C_{YX} of outcome error was not significantly different for all three electrode

subsets (p>0.47; signed Mann–Whitney–Wilcoxon test). When detecting execution error, C_{YX} for motor and other subsets was higher than C_{YX} for somatosensory subset, while the small difference of C_{YX} between motor and other subsets was not significant (C_{YX} difference: motor vs. somatosensory: 0.10±0.01; p<0.05; motor vs. other: 0.03±0.02; p=0.21; other vs. somatosensory: 0.06±0.02; p<0.05; signed Mann–Whitney–Wilcoxon test).

Anatomical sets	S1	S2	S3	S4
Motor	22	3	18	11
Somatosensory	18	2	11	14
Other	20	51	35	39

Table 12. Number of electrodes belonging to motor, somatosensory and other anatomical sets for each of the subjects.

Next, I investigated the change of detection performance if restricted to signals from one of the anatomical regions only. For each of the tolerances, I calculated the percentage of C_{YX} achieved when using signals from electrodes belonging to one of the anatomical sets in comparison to C_{YX} achieved when using signals from all ECoG grid electrodes. When averaged over tolerances, detection from motor subsets achieves 72% for outcome error and 78% for execution error of C_{YX} achieved when all electrodes are used for detection. C_{YX} from somatosensory subsets is 65% for outcome error and 50% for execution error of C_{YX} from using all electrodes. When signals from other electrode subsets are used, C_{YX} is 69% of C_{YX} achieved when all electrodes are used for both outcome and execution errors.

4.3.4. Detection from smaller electrode sets

I investigated whether one can detect error events with smaller electrode sets with accuracy similar to detection when all ECoG grid electrodes are used (Figure 31). When both frequency components are used, maximum C_{YX} from single electrodes was 60% for outcome error and 66% for execution error of the C_{YX} when all electrodes are used. For electrode quartets and both frequency components, maximum C_{YX} is 82% for outcome error and 74% for execution error of C_{YX} when all electrodes were used.

4.3.5. Effect of MRNR subtraction on the normalized mutual information

I also investigated whether MRNR subtraction affected the detection of the error events (Figure 32). Averaged over subjects and tolerance values, difference of C_{YX} when MRNR subtraction was and was not used is not significant if both LFC and HFC are used for detection (p=0.09; signed Mann–Whitney–Wilcoxon test). When only LFC is used for detection, using MRNR subtraction leads to a slight improvement (C_{YX} difference: 0.089±0.008; $p<10^{-13}$; signed Mann–Whitney–Wilcoxon test). For the high frequency component, I observed a slight, but still significant, reduction of mutual

information when the MRNR subtraction was used (C_{YX} difference: -0.028±0.006; $p<10^{-4}$; signed Mann–Whitney–Wilcoxon test).

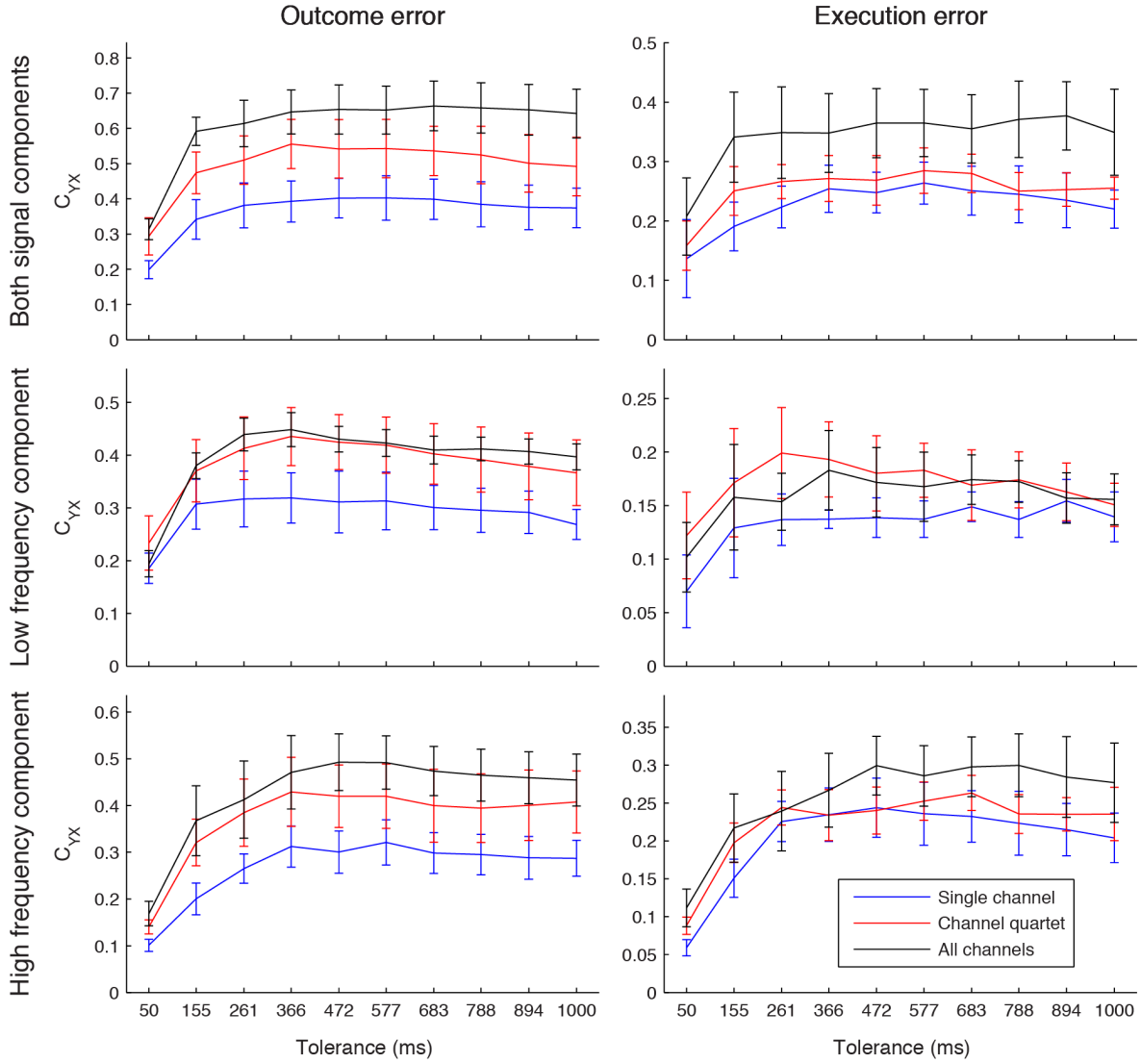

Figure 31. C_{YX} of outcome and execution error events for different electrode set sizes, maximized over all possible electrode sets and averaged over subjects. I compared electrode subsets containing single electrodes (blue line), electrode quartets (red line) and set of all grid electrodes (black line) when using low frequency component, high frequency component or both frequency components. Detection was made using rLDA. Error bars show standard error of the means.

4.3.6. Selection of the model type for detection: rLDA vs. rQDA

I compared the detection performance between rLDA and rQDA (Figure 33). rQDA is more flexible, but has a drawback that more free parameters have to be estimated from the training dataset. The number of free parameters is a quadratic function of the number of signal features, which is, in turn, a product of the number of electrodes and a number of features taken from each single electrode. Therefore, if the dataset is quite large and the total number of features used to build the model is quite small, rQDA might outperform rLDA. On the other hand, if the data is limited and the total

number of features is quite high, rLDA might outperform rQDA. I wanted to find out in which one of these two regimes was my dataset.

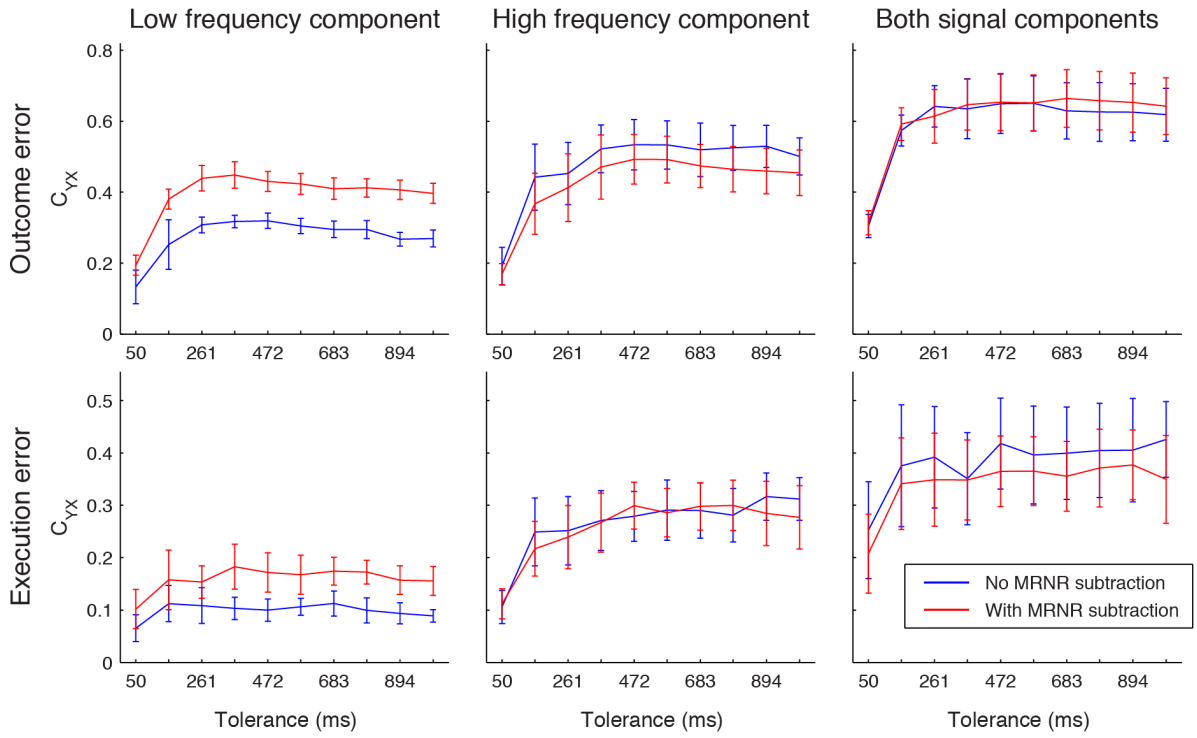

Figure 32. Normalized mutual information from signals with (red) and without (blue) MRNR subtraction when using signals from all electrodes. Different columns show detection mutual information when low frequency component (dashed lines), high frequency component (dotted lines) or both signal components (full line) were used for detection. Error bars show standard error of the means.

Electrode subsets		Outcome error			Execution error		
		LFC	HFC	LFC & HFC	LFC	HFC	LFC & HFC
Single electrodes	C_{YX} diff.	$(9\pm6)\cdot10^{-4}$	$(-17\pm6)\cdot10^{-4}$	$(86\pm7)\cdot10^{-4}$	$(-27\pm5)\cdot10^{-4}$	$(-15\pm5)\cdot10^{-4}$	$(-26\pm5)\cdot10^{-4}$
	p	0.79	$<10^{-2}$	$<10^{-2}$	$<10^{-2}$	$<10^{-2}$	$<10^{-2}$
Electrode quartets	C_{YX} diff.	$(45\pm1)\cdot10^{-3}$	$(11\pm1)\cdot10^{-3}$	$(57\pm2)\cdot10^{-3}$	$(19\pm1)\cdot10^{-3}$	$(9\pm1)\cdot10^{-3}$	$(27\pm1)\cdot10^{-3}$
	p	$<10^{-2}$	$<10^{-2}$	$<10^{-2}$	$<10^{-2}$	$<10^{-2}$	$<10^{-2}$
All electrodes	C_{YX} diff.	0.32±0.01	0.09±0.02	0.42±0.02	0.15±0.01	0.11±0.01	0.30±0.02
	p	$<10^{-2}$	$<10^{-2}$	$<10^{-2}$	$<10^{-2}$	$<10^{-2}$	$<10^{-2}$

Table 13. C_{YX} differences between detections using rLDA and rQDA. Each field shows differences and standard error of the means across subjects, all possible electrode subsets and all tolerances, together with the p value for testing equal medians using Mann–Whitney–Wilcoxon test.

If only LFC or HFC signals from single electrodes were used for detection and for both error types, rQDA either significantly outperformed rLDA, or there was no significant difference in performance (Table 13). When using both signal components for outcome error detection, rLDA significantly

outperforms rQDA, while opposite is true for execution error detection. If signals from electrode quartet or all electrodes were used, rLDA always significantly outperformed rQDA.

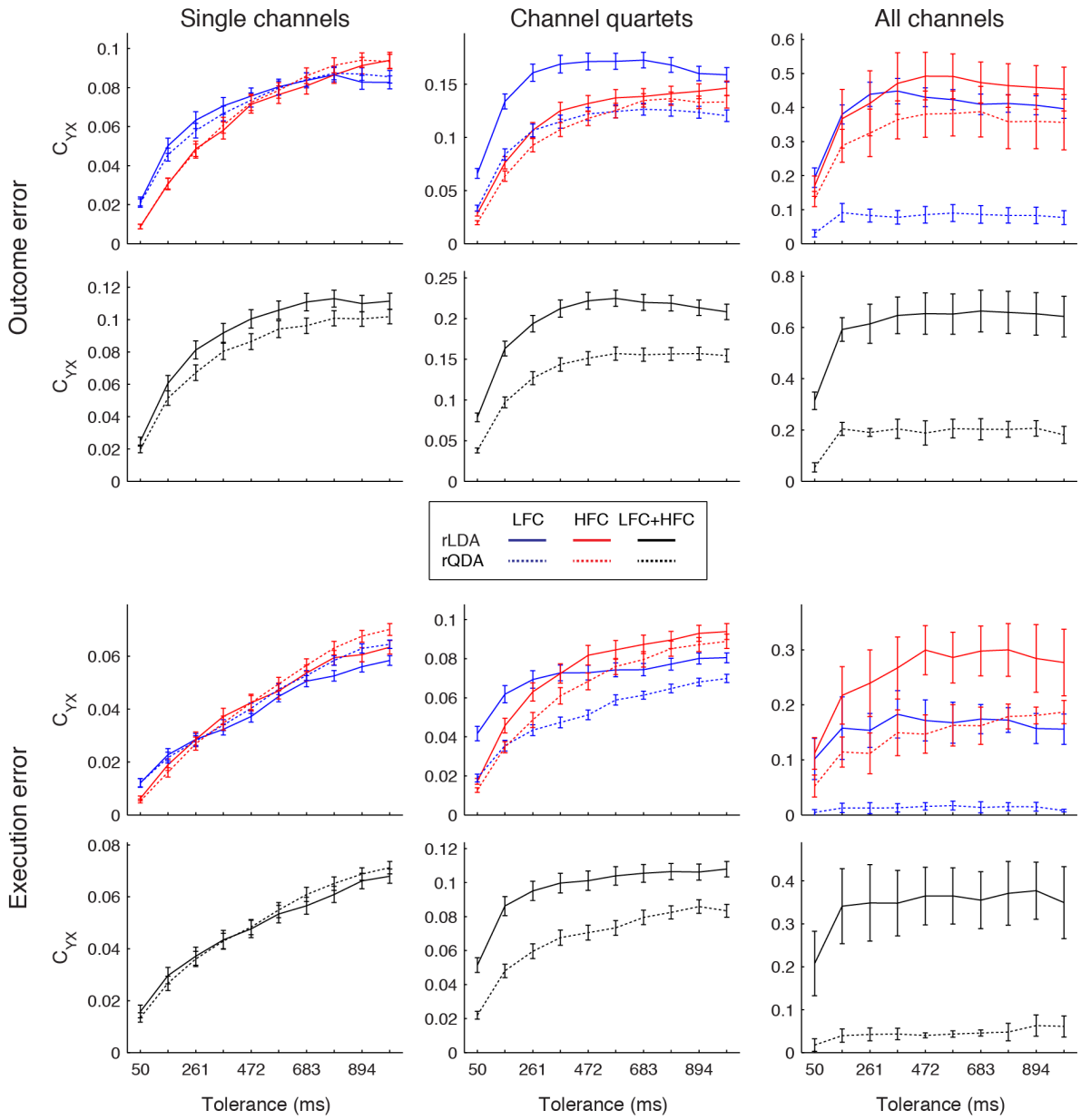

Figure 33. Normalized mutual information of outcome and execution error events for different electrode set sizes, using LFC (blue lines), HFC (red lines) or both components together (black lines) and for rLDA (full lines) and rQDA (dotted lines) based detection algorithms, averaged over all subjects and all possible electrode subsets. Error bars show standard error of the means.

4.4. Discussion

In the previous Chapter (Chapter 3), I demonstrated that ECoG signals reflect outcome and execution ERNRs and are not related to movements or caused by visual stimuli or surprise effects. Here, I show that both outcome and execution error events can be detected from continuous neuronal activity measured with ECoG electrode implants. For a tolerance windows of 366ms,

outcome error events were detected with an average TPR of 0.79 and an average FPR of 0.31. Execution error events were detected slightly less reliable, with an average TPR of 0.61 and an average FPR of 0.60 for the same temporal tolerance. These results suggest that, for both error types, it is possible to detect more than half of the errors and that the number of false positive detections is comparable to the number of true positive detections. In the experiment presented here, error events were extremely sparse. Therefore, these results suggest that error events can be detected with high reliability. This notion is supported by the values of the normalized mutual information that show that the timing of the error events, reproduced by detection process and with a tolerance of 366ms contain 61% of the information contained in the timing of the outcome errors and 34% of the information contained in the timing of the execution errors on average.

Signals informative about the time of error events were not found in one isolated cortical area but rather in several various areas. Often, it was possible to find several, mutually isolated C_{YX} peaks on one subject for the same error type and the same frequency component. In addition, C_{YX} peaks often had different locations for different error types and different location for different frequency components. This suggests that neuronal responses coding for outcome errors might be independent from the neuronal responses coding for execution errors. In addition, it suggests that low and high frequency component of the neuronal responses coding for the same error might also be independent. This is consistent with the results of the previous Chapter where it was shown that topographical distribution of ERNR's signal to noise ratio had the same property.

I also tested whether signals from a particular anatomical area gave more or less informative signals for detection. To this end, I divided the ECoG electrodes for each of the subjects into three sets: motor set, somatosensory set and the 'other' set. In S2, the ECoG grid was implanted over the more ventrally than for other subjects, thereby covering only the ventral motor and somatosensory areas. In addition, ESM was not performed on S2. Therefore, for S2, I had to use sulci reconstruction to determine which electrodes belong to motor and somatosensory sets. This resulted in motor set of only 3 electrodes and somatosensory set of only 2 electrodes (Table 12). Due to the low number of electrodes in these sets, and due to more ventral location of the ECoG implant, I decided that detection results of motor and somatosensory sets for S2 are not representative as these areas were not sufficiently covered and, therefore, excluded S2 from the anatomical area specific analysis. For the remaining subjects none of the anatomical sets provide better signals for detecting outcome errors. In the case of execution error, detection using motor and other electrode sets was similar and only a bit better then detection from somatosensory subset. On average, using signals from motor areas achieves 72% of C_{YX} when using all grid electrodes to detect outcome errors and 78% of C_{YX} when using all grid electrodes to detect outcome errors.

A complete 8x8 electrodes ECoG grid covers a surface of around 64cm^2. To implant such grids, an open wound of similar size has to be made at the side of the skull. Reducing the size of the implant would reduce the medical risk of ECoG implantations. Therefore, I investigated whether similar detection accuracy can be obtained using signals from smaller parts of the grid only. Signals from single electrodes gave much lower detection accuracy in comparison to using all ECoG electrodes, but 60% of C_{YX} when using all grid electrodes to detect outcome errors and 66% of C_{YX} when using all grid electrodes to detect execution errors could still be obtained. Detection based on signals from electrode quartets, 2x2 neighbouring electrodes, was almost at the level of the detection obtained by using signals from all electrodes, obtaining 82% of C_{YX} when using all grid electrodes to detect outcome errors and 74% of C_{YX} when using all grid electrodes to detect execution errors. These results suggest that, if the optimal location for an implant is known in advance, one could safely reduce the size of the electrode by 16 fold, with only a small loss of detection accuracy.

Besides medical risk, there are additional benefits when reducing the number of electrodes used for the detection. The numerical complexity of the detection algorithm is a quadratic function of the number of used electrodes. Therefore, reducing the number of electrodes by 16 fold could reduce the numerical complexity of the detection algorithm by up to 256 times, which could drastically reduce the hardware requirement of the detection process, allowing the process to be run on a less powerful computers, or freeing computational resources for other tasks. To find out which electrodes or electrode quartets are best for detection, one could run the whole detection process on a set of data recorded for such calibration purpose. On the other hand, such an optimization process might take a considerable amount of computation time.

A high proportion of electrodes were located above the motor and somatosensory cortical areas. Therefore, it is expected that some proportion of the recorded signal is movement related. In the previous Chapter, analysis revealed that large amounts of variance on some of the electrodes can be explained by a model predicting neuronal signals from eye and hand movements. Movement related part of the signal was then removed by using MRNR subtraction procedure (see Chapter 3 for details). In the analysis presented in this Chapter, I detected the error events using both MRNR-free signals and signals where MRNR subtraction was not used. On average, MRNR subtraction did not significantly change the detection accuracy, demonstrating that here presented detection is based on error related and not any movement related neuronal signals.

I also compared detection accuracy between detection using rLDA and rQDA. In my experiment, subjects performed around one hour of recordings, which left around 20 minutes of recordings for training the detector. In these experimental conditions, detector using rLDA clearly outperformed detector using rQDA when signals from all ECoG electrodes were used. In this case, number of

possible features used for detection greatly outnumbered the number of ERNR examples used for building the model. Since rQDA models have to estimate much higher number of parameters than the rLDA models, it is no surprise that detection based on rLDA showed better results. On the other hand, when signals from only one electrodes and single signal component were used for detection, using rQDA was as accurate or better than using rLDA. Already by using signals from 4 electrodes, detection accuracy was significantly higher when rLDA was used. In this case of low numbers of features, detection benefited from the higher flexibility of rQDA models. For larger datasets containing more ERNR examples that could be used for detection model building, rQDA might further outperform rLDA models although, based on the results presented in this Chapter, one would rather include signals from larger number of electrodes since, by doing so, gain of detection accuracy becomes higher.

4.4.1. Characteristics of signal components used for detection

Here, I used both low (0-8Hz) and high (60 Hz to 128 Hz for S1 and S2 and 60 Hz to 200 Hz for S3 and S4) frequency component of the neuronal signals to detect the error events. Results from the previous Chapter show that these signal components gave two different, possibly independent, sources of information about errors. Other studies showed that neuronal responses with similar spectro-temporal characteristics can be evoked by non-error events, such as different movements (Ball et al., 2009b; Crone et al., 1998a; Crone et al., 1998b; Crone et al., 2006; Leuthardt et al., 2004; Wang et al., 2009; Wisneski et al., 2008), somatosensory and auditory stimuli (Boatman-Reich et al., 2010; Crone et al., 2001; Ray et al., 2008), word recognition (Jerbi et al., 2009), face recognition (Lachaux et al., 2003) and attention and short term memory (Jensen et al., 2007). One could argue that detecting ERNR in a more natural environment, compared to my highly controlled task, will be hard as the ERNRs would not be differentiable from the neural responses to the non-error events. This will not necessarily hinder the applicability of the error detection system. If subjects are focused on the task at hand, they will perform minimal amount of additional movements, receive minimal amount of additional tactile stimuli and will probably not perform additional cognitive tasks. In my task, subjects were merely asked not to move too much and to try to remain focused on the task. I argue that they would show similar behaviour if they were motivated to do the task for their personal benefit, such as navigating the cursor or artificial hand towards the target. I therefore think that ECoG signals can be applied for the online continuous error detection.

Detection of error events might still be likely possible even in the environment where more somatosensory stimuli are present and more different tasks have to be made at once. ERNRs used in this study are evoked on different, often quite distant, electrodes and these evoked responses

exhibit different time courses. This makes the ERNR responses highly redundant and differentiable to other, non-error neuronal responses. Some of the before mentioned studies already used these signal properties to differentiate between neuronal responses to different non-error events (Ball et al., 2009b; Boatman-Reich et al., 2010; Wang et al., 2009) and the same principal could work for ERNRs as well. Further studies are required to test the accuracy of error detection in such noisy environments.

4.4.2. Comparison to previous detection studies

Several studies investigated the detection of epileptic seizures from neuronal recordings (Lee et al., 2007; Rana et al., 2012). Since epileptic seizures occur very rarely and cause hospital staff alarms during the epileptic assessment periods, there is a strong requirement to keep the number of false positive detections at a minimum. Therefore, when measuring accuracy of seizure detections, TPR is usually combined with the number of false positives per hour. Since frequency of decoding errors during normal BMI continuous control is much higher than the number of epileptic seizures, using the number of false positives per hour as a measure of performance does not apply well to error detection. A number of other studies used neuronal signals to detect movement related events, such as movement onset (Awwad Shiekh Hasan and Gan, 2010; Bashashati et al., 2007; Hwang and Andersen, 2009; Levine et al., 2000), movement planning phase (Achtman et al., 2007) and periods of movement related synchronization and desynchronization (Solis-Escalante et al., 2008). These studies mainly used TPR and FPR to visualize the detection results, while some of them used the Youden index $i = TPR\text{-}FPR$ (Sokolova et al., 2006) as a single measure of detection performance (Awwad Shiekh Hasan and Gan, 2010; Levine et al., 2000). Solis-Escalante et al. used mutual information to report their final results, but still used the Youden index to calibrate their detector. Here, due to its strong theoretical foundations, I used normalized mutual information to both calibrate the detector and measure its accuracy.

Afore mentioned studies used a wide variety of algorithms for detection: expectation maximization Gaussian mixture model (Awwad Shiekh Hasan and Gan, 2010), k nearest neighbours (Bashashati et al., 2007), linear discriminant analysis (Bashashati et al., 2007), local field potential β-band power threshold crossing (Hwang and Andersen, 2009), cross-correlation threshold crossing (Levine et al., 2000), support vector machine (Solis-Escalante et al., 2008), recursive Bayesian model (Achtman et al., 2007) and phase slope index threshold crossing (Rana et al., 2012). Here, I used regularized versions of linear and quadratic discriminant analyses with a variable threshold. This makes my detection algorithms quadratic in nature. Use of more complex and flexible algorithms might improve the detection, although my results show that simpler rLDA algorithms outperformed more

complex rQDA algorithms. More robust, linear algorithms might also provide improvements, but, due to the large variability of all neuronal activity not related to errors, finding an efficient linear decision boundary might prove impossible.

In addition, afore mentioned studies detecting movement states also failed to investigate the effect of tolerance on the precision of the detector. In this Chapter, I show that detection accuracy rises with the tolerance until it saturates at around 300-500ms. This implies that ERNRs used to detect error events are not perfectly synched with those events, and that variability or ERNRs in response to error events is on the level of 300-500ms. Cause of such variability in ERNRs response time might be the variability in the time subjects need to recognizinge the error. This is in line with the measurements of choice reaction time variability (Kirkeby and Robinson, 2005) where 95% of reactions fell within approximately 400ms around the mean reaction time. In any case, variability caused by limited detection frequency of 32Hz should be negligible compared to other effects.

4.4.3. Comparison to previous ERNR studies

Most of the earlier ERNR studies concentrated on the activation of anterior cingulate cortex (ACC) and its functional meaning (for review see Bechtereva et al., 2005; Jocham and Ullsperger, 2009; van Veen and Carter, 2006). ERNRs have also previously been found in motor cortex (Diedrichsen et al., 2005; Koelewijn et al., 2008; van Schie et al., 2004), somatosensory cortex (Diedrichsen et al., 2005) and in other cortical areas (Diedrichsen et al., 2005; Jung et al., 2010; Ojemann, 2003; Ojemann et al., 2004; Ullsperger and von Cramon, 2003; Walton et al., 2004; Zanolie et al., 2008). My study extends on the findings from the previous Chapter by showing that error related neuronal responses recorded by ECoG can be detected in continuous neuronal activity recordings. Furthermore, I demonstrated that outcome errors can be detected with higher accuracy than execution errors.

4.4.4. Relevance for brain machine interfaces

One motivation for this study was to investigate whether ERNRs can be used to improve the performance of continuous movement BMIs (Carmena et al., 2003; Hochberg et al., 2006; Kim et al., 2008; McFarland and Wolpaw, 2005; Serruya et al., 2002; Taylor et al., 2002; Velliste et al., 2008).

To improve the continuous movement BMIs, (i) error related signals have to be present in the given recording of neuronal activity, (ii) these errors related signals would have to be detectable, (iii) proper errors would have to be differentiable from other error types and (iv) adaptive algorithms facilitating error detection would have to be available. Extensive research in error related signals already showed that error related signal can be recorded with wide range of recording techniques. Previous chapter shows that error signals can be recorded using ECoG during continuous tasks and

that execution errors can be differentiated from outcome errors, thereby resolving points (i) and (iii) in the case of ECoG based BMIs. Rotermund et al. (Rotermund et al., 2006) showed that adaptive algorithms decoding continuous movements can indeed benefit from error detection, resolving the point (iv). In this Chapter, I showed that error detection is possible, thereby resolving the point (ii). Even though all points have now been resolved, it is still necessary to demonstrate the proposed continuous BMI decoding system that facilitates error detection in an online study, making this an interesting topic for a future study.

My study also shows that both outcome and execution errors can be reliably detected. Instead of just providing binary information, whether decoding error has been made or not, detection of multiple error types could further improve BMI operation. Outcome error detection can be used to subsequently correct the errors (Blankertz et al., 2003; Buttfield et al., 2006; Ferrez and del R Millan, 2008; Parra et al., 2003). Such use might not be used to directly correct the decoded trajectory, since BMI users will try to correct the decoding mistake using corrective movements. On the other hand, in a task where movements are made to perform some kind of selection, e.g. guiding a cursor to one of several target locations, detecting that such selection was incorrect might make such BMI more efficient. In addition, outcome errors can also be used as a critic within the reinforcement learning algorithm (DiGiovanna et al., 2009). Such algorithms tend to require long recording sessions, making them much slower in their adaptation towards more efficient BMI decoder.

Detection of execution errors can be used to directly label the incorrectly decoded trajectories and the part of the recordings that were incorrectly interpreted. Such information can be used to facilitate BMI algorithm adaptation (Rotermund et al., 2006).

For most invasive BMIs, motor cortex is the target area for the implantation of electrodes whose signals are to be used to extract intended motor actions. I demonstrated that one can detect error signals with high accuracy based on motor cortical signals only. Therefore, movement decoding and error detection may be implemented using the same electrode implants. Consequently, no additional implants over other cortical areas would be required for BMIs employing such neuronal error signals, thereby removing additional medical risk when adding error detection to a BMI system.

Chapter 5

Inference based method for re-alignment of single trial neuronal responses

Summary. Many neuroscientific studies are trying to identify neuronal responses to certain stimuli or neuronal signals that code for certain behaviours. Usual way to extract such neuronal responses is to average neuronal activity over large number of experimental trials in order to reduce the noise. If observed neuronal responses are jittered in time with respect to the corresponding stimulus or behaviour, averaging over trials distorts the estimation of the underlying neuronal response. In this Chapter, I present a novel algorithm ($dTAV$ algorithm) for realigning the recorded neuronal activity to an arbitrary internal trigger based on an inference algorithm and time averaging of variance across trials. Using simulated data, I show that $dTAV$ algorithm can reduce the jitter of neuronal responses for signal to noise ratios of 0.2 or higher. In addition, I demonstrate that $dTAV$ algorithm outperforms another competitive algorithm published by Nawrot et al. {Nawrot, 2003 #548}.

5.1. Introduction

Large numbers of neurophysiological studies are investigating neuronal responses to external events. These studies range from simple stimulus evoked neuronal responses in the corresponding primary sensory areas, e.g. neuronal responses to light flashes in the primary visual cortex (Dagnelie et al., 1989), to neuronal activity correlates to complex behaviours, e.g. neuronal correlates of abstract problem solving (Gaona et al., 2011; Gunduz et al., 2011). In such studies, neuronal responses are usually extracted by averaging the neuronal signal in order to reduce the noise non-correlated to the neuronal responses. Extraction of the neuronal responses by averaging relies on the assumption that neuronal responses are similar and time locked to the corresponding stimulus or behaviour. On the other hand, neuronal responses show temporal variability in relation to the corresponding stimulus or behaviour (Radons et al., 1994; Requin et al., 1988; Seal et al., 1983; Seidemann et al., 1996; Vaadia et al., 1988). Depending on the amount of such temporal jitter, underlying neuronal response estimated by averaging will be distorted (Figure 34), possibly leading to mistakes in subsequent analysis and mistakes in conclusions of the studies.

In this chapter, I propose an inference based algorithm for realignment of neuronal responses ($dTAV$ algorithm). It is a parametric algorithm that uses the reduction of variability, integrated over the time course of the neuronal response, to select the parameter values and, therefore, optimize the realignment procedure. In addition, I show, by means of analytic calculations, that the reduction of time averaged variability can be used as a measure of jitter reduction and, therefore, the amount of neuronal response alignment. To show this, I built a simple model of neuronal responses and demonstrated the usability of my algorithm in variety of noise levels using simulated data. $dTAV$ algorithm is also compared to another non-parametric realignment algorithm published by Nawrot et al. (Nawrot et al., 2003).

5.2. Methods

Methods section is presented in the following order. First, I construct a simple model of neuronal responses to a given external stimulus. Next, I present the analytic tools used to predict the jitter reduction after the algorithm finished with the re-alignment procedure. Since the underlying brain triggers are not known, it is necessary to design such unsupervised measure of jitter reduction in order to optimize the values of the $dTAV$ algorithm parameters. In the following section, I describe $dTAV$ realignment algorithm in detail. Finally, I describe the details of simulated data used to assess the usefulness of $dTAV$ realignment algorithm and to compare it to a realignment algorithm published by Nawrot et al. (Nawrot et al., 2003).

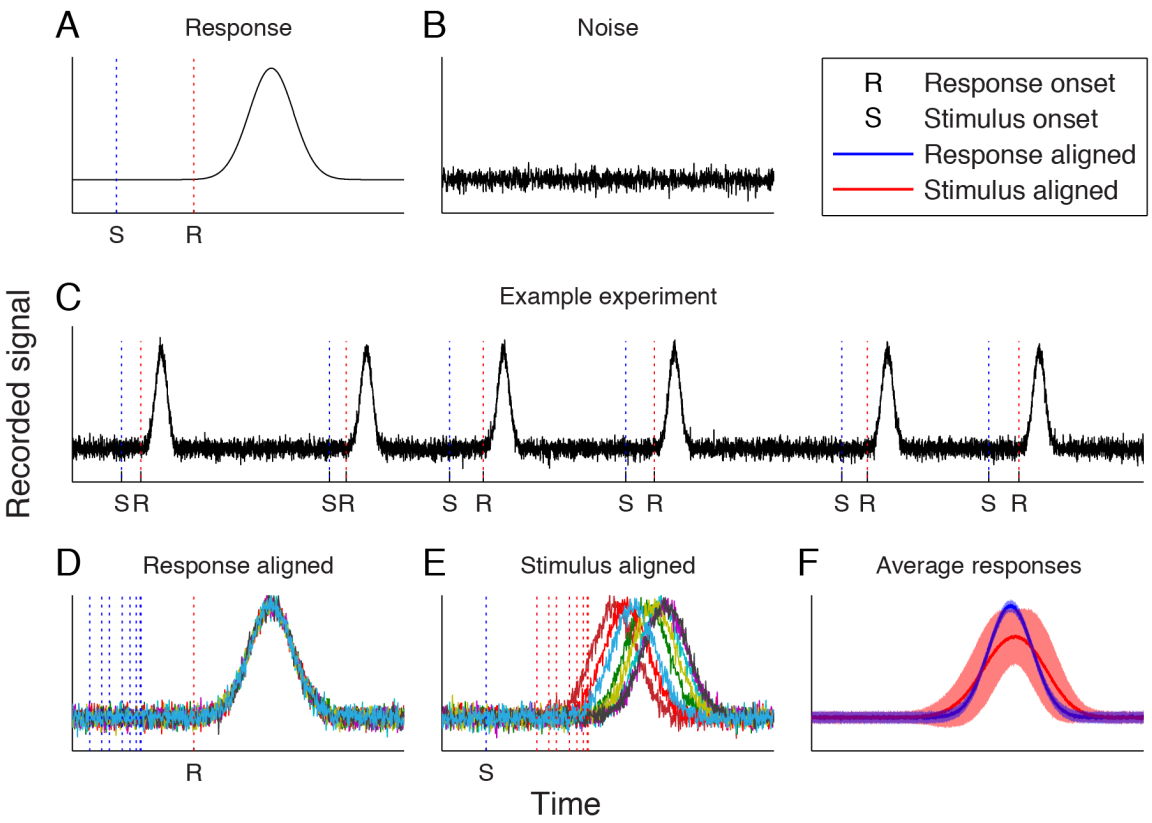

Figure 34. Effect of neuronal response jitter on estimation of the underlying neuronal response. A: Neuronal responses follow the stimulus onset (S), but are triggered (R) by some internal stochastic process. B: A certain amount of noise is recorded together with the relevant neuronal response. C: During the experiment, stimulus presentation is repeated many times. Following every stimulus presentation, neuronal signal is recorded. D: When neuronal responses are aligned on the response onset, trial average response (F: blue line) is going to approximate the real neuronal response. But the response onset is not known. Average response over trials aligned on the stimulus onset triggers (F: red line) will badly reproduce the real neuronal response. In addition, when stimulus onset triggers are used, calculated standard deviation (F: blue and red shaded tubes) badly estimates the noise.

5.2.1. Neuronal response model

I constructed the neuronal signal as a convolution of neuronal responses $r(t)$ triggered at times t_i with the addition of Gaussian white noise η:

$$signal(t) = \sum_i r\left(t - t_i\right) + \eta \qquad \eta \in N(0, \sigma_\eta) \tag{5.1}$$

where σ_η is the standard deviation of the noise. After recording the neuronal signal, one can estimate the neuronal response by calculating the response-triggered average $\hat{r}(t)$:

$$\hat{r}(t) = \frac{1}{M}\sum_{i=1}^{M} signal\left(t - t_i\right) = r\left(t\right) + \frac{1}{M}\sum_{i=1}^{M}\eta_{i,t} \tag{5.2}$$

$$\hat{s}_\eta = \frac{1}{M}\sum_{i=1}^{M}\eta_{i,t} \in N\left(0, \frac{\sigma_\eta}{\sqrt{M}}\right) \tag{5.3}$$

where M is the number of responses used to calculate the average and $\hat{s}_\eta$ is the random variable drawn from a Gaussian distribution that follows from the presence of noise. Estimated variance of the signal $\hat{V}\left(r(t)\right)$ is given by:

$$\hat{V}\left(r(t)\right)=\frac{1}{M-1}\sum_{i=1}^{M}\left(signal\left(t-t_i\right)-\hat{r}(t)\right)^2=\frac{1}{M-1}\sum_{i=1}^{M}\left(\eta_{i,t}-\hat{s}_\eta\right)^2=\sigma_\eta^2+\hat{s}_V^2 \tag{5.4}$$

where $\hat{s}_V$ is the random variable drawn from a Gaussian distribution. Expected variance of the estimated variance is given by:

$$\hat{V}\left(\hat{V}\left(r(t)\right)\right)=\frac{\left(M-1\right)^2}{M^3}m_4-\frac{\left(M-1\right)\left(M-3\right)}{M^3}m_2^2 \tag{5.5}$$

where m_2 and m_4 are the second and fourth moments of the distribution (Kenney and Keeping, 1951; Rose and Smith, 2002). For the Gaussian distribution, this reduces to:

$$\hat{V}\left(\hat{V}\left(r(t)\right)\right)=\frac{2\left(M-1\right)}{M^2}\sigma_\eta^4 \qquad \hat{s}_V\in N\left(0,\frac{\sigma_\eta^2}{M}\sqrt{2\left(M-1\right)}\right) \tag{5.6}$$

During the experiments, onsets of the neuronal responses are not known, since these are triggered by brain-internal processes. Experiments are usually designed in such a way that the studied neuronal responses are elicited as a response to a certain stimulus. Time elapsed between the stimulus times ts_i and the times of the neuronal response onset t_i can be regarded as a stochastic process. In my model, difference between the stimulus times and the neuronal response onsets are modelled by a Gaussian distribution:

$$t_i-ts_i\in N\left(\mu_J,\sigma_J\right) \tag{5.7}$$

where μ_J and σ_J are mean and the standard deviation of the distribution. If one has access to stimulus times only, it is possible to estimate the neuronal response by calculating the stimulus-triggered average $\tilde{r}(t)$:

$$\tilde{r}(t)=\frac{1}{M}\sum_{i=1}^{M}signal\left(t-ts_i\right)=\frac{1}{M}\sum_{i=1}^{M}r\left(t-t_i+\left(t_i-ts_i\right)\right)+\frac{1}{M}\sum_{i=1}^{M}\eta_{i,t}=\overline{r}(t)+\hat{s}_\eta \tag{5.8}$$

where $\overline{r}(t)$ is the average signal in the presence of the jitter, independent of the noise. Variance is given by:

$$\begin{aligned}\tilde{V}\left(r(t)\right) &= \frac{1}{M-1}\sum_{i=1}^{M}\left(signal\left(t-ts_i\right)-\tilde{r}(t)\right)^2 \\ &= \frac{1}{M-1}\sum_{i=1}^{M}\left(r\left(t-t_i+\left(t_i-ts_i\right)\right)-\overline{r}(t)+\eta_{i,t}-\hat{s}_\eta\right)^2 \\ &= \frac{1}{M-1}\sum_{i=1}^{M}\left(\eta_{i,t}-\hat{s}_\eta\right)^2+\frac{1}{M-1}\sum_{i=1}^{M}\left(r\left(t-t_i+\left(t_i-ts_i\right)\right)-\overline{r}(t)\right)^2 \\ &+2\hat{Cov}\left(r\left(t-t_i+\left(t_i-ts_i\right)\right),\eta_{i,t}\right) \\ &= \sigma_\eta^2+\hat{s}_V^2+\hat{s}_J^2+\hat{s}_{Cov}^2\end{aligned} \tag{5.9}$$

where $\hat{s}_J$ is drawn from a distribution that depends on the neuronal response $r(t)$, but is independent of the noise, and $\hat{s}_{Cov}$ is the random variable drawn from a Gaussian distribution that follows from the covariance term. Using the identity (Unnikrishnan et al., 2007):

$$\begin{aligned}V\left(\hat{Cov}(X,Y)\right) = \frac{1}{M}\Bigg(&E\left(\left(X-\overline{X}\right)^2\left(Y-\overline{Y}\right)^2\right)+\frac{1}{M-1}V(X)V(Y) \\ &-\frac{M-2}{M-1}E\left(\left(X-\overline{X}\right)\left(Y-\overline{Y}\right)\right)^2\Bigg)\end{aligned} \tag{5.10}$$

it can be shown that $\hat{s}_{Cov}$ is drawn from:

$$\hat{s}_{Cov} \in N\left(0,\frac{\sigma_\eta}{\sqrt{M-1}}\sqrt{V\left(\hat{s}_J\right)}\right) \tag{5.11}$$

Since $V\left(\hat{s}_J\right)$ goes down with M^{-1}, variance of the $\hat{s}_{Cov}$ drops down with M^{-2}. Therefore, for all practical purposes, $\hat{s}_{Cov}$ is negligible.

5.2.2. Time-average of signal variance

To measure the amount of temporal jitter of the neuronal responses, one can use jitter standard deviation (jitter std, σ_J). But, in order to use parametric models, it is necessary to estimate the amount of jitter without the knowledge of the neuronal response triggers t_i. One could simply measure the variance of the stimulus triggered response $\tilde{V}\left(r(t)\right)$ (Equation 5.9) at one particular time point and compare the measured values before and after the realignment procedure. If the realignment was successful, $\hat{s}_J$ will be smaller after the realignment. But, since the $\hat{s}_V$ term, arising from the noise in the signal, comes from a stochastic process, its value might go up and mask the reduction in $\hat{s}_J$. Neighbouring time points of the neuronal response are correlated in time and so is the variance term $\hat{s}_J$ arising from the jitter. On the other hand, noise often exhibits correlation on a

smaller time scale. Therefore, to improve the reliability of the jitter measure, I have averaged the variance of the stimulus triggered response over time (time-averaged variance, TAV):

$$TAV = \left\langle \tilde{V}\left(r(t)\right)\right\rangle = \frac{1}{\left(T_E - T_S\right)} \int_{T_S}^{T_E} V\left(\bar{r}(t)\right) dt \tag{5.12}$$

Variance of the TAV can be estimated by:

$$V\left(TAV\right) = \frac{1}{\left(T_E - T_S\right)^2} \int_{T_S}^{T_E} \int_{T_S}^{T_E} Cov\left(V\left(\bar{r}(t')\right), V\left(\bar{r}(t'')\right)\right) dt' dt'' \tag{5.13}$$

From equation (5.9) it follows that TAV is a stochastic measure of the jitter in a sense that:

$$\sigma_J' > \sigma_J'' \Rightarrow p\left(TAV' > TAV''\right) > 0.5 \tag{5.14}$$

where σ_J' and σ_J'' are the initial and the final jitter std.

As discussed before, averaging over time can reduce the variance of the TAV, thereby increasing the reliability of the measure. On the other hand, integrating over periods of time where neuronal response is low compared to the noise, or not present at all, will clearly reduce the TAV faster than reducing its variance. Therefore, the optimal integration time interval, for which the TAV measure shows highest reliability, exists.

I measured the jitter reduction using a difference of TAV ($dTAV$):

$$dTAV\left(\sigma_J', \sigma_J''\right) = TAV\left(\sigma_J''\right) - TAV\left(\sigma_J'\right) \tag{5.15}$$

and used these assumptions to perform calculations:

$$V\left(dTAV\left(\sigma_J', \sigma_J''\right)\right) = V\left(TAV\left(\sigma_J'\right)\right) + V\left(TAV\left(\sigma_J''\right)\right) \tag{5.16}$$

$$p\left(dTAV\left(\sigma_J', \sigma_J''\right) > 0\right) = \Phi\left(-dTAV\left(\sigma_J', \sigma_J''\right), \sqrt{V\left(dTAV\left(\sigma_J', \sigma_J''\right)\right)}\right) \tag{5.17}$$

where Φ is the cumulative distribution function of the Gaussian distribution.

5.2.3. Reliability of *dTAV* as a measure of jitter reduction

For the purposes of analytic calculations, I have modelled the distribution of the shifts ρ_J as Gaussian with zero mean and standard deviation σ_J:

$$\rho_J(\Delta t = t_i - ts_i) = N\left(0, \sigma_J\right) \tag{5.18}$$

Noise is modelled as white Gaussian noise with zero mean and standard deviation σ_η:

$$\rho_\eta(\eta) = N\left(0, \sigma_\eta\right) \tag{5.19}$$

Expectation and variance of the stimulus-triggered neuronal response are then given by:

$$\bar{r}(t) = \int_{-\infty}^{\infty}\int_{-\infty}^{\infty} \rho(\eta)\rho(\Delta t)\left(r(t-\Delta t)+\eta\right) d\eta d\Delta t \tag{5.20}$$

$$V\left(\bar{r}(t)\right) = \int_{-\infty}^{\infty}\int_{-\infty}^{\infty} \rho(\eta)\rho(\Delta t)\left(r(t-\Delta t)+\eta-\bar{r}(t)\right)^2 d\eta d\Delta t \tag{5.21}$$

In the case of limited number of trials M, variance needs to be estimated. Such estimation is also a normally distributed random variable with the variance given by:

$$V\left(\hat{V}\left(\bar{r}(t)\right)\right) = \frac{2V\left(\bar{r}(t)\right)^2}{n-1} + \frac{m_4}{n} \tag{5.22}$$

where m_4 is the fourth central moment of the distribution:

$$m_4 = \int_{-\infty}^{\infty}\int_{-\infty}^{\infty} \rho(\eta)\rho(\Delta t)\left(r(t-\Delta t)+\eta-\bar{r}(t)\right)^4 d\eta d\Delta t \tag{5.23}$$

As a model for neuronal responses, I designed mono-phasic and bi-phasic signals using one or two Gaussian functions:

$$r_{mono}(t) = N\left(0,\sigma_R\right) = \frac{1}{\sqrt{2\pi\sigma_R}} e^{-\frac{t^2}{2\sigma_R^2}} \tag{5.24}$$

$$r_{bi}(t) = N\left(0,\sigma_R\right) - 1.5N\left(5\sigma_R, 3\sigma_R\right) \tag{5.25}$$

Using the convolution theorem and the simple identity:

$$N(\mu_1,\sigma_1)\cdot N(\mu_2,\sigma_2) = \frac{1}{\sqrt{2\pi\left(\sigma_1^2+\sigma_2^2\right)}} e^{-\frac{(\mu_1-\mu_2)^2}{2\left(\sigma_1^2+\sigma_2^2\right)}} N\left(\frac{\mu_1\sigma_2^2+\mu_2\sigma_1^2}{\sigma_1^2+\sigma_2^2}, \frac{\sigma_1\sigma_2}{\sqrt{\sigma_1^2+\sigma_2^2}}\right) \tag{5.26}$$

this choice of neuronal responses significantly simplified the calculations in equations (5.22-5.25):

$$\bar{r}_{mono}(t) = N\left(0,\sqrt{\sigma_R^2+\sigma_S^2}\right) \tag{5.27}$$

$$V\left(\bar{r}_{mono}(t)\right) = \frac{1}{\sqrt{4\pi\sigma_R^2}} N\left(0,\sqrt{\frac{\sigma_R^2}{2}+\sigma_S^2}\right) - N\left(0,\sqrt{\sigma_R^2+\sigma_S^2}\right)^2 + \sigma_\eta^2 \tag{5.28}$$

$$\bar{r}_{bi}(t) = N\left(0,\sqrt{\sigma_R^2+\sigma_S^2}\right) - 1.5N\left(5\sigma_R,\sqrt{9\sigma_R^2+\sigma_S^2}\right) \tag{5.29}$$

$$
\begin{aligned}
V\left(\overline{r}_{bi}(t)\right) = {} & \frac{1}{2\sqrt{\pi}\sigma_R} N\left(0, \sqrt{\frac{\sigma_R^2}{2} + \sigma_S^2}\right) - \frac{3}{4\sqrt{5\pi}\sigma_R} e^{-\frac{5}{4}} N\left(\frac{\sigma_R}{2}, \sqrt{\frac{9\sigma_R^2}{10} + \sigma_S^2}\right) \\
& - \frac{1}{2\sqrt{\pi\left(\sigma_R^2 + \sigma_S^2\right)}} N\left(0, \sqrt{\frac{\sigma_R^2 + \sigma_S^2}{2}}\right) \\
& + \frac{3}{2\sqrt{\pi\left(5\sigma_R^2 + \sigma_S^2\right)}} e^{-\frac{25\sigma_R^2}{4\left(5\sigma_R^2 + \sigma_S^2\right)}} N\left(\frac{5\left(\sigma_R^2 + \sigma_S^2\right)}{2\left(5\sigma_R^2 + \sigma_S^2\right)}\sigma_R, \sqrt{\frac{\left(\sigma_R^2 + \sigma_S^2\right)\left(9\sigma_R^2 + \sigma_S^2\right)}{2\left(5\sigma_R^2 + \sigma_S^2\right)}}\right) \\
& + \frac{3}{8\sqrt{\pi}\sigma_R} N\left(5\sigma_R, \sqrt{\frac{9\sigma_R^2}{2} + \sigma_S^2}\right) - \frac{9}{8\sqrt{\pi\left(9\sigma_R^2 + \sigma_S^2\right)}} N\left(5\sigma_R, \sqrt{\frac{9\sigma_R^2 + \sigma_S^2}{2}}\right) + \sigma_\eta^2
\end{aligned}
\tag{5.30}
$$

Using equations (5.14) and (5.15), I calculated the expectation and the variance of the TAV for different times of integration, noise levels and amounts of jitter. In my calculations, integration time was symmetric around 0:

$$
TAV\left(T_I, \sigma_\eta, \sigma_J\right) = \frac{1}{2T_I} \int_{-T_I}^{T_I} V\left(\overline{r}\left(t; \sigma_\eta, \sigma_J\right)\right) dt \tag{5.31}
$$

$$
V\left(TAV\left(T_I, \sigma_\eta, \sigma_J\right)\right) = \frac{1}{4T_I^2} \int_{-T_I}^{T_I} \int_{-T_I}^{T_I} Cov\left(V\left(\overline{r}(t'; \sigma_\eta, \sigma_J)\right), V\left(\overline{r}(t''; \sigma_\eta, \sigma_J)\right)\right) dt' dt'' \tag{5.32}
$$

To calculate the covariance function of the stimulus-triggered response variance (Equation 5.32), I simulated 1000 repetitions of the 100 trial experiment. Reliability of the $dTAV$ as a measure of the jitter depends on the initial and the final amounts of the jitter. I used the value of 100ms for the initial jitter standard deviation and calculated the reliability of the $dTAV$ using equation (5.19) for values of final jitter standard deviation of 0ms to 120ms in steps of 1. Calculations were made for integration times ranging from 30ms to 850ms in steps of 30ms. To define different noise levels, we used signal to noise ratio (SNR) defined as the ratio of the peak of the signal and the standard deviation of the noise. Standard deviation of the noise was chosen such that SNR values were 0.03, 0.05, 0.08, 0.13, 0.20, 0.32, 0.50, 0.79, 1.26 and 2.00 for both mono and bi-phasic responses.

5.2.4. $dTAV$ realignment algorithm

$dTAV$ realignment algorithm (Figure 35) relies on the assumption that the distribution of shifts in the recorded neuronal signal is unimodal and that the neuronal responses can be represented with a small number of discrete features ($f_1,...,f_n$). In my case, these features were neuronal signals recorded at different time points after the stimulus ($\tau_1,...,\tau_n$):

$$
signal\left(t_i\right) = r\left(t - t_i\right) \Leftrightarrow \left(f_{1,i},...,f_{n,i}\right) \qquad f_{k,i} = signal\left(t_i + \tau_k\right) \tag{5.33}
$$

First step of my realignment algorithm is to select a subgroup of trials S that are already well aligned. In that case, stimulus times and neuronal response onset times can be used interchangeably, given an arbitrary bias. I selected a subgroup of trials containing half of the total number of trials, with the property of smallest variance in the Euklidian space spanned by the features of all possible such subgroups. I labelled the features from this trial subset as "positive" class (P_{class}). All the features from the same trial subset, but shifted arbitrarily in time, were labelled as "negative" class (N_{class}).

$$\begin{aligned} P_{class} &= \left\{ \left(f_{1,i}, ..., f_{n,i} \right), i \in S \right\} \\ N_{class} &= \left\{ \left(signal\left(ts_i + \tau_1 + \tau \right), ..., signal\left(ts_i + \tau_n + \tau \right) \right), i \in S, \tau \neq 0 \right\} \end{aligned} \tag{5.34}$$

These classes were used to build a quadratic discriminant analysis (QDA) model, which fits Gaussian distributions to each of the classes and gives the probability to belong to one of the classes for any arbitrary point in the feature space.

One could have selected a larger or a smaller trial subset, but certain issues arise from building the QDA model. If the number of the subset trials is two small, it will be hard to make a reliable estimation of the Gaussian distribution that fits the positive class. If the subset is too large, the mean of the positive Gaussian distribution will not represent the neuronal response properly, but rather the stimulus-triggered average neuronal response. Furthermore, the covariance matrix of the positive distribution will be overestimated, since it will include the larger jitter contribution. I found that using half of the trials worked well for the 100 trial experiment.

In the next step, QDA model is used to give a probability that a feature set from a given trial belongs to a positive class. I located the time of the maximum probability in a certain time range:

$$\tau_{i,MAX} = \max_{\tau} \arg\left(p_P\left(\left(signal\left(ts_i + \tau_1 + \tau \right), ..., signal\left(ts_i + \tau_n + \tau \right) \right) \right), t_S < \tau < t_E \right) \tag{5.35}$$

and used it to re-align the stimulus-triggered neuronal responses and calculate $dTAV$:

$$\breve{r}(t) = \frac{1}{M} \sum_{i=1}^{M} signal\left(t - ts_i - \tau_{i,MAX} \right) \tag{5.36}$$

$$dTAV\left(\tau_1, ..., \tau_n \right) = TAV_{START} - TAV\left(\tau_{1,MAX}, ..., \tau_{M,MAX} \right) \tag{5.37}$$

The whole procedure is then repeated for a different selection of features representing the neuronal response.

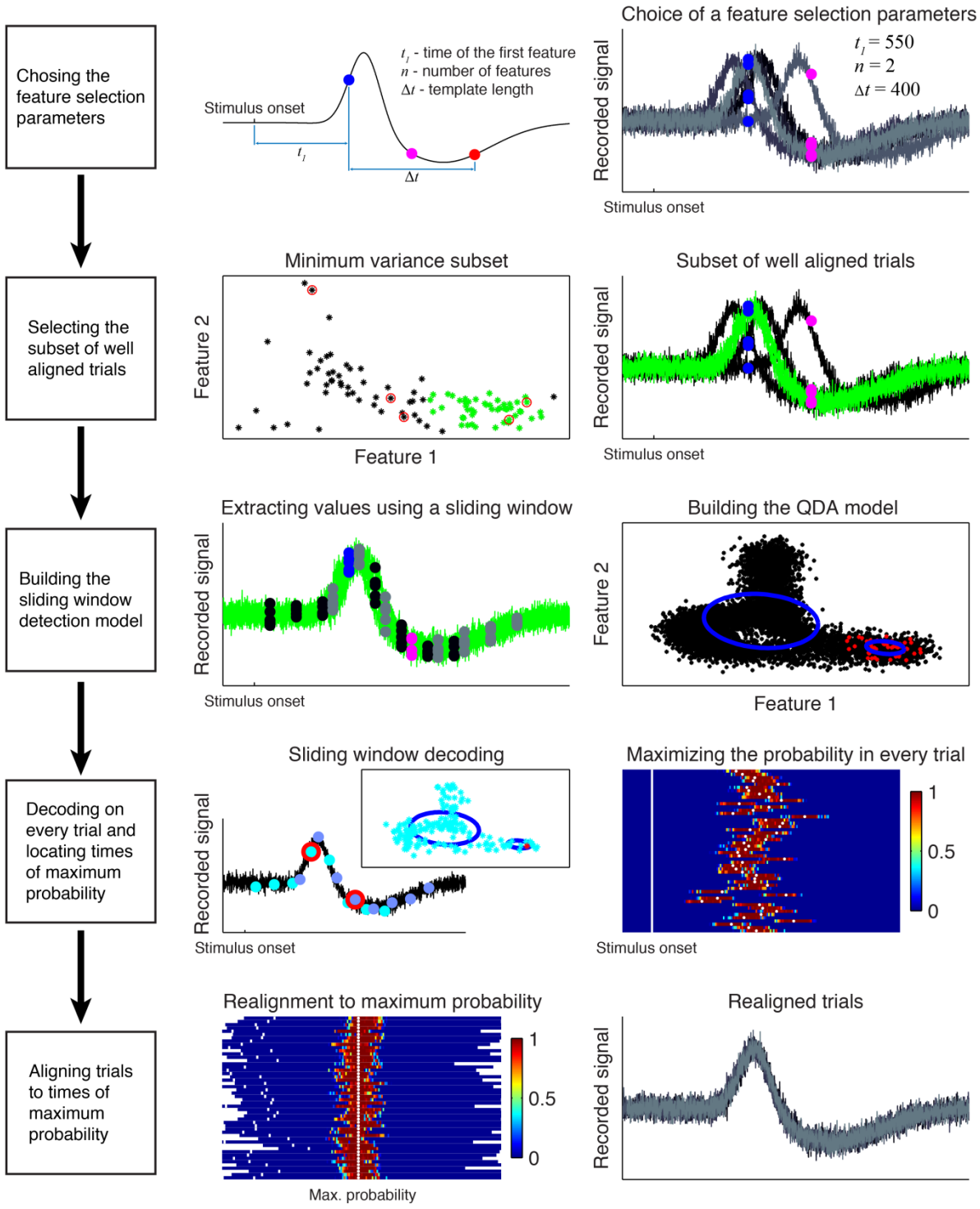

Figure 35. Steps of the *dTAV* inference realignment algorithm. First step: Response is represented by a small number of features. Left: Selected features are determined by the chosen array of equidistant time points parameterized by the time of the first feature t_1, number of features n and the temporal length of the array t_n- t_1. Values of these parameters are chosen arbitrarily. Right: Five example trials and the values of the chosen response features (blue and magenta circles). Second step: Subset of trials with the smallest within-subset variance is selected. Left: Values of the chosen response features for every trial shown in the feature space. Green stars show the chosen subset. Right: Five example trials with trials belonging to the chosen subset shown in green. Red circles in the left panel show the feature values of the five example trials. Third step: QDA model is built from the population of values extracted by the time sliding template. Left: Feature values for the model building are taken only from the selected subset of trials. Right: Positive class is made by extracting features using the previously chosen array (left: blue and magenta dots; right: red stars), while the "negative" class is made by sliding the same array in time (left: black and gray dots; right: black stars). Blue ellipses show the estimated standard deviation for "positive" and "negative" class. Fourth step: Posterior probability of

belonging to the "positive" class is calculated for every set of features extracted by sliding the chosen array in every trial. Left: Extracted features in one trial and in feature space. Red circle and red star represent the feature with the maximum probability for "positive" class. Right: Features with maximum probability for "positive" class are found in each trial (white dots). Fifth step: Left: Trials are realigned to the points of maximum probability. Right: Five example trials realigned to the point of maximum probability.

In addition to parameters that determine feature extraction, it is possible to introduce other parameters in the realignment algorithm, such as the integration time used to calculate the TAV or the size of the trial subgroup used to build the QDA model. After all the parameter values have been exhausted, a set of time shifts is chosen by maximizing $dTAV$:

$$\left(\tau_{1,MAX},\ldots,\tau_{M,MAX}\right)_{Chosen} = \max_{parameters}\arg\left(dTAV\right) \tag{5.38}$$

According to equation (5.19), using these time shifts gives the highest probability that the jitter is reduced.

5.2.5. Simulated data

I used $dTAV$ realignment algorithm to realign the neuronal responses in a range of simulated experiments to identify the range of noise levels for which $dTAV$ algorithm reduces the jitter. In addition to $dTAV$ algorithm, I also used the algorithm published by Nawrot et al. (Nawrot et al., 2003) and compared the results.

Simulations were made for two neuronal responses, mono-phasic and bi-phasic response, whose shape resembled a large number of reported neurophysiological responses. Each simulation consisted of 100 simulated experiments, each consisting of 200 trials. In each trial, single channel neuronal response to an arbitrary stimulus was recorded at 1KHz. Neuronal responses were modelled as (Figure 36):

$$f(\tau)=\begin{cases} e^{\frac{(\tau-250)^2}{2\cdot(83)^2}} & \text{for } 0\le\tau<500 \\ 0 & \text{othervise}\end{cases} \tag{5.39}$$

$$f(\tau)=\begin{cases} e^{\frac{(\tau-125)^2}{2\cdot(25)^2}} - 1.5e^{\frac{(\tau-250)^2}{2\cdot(83)^2}} & \text{for } 0\le\tau<500 \\ 0 & \text{othervise}\end{cases} \tag{5.40}$$

Noise in the recordings was simulated as white Gaussian noise with standard deviation σ_η of: 31.62, 19.95, 12.59, 7.94, 5.01, 3.16, 2.00, 1.26, 0.79 and 0.50 (SNR of 0.03, 0.05, 0.08, 0.13, 0.20, 0.32, 0.50, 0.79, 1.26 and 2.00). Temporal distances between the stimulus times were drawn from a Gaussian distribution N(10000,10000). To keep neuronal responses from overlapping, values bellow 3000 were redrawn. Times of the neuronal response offset were drawn from a Gaussian distribution

$N(0,100)$. To keep the recorded triggers from being too far from the real triggers, all shift values smaller than -300 or bigger than 300 were redrawn. Therefore simulated data can be shown in form:

$$data_i(t) = \sum_j f\left(t - \left(t_j + \tau_j\right)\right) + \eta$$
$$\eta \in N(0, \sigma_{\eta,i});\ t_{j+1} - t_j \in N(10000,10000);\ \tau_j \in N(0,100) \tag{5.41}$$

To fairly simulate the outcome of the experiment, I assumed that the person analyzing the data would filter the data using a low-pass filter, since neuronal responses are present in a narrow low frequency band. Therefore, I filtered the simulated recordings using the 2nd order symmetric Savitzky-Golay filter (Savitzky and Golay, 1964; Steinier et al., 1972) with a time window of 100ms, 250ms, 500ms or 1000ms.

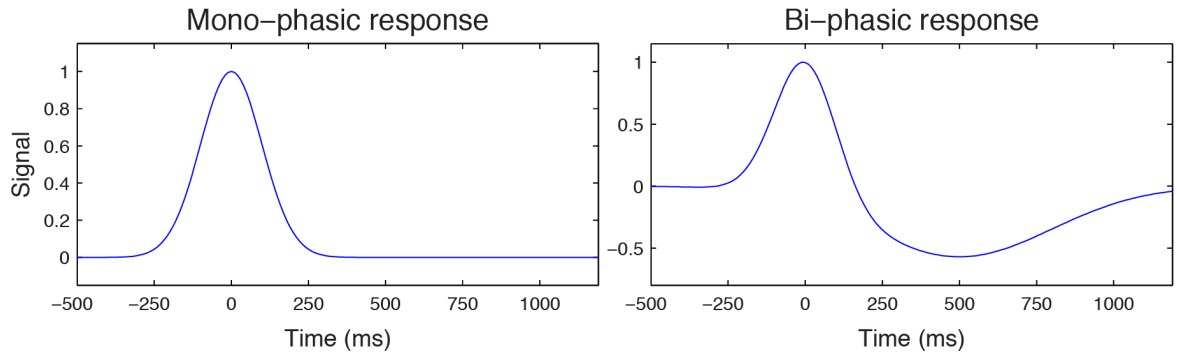

Figure 36. Simulated mono-phasic (left) and bi-phasic (right) neuronal responses.

Array of time points used to extract features of neuronal responses was controlled by three parameters: time of the first feature in respect to the stimulus τ_1 (used values from -125ms to 1324ms in steps of 63ms), temporal distance between first and the last feature τ_1- τ_n (100ms, 250ms, 500ms or 1000ms) and the number of features n (2, 4, 8 or 12). I used the integration T_I of 350ms and the probability maximum was searched in the time range from 300ms before the stimulus till 300ms after the stimulus.

To fit the quadratic function in the algorithm published by Nawrot et al. (Nawrot et al., 2003), I used the neighbourhood of 10ms. Since the data was filtered before using the algorithm, I assumed that size of the neighbourhood will not have a large effect on the precision of the 1st and 2nd derivative estimate at the point of the function maximum. In their study, Nawrot et al. do not specify how to fit the quadratic function and do not discuss the algorithm's behaviour in respect to the neighbourhood used for fitting.

5.3. Results

5.3.1. Analytical analysis

Assuming the neuronal responses model defined in section 5.2.1, I calculated the dependence of $dTAV$ on the reduction of the jitter for different noise levels and integration times. Results are summarized on Figure 37 for mono-phasic signal and on Figure 38 for bi-phasic signal.

For integration times similar to the width of the response, expectation of the $dTAV$ increases almost linearly with the reduction of the jitter standard deviation (Figure 37a, Figure 38a). Expectation of the $dTAV$ does not depend on the level of the noise. On the other hand, standard deviation of $dTAV$ (Figure 37b, Figure 38b) is, in my examples, dominated by noise for high noise levels and comparable or bigger than the estimation of the $dTAV$. For low noise levels, $dTAV$ becomes dominated by the jitter. In such cases the realignment problem becomes trivial.

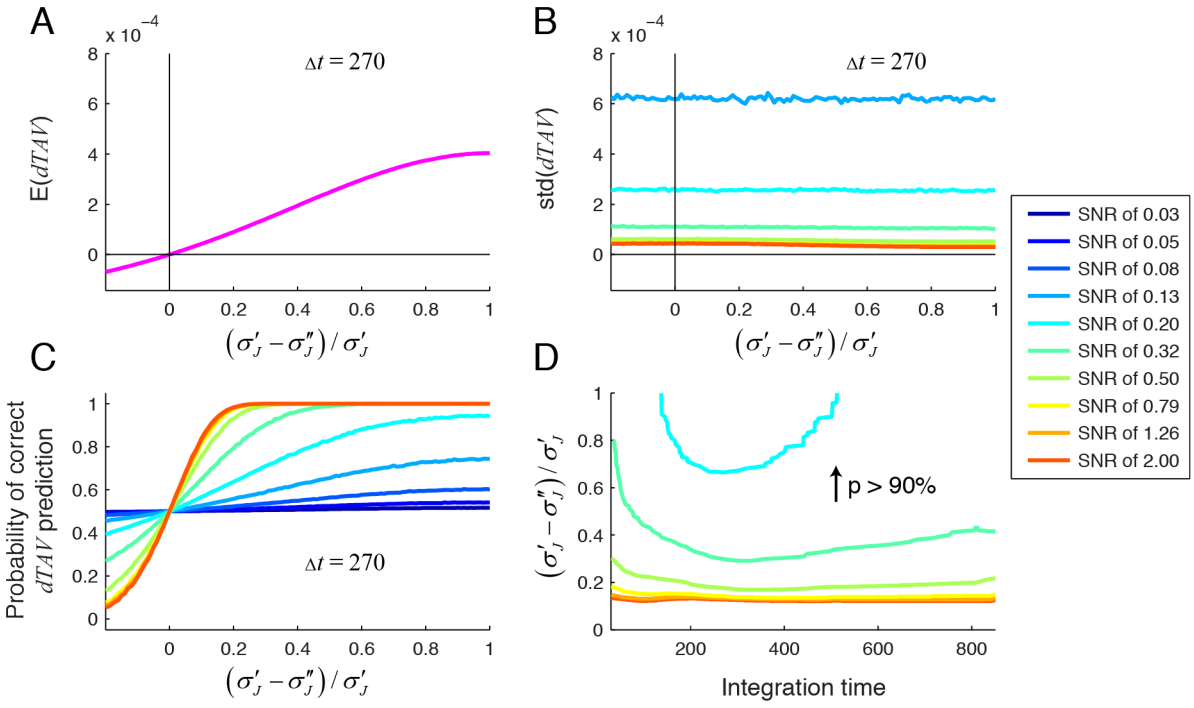

Figure 37. Reliability of $dTAV$ as a measure of jitter reduction for different SNRs and for mono-phasic neuronal response. Calculation is made experiment consisting of 100 trials. A: Expectation of $dTAV$ as a function of jitter std reduction. Function is independent of the noise. B: Standard error of the $dTAV$ as a function of jitter std reduction for different SNRs. Standard errors of $dTAV$ for SNR of 0.13 and lower are above 5.5 x 10^{-4} and are, therefore, not shown. C: Probability of correct $dTAV$ prediction as a function of jitter std reduction for different SNRs. D: Values of jitter std. reduction and integration times in which probability of correct $dTAV$ prediction reaches 90% for different SNRs. For all pairs of jitter std reduction values and integration times above the line correct $dTAV$ prediction is above 90%. For SNRs of 0.13 and lower, probability of correct $dTAV$ prediction never reaches 90%.

To measure how well can one rely on the $dTAV$ as a measure of jitter reduction, I calculated the probability of correct $dTAV$ prediction, defined as probability that the $dTAV$ is positive if the jitter is reduced (Figure 37c, Figure 38c). As the noise level is reduced, the probability increases up to 1,

even for the smallest jitter reductions. If the noise level is high, probability will never reach 1, even when the jitter is completely removed.

To give an insight on the dependence of the probability of correct $dTAV$ prediction on the integration time, I calculated the values of integration times and reductions of jitter std for which the probability of correct $dTAV$ prediction reaches 90% (Figure 37d, Figure 38d). For each noise level there is an optimal integration time. $dTAV$ prediction improves sharply for times smaller than the optimal integration time, while it is dropping slowly for integration times bigger than the optimal integration time. Therefore, choosing a short integration times could be more disadvantageous than choosing a longer integration time.

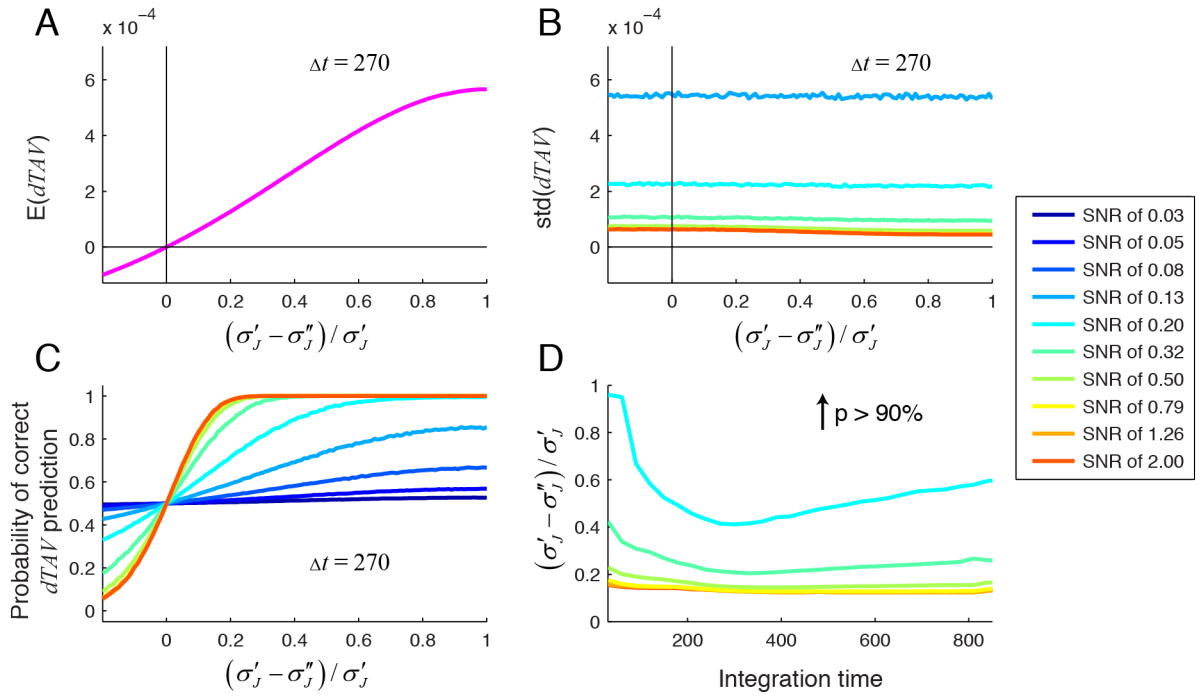

Figure 38. Reliability of $dTAV$ as a measure of jitter reduction for different SNRs and bi-phasic neuronal response. See Figure 36 caption for details.

5.3.2. Re-alignment of simulated data

I ran $dTAV$ and Nawrot realignment algorithms on 100 simulated experiments for mono-phasic and by-phasic neuronal responses and different levels of noise (Figure 39). For high levels of noise (filter window of 250ms; mono-phasic signal: SNR<0.2; bi-phasic signal: SNR<0.32) both algorithms increase the amount of jitter, rather than decrease it. For medium noise levels (filter window of 250ms; mono-phasic signal: 0.2<SNR<0.75; bi-phasic signal: 0.32<SNR<1.26) $dTAV$ algorithm outperforms the Nawrot algorithm ($p<10^{-9}$, Mann–Whitney–Wilcoxon signed test). For low noise conditions (mono-phasic signal: 0.8<SNR; bi-phasic signal: 1.5<SNR), both algorithms remove almost all jitter from the recorded signal. In some of the low noise cases Nawrot algorithm achieves higher

jitter reduction, but the difference is very small (<0.08) and significant only in the case of mono-phasic signal for SNR=0.79 (p=0.026, Mann–Whitney–Wilcoxon signed test).

Choice of the filter can be important for successful re-alignment. For both algorithms, re-alignment worked best when filter length of 250ms was used. For $dTAV$ algorithm, differences in the jitter reduction between using filter window length of 250ms and using filter window lengths of 100ms and 500ms were small. For Nawrot algorithm, variability of jitter reduction with the choice of filter window length was much larger. When filter window length of 1000ms was used, jitter reduction was much smaller than when using other filter window lengths for both algorithms.

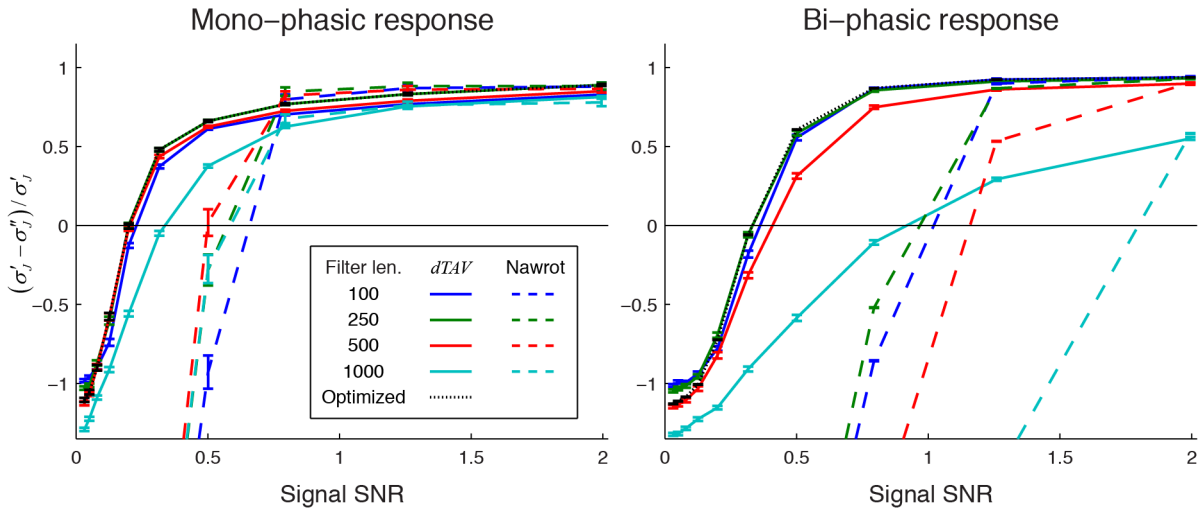

Figure 39. Reduction of jitter standard deviation for $dTAV$ algorithm (full lines) and the algorithm published by Nawrot et al. (dashed lines) for mono-phasic (left) and bi-phasic (right) simulated neural responses and different SNRs. Reduction is shown for different low-pass filters, averaged over the simulation repetitions. In addition, for $dTAV$ algorithm, reduction is shown when the filter length is optimized as one of the algorithm parameters (dotted lines). Error bars show the standard errors of the mean.

When filter window length is included as an additional parameter whose value was chosen by maximizing $dTAV$, final jitter reduction is not significantly different from the jitter reduction when only filter length of 250ms is used (Figure 1). Thus, $dTAV$ algorithm can automatically select the proper filter length if filter length is included as an additional parameter. On the other hand, Nawrot algorithm has no way of estimating whether the filter length was correctly chosen. The success of such non-parametric algorithm depends on the proper choice of the person performing the data analysis.

5.4. Discussion

In this chapter, I presented a novel method, $dTAV$ inference based algorithm for realignment of neuronal responses. Algorithm is based on using $dTAV$ as a measure of jitter reduction and inference algorithms for recognizing the temporal shifts of single trial neuronal responses. I show that, by

using $dTAV$ algorithm, it is possible to realign mono and bi-phasic single trial neuronal responses for the noise levels commonly present in the neurophysiologic experiments.

As examples of neuronal responses, I used mono and bi-phasic responses composed out of one and two Gaussian functions. Realignment results on simulated data show differences between mono and bi-phasic response shapes, suggesting that signal shape plays a role on the applicability of the $dTAV$ algorithm. Still, the success of the method in reducing the jitter in the medium and low noise levels (SNR>0.32), frequently reported in neurophysiological studies (Hu et al., 2011; Matsuo et al., 2011; Maynard et al., 1997; Pistohl et al., 2012; Rohde et al., 2002), suggests that the algorithm can still be used in large number of cases.

My simulations used an example of a neurophysiologic study where the recorded signal is analogue. On the other hand, many neuroscietific studies have been performed by recording and analyzing the spikes of neuronal cells (Boraud et al., 2002; Georgopoulos et al., 1986; Hochberg et al., 2006; Hubel and Wiesel, 2009), essentially a point process signal. Even though my algorithm cannot be directly applied to the point processes, single unit spike times can be used to estimate instantaneous neuronal firing rates (Cunningham et al., 2007), which is an analogue function. By using such methods, it is possible to apply my realignment algorithm to spike signals.

I compared my $dTAV$ algorithm to the algorithm published by Nawrot et al. (Nawrot et al., 2003) which was designed for the same purpose of reducing the temporal jitter in the neuronal responses. $dTAV$ algorithm outperformed the algorithm by Nawrot et al. $dTAV$ algorithm works with a large number of parameters whose values have to be determined. This process may be computationally demanding and, therefore, may be time consuming. On the other hand, optimal parameter values can provide additional information about the underlying neuronal response. Integration time T_I and time of the first and the last feature t_1 and t_n can provide a good estimate on the temporal location and duration of the stimulus related neuronal response, while the number of features n can give an insight into response complexity. In contrast, algorithm published by Nawrot et al. has no parameters. Therefore, in the case of limited computational resources, Nawrot et al. algorithm might be the only possible solution. One should take into account that, and my simulation results suggest that, in the case of medium and high noise levels (SNR<1) Nawrot et al. algorithm might even be counterproductive, increasing the amount of jitter in the signal.

In general, realignment algorithms can be used to improve the analysis of neurophysiologic signals by improving the estimation of the underlying neuronal responses. The obvious case is the estimation of the neuronal responses by calculating trial averages. As shown in my example (Figure 34), even for the case where all neuronal responses are identical and the noise is uncorrelated to the

signal, averaging the jittered neuronal responses can lead to distorted estimation of the neuronal responses and the incorrect estimation of the amount of noise. In such simple situation, removing the jitter improves the estimation of the neuronal response and improves the estimation of the noise. A large number of neurophysiologic studies look at neuronal responses to different stimuli. In studies looking at the sensory brain regions, neuronal responses seem to be well locked to the stimulus (Richmond and Optican, 1990). Therefore, realignment methods might be of limited use for studies looking at sensory neuronal responses. On the other hand, neuronal responses related to higher level processing may not solely depend on the stimulus and, therefore, might be initiated with variable lags after the stimulus presentation. In such cases, temporal jitter may be present. Therefore, realignment algorithms could largely improve the examination of such neuronal response, making it easier to analyze the recordings and compare the results with other studies.

Additionally, systems using detection of events based on neuronal recordings (Achtman et al., 2007; Awwad Shiekh Hasan and Gan, 2010; Bashashati et al., 2007; Hwang and Andersen, 2009; Levine et al., 2000; Solis-Escalante et al., 2008) might benefit from re-alignment algorithms. Such systems require a certain number of trials containing the neuronal responses to build the model used to detect the events related to those neuronal responses. If the jitter or the neuronal responses used to train the model is removed, detection may perform better.

In summary, I showed that $dTAV$ realignment algorithm can reduce the jitter of the analogue neuronal responses for the commonly encountered neuronal response shapes and in commonly reported noise levels. Use of this algorithm could improve data analysis and comparison of neuronal responses and improve the performance of asynchronous detection systems.

Chapter 6

Conclusions

In this thesis, I presented the first online BMI based on extracting movement parameters of a subject's arm from ECoG recordings. The same approach has been used to achieve the most powerful BMIs up to date (Hochberg et al., 2006; Kim et al., 2008; Santhanam et al., 2006; Velliste et al., 2008). Unlike the BMI presented here, these powerful BMIs used SUA recordings. To record SUA signals, it is necessary to implant electrodes into the cortex, making the implantation procedure highly invasive. In addition, SUA recordings require spike sorting and can be unstable (Moran, 2010), which can lead to reduced reliability of operating such BMIs. On the other hand, ECoG does not require penetration of the cortex and shows stability of recordings over several months (Chao et al., 2010). Therefore, ECoG is a possible alternative for achieving BMIs (Schalk, 2010).

The BMI presented here is not capable of providing multidimensional continuous control needed to operate hand and arm prosthesis, such as shown to be controlled using SUA based BMIs (Hochberg et al., 2006; Velliste et al., 2008). BMI presented here merely demonstrates a proof of concept that approach of using movement parameters of a subject's arm from ECoG recordings can be used to achieve a BMI. To reach the level of control currently shown by SUA based BMIs, it is necessary to improve on the demonstrated level of control. There are numerous reasons why this is highly likely to be possible.

Most of the ECoG studies so far have been conducted by performing studies on human patients undergoing epilepsy assessments (Keene et al., 2000). Benefit of such procedures is an ability to perform human invasive recordings without additional medical risk. On the other hand, these studies are restricted on using epilepsy assessment ECoG implants that feature electrodes of 4mm in diameter and 1cm apart. Large number of studies suggested that epicortical potentials recorded with higher spatial resolution would be more informative (Slutzky et al., 2010; Weliky et al., 2003). These studies led to the development of ECoG implants with spatial resolution on the level of micrometers (µECoG; Gierthmuehlen et al., 2011; Leuthardt et al., 2009; Rubehn et al., 2009; Wang et al., 2009). A number of such implants are currently undergoing clinical evaluation and should soon be used in clinical trials designed to help paralyzed patients control prosthetic devices though BMIs (Thongpang et al., 2011; Wang et al., 2010).

BMI studies have shown that subjects can improve BMI control through repeated use (Ganguly and Carmena, 2009; McFarland et al., 2010; Wang et al., 2010). These studies shown that improvement

in control can be quite slow and requires at least several days to make a significant impact. Unfortunately, this principle could not be used with the here presented BMI, since patients undergoing epilepsy assessment were allowed to dedicate only a couple of hours for research experiments. If the ECoG grids were implanted for BMI use, subjects would use BMIs continuously during every day. This would improve the accuracy of the current level of control or even increase the level of control of such BMIs.

Such improvement through learning and continuous use would be greatly facilitated if the BMI algorithm could recognize whether it is consistently making decoding errors (Blumberg et al., 2007; Rotermund et al., 2006). A number of studies showed that error related neuronal responses (ERNR) are present in the brain (Bechtereva et al., 2005; Diedrichsen et al., 2005; Krigolson et al., 2008). In the third chapter of this thesis, I demonstrated that ERNRs to two different types of errors, outcome error and execution error, can be recorded using the ECoG and can also be differentiated based on the same signals. Outcome error appears when subject fails to achieve the intended goal (Krigolson et al., 2008), while execution error arises when the decoded trajectory is different enough from the intended trajectory (Diedrichsen et al., 2005). Both of these errors can be used to facilitate the adaptation of the BMI decoder in a separate way. Outcome error can provide a more general feedback on the BMI performance, possibly serving as critic in the reinforcement learning algorithms. Execution errors provide a more direct feedback, possibly marking the part of the trajectory that BMI decoded incorrectly.

Findings presented in chapter 3 were used in chapter 4 to demonstrate that ERNRs can be used for detection of outcome and execution error events. In both chapters 3 and 4, I showed that there is no specific cortical region that is a source of ECoG ERNR signals, but that both outcome and execution ERNRs could be identified and detected in motor cortex. This is of high importance since motor cortex is a primary target for BMI implants. Future ECoG implants implanted for the purpose of BMI could be much smaller in size (Leuthardt et al., 2009; Rubehn et al., 2009; Wang et al., 2009), thereby covering only a limited part of the cortex. Using the same ECoG implant for both BMI control and error detection will greatly reduce the size of the open wound necessary during the implantation procedure, thereby reducing the medical risk of the surgical procedure. Such advancement would make ECoG based BMIs safer for future users.

Whether the here shown detection accuracy is good enough to improve the BMI decoder is an open question. To fully answer this question, one would need to demonstrate an online ECoG based BMI with an adaptive algorithm using error detection and show that it superior to ECoG based BMI not using error detection. This is an interesting topic for future studies, but some other simulation studies suggest that error signals carrying some information about the decoding errors could be

beneficial for the BMI operation (Blumberg et al., 2007; Rotermund et al., 2006). These studies have also showed that improving the reliability of the detector increases the speed of the BMI decoder improvement. In chapter 5, I presented a method for re-alignment of neuronal responses. This method is designed to reduce the variability of neuronal responses. Results from chapter 4 suggest that most of the ERNR can be reliably detected given the tolerance of less than 400ms, while using a much smaller tolerance of 50ms greatly reduces detection. This suggests that variability of ERNRs in respect to the error events that elicited those ERNRs is not negligible. When designing a detection algorithm in Chapter 4, I assumed that all ERNR are synced with corresponding error events. Training the detection algorithm under such assumptions may have caused some detection errors. Re-alignment method presented in chapter 5 might be used to re-align ERNRs used to train error detection algorithm and, therefore, possibly improve the error detection accuracy.

This thesis demonstrates a proof of concept for a BMI based on extracting movement parameters of a subject's arm from ECoG recordings. It also demonstrates that error events can be identified and detected from ECoG recordings. Detection of error events can be used to improve the accuracy and level of control of a ECoG based BMI. In addition, a novel method for re-alignment of neuronal responses is presented. This method could further improve ECoG based error detection and, therefore, improve the ECoG based BMIs as well. Taken together, presented research significantly improves the prospects that ECoG based BMI may be used to provide paralyzed patients with a medically safe way to operate anthropomorphic hand and arm prosthetic devices in the future.

Bibliography

One Degree of Separation, Paralysis and Spinal Cord Injury in the United States. Christopher Dana Reeve Foundation, 2009.

Abdelnour AF, Huppert T. Real-time imaging of human brain function by near-infrared spectroscopy using an adaptive general linear model. NeuroImage, 2009; 46: 133-43.

Achtman N, Afshar A, Santhanam G, Yu BM, Ryu SI, Shenoy KV. Free-paced high-performance brain-computer interfaces. J Neural Eng, 2007; 4: 336-47.

Allison BZ, McFarland DJ, Schalk G, Zheng SD, Jackson MM, Wolpaw JR. Towards an independent brain-computer interface using steady state visual evoked potentials. Clin Neurophysiol, 2008; 119: 399-408.

Arno PS, Levine C, Memmott MM. The economic value of informal caregiving. Health Aff (Millwood), 1999; 18: 182-8.

Awwad Shiekh Hasan B, Gan JQ. Unsupervised movement onset detection from EEG recorded during self-paced real hand movement. Med Biol Eng Comput, 2010; 48: 245-53.

Ball T, Kern M, Mutschler I, Aertsen A, Schulze-Bonhage A. Signal quality of simultaneously recorded invasive and non-invasive EEG. NeuroImage, 2009a; 46: 708-16.

Ball T, Schulze-Bonhage A, Aertsen A, Mehring C. Differential representation of arm movement direction in relation to cortical anatomy and function. J Neural Eng, 2009b; 6: 016006.

Bartels J, Andreasen D, Ehirim P, Mao H, Seibert S, Wright EJ, Kennedy P. Neurotrophic electrode: method of assembly and implantation into human motor speech cortex. J Neurosci Methods, 2008; 174: 168-76.

Bashashati A, Ward RK, Birch GE. Towards development of a 3-state self-paced brain-computer interface. Comput Intell Neurosci, 2007: 84386.

Bechtereva NP, Shemyakina NV, Starchenko MG, Danko SG, Medvedev SV. Error detection mechanisms of the brain: background and prospects. International journal of psychophysiology : official journal of the International Organization of Psychophysiology, 2005; 58: 227-34.

Benjamini Y, Hochberg Y. Controlling the False Discovery Rate - a Practical and Powerful Approach to Multiple Testing. J Roy Stat Soc B Met, 1995; 57: 289-300.

Benjamini Y, Yekutieli D. The control of the false discovery rate in multiple testing under dependency. Journal of the Royal Statistical Society. Series B (Methodological), 2001; 29: 1165–88.

Birbaumer N. Breaking the silence: brain-computer interfaces (BCI) for communication and motor control. Psychophysiology, 2006; 43: 517-32.

Birbaumer N, Ghanayim N, Hinterberger T, Iversen I, Kotchoubey B, Kubler A, Perelmouter J, Taub E, Flor H. A spelling device for the paralysed. Nature, 1999; 398: 297-8.

Bjornsson CS, Oh SJ, Al-Kofahi YA, Lim YJ, Smith KL, Turner JN, De S, Roysam B, Shain W, Kim SJ. Effects of insertion conditions on tissue strain and vascular damage during neuroprosthetic device insertion. J Neural Eng, 2006; 3: 196-207.

Blankertz B, Dornhege G, Krauledat M, Muller KR, Curio G. The non-invasive Berlin Brain-Computer Interface: fast acquisition of effective performance in untrained subjects. NeuroImage, 2007; 37: 539-50.

Blankertz B, Dornhege G, Schäfer C, Krepki R, Kohlmorgen J, Müller K-R, Kunzmann V, Losch F, Curio G. Boosting bit rates and error detection for the classification of fast-paced motor commands based

on single-trial EEG analysis. IEEE transactions on neural systems and rehabilitation engineering : a publication of the IEEE Engineering in Medicine and Biology Society, 2003; 11: 127-31.

Blumberg J, Rickert J, Waldert S, Schulze-Bonhage A, Aertsen A, Mehring C. Adaptive classification for brain computer interfaces. Conf Proc IEEE Eng Med Biol Soc, 2007; 2007: 2536-9.

Boatman-Reich D, Franaszczuk PJ, Korzeniewska A, Caffo B, Ritzl EK, Colwell S, Crone NE. Quantifying auditory event-related responses in multichannel human intracranial recordings. Front Comput Neurosci, 2010; 4: 4.

Boraud T, Bezard E, Bioulac B, Gross CE. From single extracellular unit recording in experimental and human Parkinsonism to the development of a functional concept of the role played by the basal ganglia in motor control. Prog Neurobiol, 2002; 66: 265-83.

Brazy JE. Near-infrared spectroscopy. Clin Perinatol, 1991; 18: 519-34.

Brunner P, Ritaccio AL, Emrich JF, Bischof H, Schalk G. Rapid Communication with a "P300" Matrix Speller Using Electrocorticographic Signals (ECoG). Front Neurosci, 2011; 5: 5.

Buttfield A, Ferrez P, Millán Jd. Towards a robust BCI: error potentials and online learning. IEEE transactions on neural systems and rehabilitation engineering : a publication of the IEEE Engineering in Medicine and Biology Society, 2006; 14: 164-8.

Buzsaki G. Large-scale recording of neuronal ensembles. Nat Neurosci, 2004; 7: 446-51.

Carmena JM, Lebedev MA, Crist RE, O'Doherty JE, Santucci DM, Dimitrov DF, Patil PG, Henriquez CS, Nicolelis MA. Learning to control a brain-machine interface for reaching and grasping by primates. PLoS Biol, 2003; 1: E42.

Chao ZC, Nagasaka Y, Fujii N. Long-term asynchronous decoding of arm motion using electrocorticographic signals in monkeys. Front Neuroengineering, 2010; 3: 3.

Cohen D. Magnetoencephalography: detection of the brain's electrical activity with a superconducting magnetometer. Science, 1972; 175: 664-6.

Crone NE, Boatman D, Gordon B, Hao L. Induced electrocorticographic gamma activity during auditory perception. Brazier Award-winning article, 2001. Clin Neurophysiol, 2001; 112: 565-82.

Crone NE, Miglioretti DL, Gordon B, Lesser RP. Functional mapping of human sensorimotor cortex with electrocorticographic spectral analysis. II. Event-related synchronization in the gamma band. Brain, 1998a; 121 (Pt 12): 2301-15.

Crone NE, Miglioretti DL, Gordon B, Sieracki JM, Wilson MT, Uematsu S, Lesser RP. Functional mapping of human sensorimotor cortex with electrocorticographic spectral analysis. I. Alpha and beta event-related desynchronization. Brain, 1998b; 121 (Pt 12): 2271-99.

Crone NE, Sinai A, Korzeniewska A. High-frequency gamma oscillations and human brain mapping with electrocorticography. Prog Brain Res, 2006; 159: 275-95.

Cunningham JP, Yu BM, Sahani M, Shenoy KV. Inferring neural firing rates from spike trains using {G}aussian processes. Neural Coding, Computation and Dynamics (NCCD), 2007.

Dagnelie G, Spekreijse H, van Dijk B. Topography and homogeneity of monkey V1 studied through subdurally recorded pattern-evoked potentials. Vis Neurosci, 1989; 3: 509-25.

Daly JJ, Wolpaw JR. Brain-computer interfaces in neurological rehabilitation. Lancet Neurol, 2008; 7: 1032-43.

Demirer RM, Ozerdem MS, Bayrak C. Classification of imaginary movements in ECoG with a hybrid approach based on multi-dimensional Hilbert-SVM solution. J Neurosci Methods, 2009; 178: 214-8.

Dickey AS, Suminski A, Amit Y, Hatsopoulos NG. Single-unit stability using chronically implanted multielectrode arrays. J Neurophysiol, 2009; 102: 1331-9.

Diedrichsen J, Hashambhoy Y, Rane T, Shadmehr R. Neural correlates of reach errors. The Journal of neuroscience : the official journal of the Society for Neuroscience, 2005; 25: 9919-31.

DiGiovanna J, Mahmoudi B, Fortes J, Principe J, Sanchez J. Coadaptive brain-machine interface via reinforcement learning. IEEE transactions on bio-medical engineering, 2009; 56: 54-64.

Donoghue JP, Nurmikko A, Black M, Hochberg LR. Assistive technology and robotic control using motor cortex ensemble-based neural interface systems in humans with tetraplegia. J Physiol-London, 2007; 579: 603-11.

Donoghue JP, Nurmikko A, Friehs G, Black M. Development of neuromotor prostheses for humans. Suppl Clin Neurophysiol, 2004; 57: 592-606.

Efron B, Tibshirani R. An introduction to the bootstrap. Chapman & Hall: New York, 1993.

Falkenstein M, Hohnsbein J, Hoormann J, Blanke L. Effects of crossmodal divided attention on late ERP components. II. Error processing in choice reaction tasks. Electroencephalogr Clin Neurophysiol, 1991; 78: 447-55.

Fan R-E, Chen P-H, Lin C-J. Working Set Selection Using Second Order Information for Training Support Vector Machines. Journal of Machine Learning Research, 2005; 6: 1889–918.

Farwell LA, Donchin E. Talking off the top of your head: toward a mental prosthesis utilizing event-related brain potentials. Electroencephalogr Clin Neurophysiol, 1988; 70: 510-23.

Ferrez P, del R Millan J. Error-related EEG potentials generated during simulated brain-computer interaction. IEEE transactions on bio-medical engineering, 2008; 55: 923-9.

Fetz EE. Operant conditioning of cortical unit activity. Science, 1969; 163: 955-8.

Fetz EE, Finocchio DV, Baker MA, Soso MJ. Sensory and motor responses of precentral cortex cells during comparable passive and active joint movements. J Neurophysiol, 1980; 43: 1070-89.

Foerster O. The cerebral cortex in man. Lancet, 1931; 221: 309–12.

Fraser GW, Chase SM, Whitford A, Schwartz AB. Control of a brain-computer interface without spike sorting. J Neural Eng, 2009; 6: 055004.

Freeman WJ, Rogers LJ, Holmes MD, Silbergeld DL. Spatial spectral analysis of human electrocorticograms including the alpha and gamma bands. J Neurosci Methods, 2000; 95: 111-21.

Friedman JH. Regularized Discriminant-Analysis. J Am Stat Assoc, 1989; 84: 165-75.

Ganguly K, Carmena JM. Emergence of a stable cortical map for neuroprosthetic control. PLoS Biol, 2009; 7: e1000153.

Gaona CM, Sharma M, Freudenburg ZV, Breshears JD, Bundy DT, Roland J, Barbour DL, Schalk G, Leuthardt EC. Nonuniform high-gamma (60-500 Hz) power changes dissociate cognitive task and anatomy in human cortex. J Neurosci, 2011; 31: 2091-100.

Gehring W, Goss B, Coles M, Meyer D, Donchin E. A neural system for error detection and compensation. Psychological Science, 1993; 4: 385-90.

Georgopoulos AP, Caminiti R, Kalaska JF, Massey JT. Spatial coding of movement: a hypothesis concerning the coding of movement direction by motor cortical populations. Exp. Brain Res., 1983; Supplement 7: 327–36.

Georgopoulos AP, Langheim FJ, Leuthold AC, Merkle AN. Magnetoencephalographic signals predict movement trajectory in space. Exp Brain Res, 2005; 167: 132-5.

Georgopoulos AP, Schwartz AB, Kettner RE. Neuronal Population Coding of Movement Direction. Science, 1986; 233: 1416-9.

Gierthmuehlen M, Ball T, Henle C, Wang X, Rickert J, Raab M, Freiman T, Stieglitz T, Kaminsky J. Evaluation of muECoG electrode arrays in the minipig: experimental procedure and neurosurgical approach. J Neurosci Methods, 2011; 202: 77-86.

Guenther FH, Brumberg JS, Wright EJ, Nieto-Castanon A, Tourville JA, Panko M, Law R, Siebert SA, Bartels JL, Andreasen DS, Ehirim P, Mao H, Kennedy PR. A wireless brain-machine interface for real-time speech synthesis. PLoS One, 2009; 4: e8218.

Gunduz A, Brunner P, Daitch A, Leuthardt EC, Ritaccio AL, Pesaran B, Schalk G. Neural correlates of visual-spatial attention in electrocorticographic signals in humans. Front Hum Neurosci, 2011; 5: 89.

Hochberg LR, Serruya MD, Friehs GM, Mukand JA, Saleh M, Caplan AH, Branner A, Chen D, Penn RD, Donoghue JP. Neuronal ensemble control of prosthetic devices by a human with tetraplegia. Nature, 2006; 442: 164-71.

Hoffmann U, Vesin JM, Ebrahimi T, Diserens K. An efficient P300-based brain-computer interface for disabled subjects. J Neurosci Methods, 2008; 167: 115-25.

Hu L, Zhang ZG, Hung YS, Luk KD, Iannetti GD, Hu Y. Single-trial detection of somatosensory evoked potentials by probabilistic independent component analysis and wavelet filtering. Clin Neurophysiol, 2011; 122: 1429-39.

Hubel DH, Wiesel TN. Republication of The Journal of Physiology (1959) 148, 574-591: Receptive fields of single neurones in the cat's striate cortex. 1959. J Physiol, 2009; 587: 2721-32.

Huettel SA, Song AW, McCarthy G. Functional magnetic resonance imaging, 2nd ed. Sinauer Associates: Sunderland, Mass., 2008.

Hwang EJ, Andersen RA. Brain control of movement execution onset using local field potentials in posterior parietal cortex. J Neurosci, 2009; 29: 14363-70.

Ince NF, Gupta R, Arica S, Tewfik AH, Ashe J, Pellizzer G. High accuracy decoding of movement target direction in non-human primates based on common spatial patterns of local field potentials. PLoS One, 2010; 5: e14384.

Jensen O, Kaiser J, Lachaux JP. Human gamma-frequency oscillations associated with attention and memory. Trends Neurosci, 2007; 30: 317-24.

Jerbi K, Ossandon T, Hamame CM, Senova S, Dalal SS, Jung J, Minotti L, Bertrand O, Berthoz A, Kahane P, Lachaux JP. Task-related gamma-band dynamics from an intracerebral perspective: review and implications for surface EEG and MEG. Hum Brain Mapp, 2009; 30: 1758-71.

Jocham G, Ullsperger M. Neuropharmacology of performance monitoring. Neurosci Biobehav Rev, 2009; 33: 48-60.

Jung J, Jerbi K, Ossandon T, Ryvlin P, Isnard J, Bertrand O, Guenot M, Mauguiere F, Lachaux JP. Brain responses to success and failure: Direct recordings from human cerebral cortex. Hum Brain Mapp, 2010; 31: 1217-32.

Keene DL, Whiting S, Ventureyra EC. Electrocorticography. Epileptic Disord, 2000; 2: 57-63.

Kellis S, Miller K, Thomson K, Brown R, House P, Greger B. Decoding spoken words using local field potentials recorded from the cortical surface. J Neural Eng, 2010; 7: 056007.

Kenney JF, Keeping ES. Mathematics of Statistics ... Second edition. (Part Two by J. F. Kenney and E. S. Keeping.). 2 vol. D. Van Nostrand Co.: New York, 1951, 1951.

Kim J, Wilson JA, Williams JC. A cortical recording platform utilizing microECoG electrode arrays. Conf Proc IEEE Eng Med Biol Soc, 2007; 2007: 5353-7.

Kim SP, Simeral JD, Hochberg LR, Donoghue JP, Black MJ. Neural control of computer cursor velocity by decoding motor cortical spiking activity in humans with tetraplegia. J Neural Eng, 2008; 5: 455-76.

Kirkeby BS, Robinson MD. Impulsive behavior and stimulus–response variability in choice reaction time. Journal of Research in Personality, 2005; 39: 263-77.

Koelewijn T, van Schie H, Bekkering H, Oostenveld R, Jensen O. Motor-cortical beta oscillations are modulated by correctness of observed action. NeuroImage, 2008; 40: 767-75.

Kovalev D, Spreer J, Honegger J, Zentner J, Schulze-Bonhage A, Huppertz HJ. Rapid and fully automated visualization of subdural electrodes in the presurgical evaluation of epilepsy patients. AJNR Am J Neuroradiol, 2005; 26: 1078-83.

Koyama S, Chase SM, Whitford AS, Velliste M, Schwartz AB, Kass RE. Comparison of brain-computer interface decoding algorithms in open-loop and closed-loop control. J Comput Neurosci, 2010; 29: 73-87.

Krigolson O, Holroyd C, Van Gyn G, Heath M. Electroencephalographic correlates of target and outcome errors. Experimental brain research. Experimentelle Hirnforschung. Expérimentation cérébrale, 2008; 190: 401-11.

Krusienski DJ, Shih JJ. Control of a visual keyboard using an electrocorticographic brain-computer interface. Neurorehabil Neural Repair, 2011; 25: 323-31.

Kubanek J, Miller KJ, Ojemann JG, Wolpaw JR, Schalk G. Decoding flexion of individual fingers using electrocorticographic signals in humans. J Neural Eng, 2009; 6: 066001.

Kubler A, Kotchoubey B, Kaiser J, Wolpaw JR, Birbaumer N. Brain-computer communication: unlocking the locked in. Psychol Bull, 2001; 127: 358-75.

Lachaux JP, Rudrauf D, Kahane P. Intracranial EEG and human brain mapping. J Physiol Paris, 2003; 97: 613-28.

Lal TN, Schroder M, Hinterberger T, Weston J, Bogdan M, Birbaumer N, Scholkopf B. Support vector channel selection in BCI. IEEE Trans Biomed Eng, 2004; 51: 1003-10.

Lebedev MA, Nicolelis MA. Brain-machine interfaces: past, present and future. Trends Neurosci, 2006a; 29: 536-46.

Lebedev MA, Nicolelis MAL. Brain-machine interfaces: past, present and future. Trends in Neurosciences, 2006b; 29: 536-46.

Lee HC, van Drongelen W, McGee AB, Frim DM, Kohrman MH. Comparison of seizure detection algorithms in continuously monitored pediatric patients. J Clin Neurophysiol, 2007; 24: 137-46.

Leuthardt EC, Freudenberg Z, Bundy D, Roland J. Microscale recording from human motor cortex: implications for minimally invasive electrocorticographic brain-computer interfaces. Neurosurg Focus, 2009; 27: -.

Leuthardt EC, Schalk G, Wolpaw JR, Ojemann JG, Moran DW. A brain-computer interface using electrocorticographic signals in humans. J Neural Eng, 2004; 1: 63-71.

Levine SP, Huggins JE, BeMent SL, Kushwaha RK, Schuh LA, Rohde MM, Passaro EA, Ross DA, Elisevich KV, Smith BJ. A direct brain interface based on event-related potentials. IEEE Trans Rehabil Eng, 2000; 8: 180-5.

Lewicki MS. A review of methods for spike sorting: the detection and classification of neural action potentials. Network, 1998; 9: R53-78.

Machado S, Araujo F, Paes F, Velasques B, Cunha M, Budde H, Basile LF, Anghinah R, Arias-Carrion O, Cagy M, Piedade R, de Graaf TA, Sack AT, Ribeiro P. EEG-based brain-computer interfaces: an overview of basic concepts and clinical applications in neurorehabilitation. Rev Neurosci, 2010; 21: 451-68.

Matsuo T, Kawasaki K, Osada T, Sawahata H, Suzuki T, Shibata M, Miyakawa N, Nakahara K, Iijima A, Sato N, Kawai K, Saito N, Hasegawa I. Intrasulcal electrocorticography in macaque monkeys with minimally invasive neurosurgical protocols. Front Syst Neurosci, 2011; 5: 34.

Maulsby R, Winter D, Crawley J, Kellaway P. Electroencephalography. Prog Neurol Psychiatry, 1963; 18: 348-91.

Maynard EM, Nordhausen CT, Normann RA. The Utah intracortical Electrode Array: a recording structure for potential brain-computer interfaces. Electroencephalogr Clin Neurophysiol, 1997; 102: 228-39.

McFarland DJ, Krusienski DJ, Sarnacki WA, Wolpaw JR. Emulation of computer mouse control with a noninvasive brain-computer interface. J Neural Eng, 2008; 5: 101-10.

McFarland DJ, Sarnacki WA, Wolpaw JR. Electroencephalographic (EEG) control of three-dimensional movement. J Neural Eng, 2010; 7: 036007.

McFarland DJ, Wolpaw JR. Sensorimotor rhythm-based brain-computer interface (BCI): feature selection by regression improves performance. IEEE Trans Neural Syst Rehabil Eng, 2005; 13: 372-9.

Mehring C, Nawrot MP, de Oliveira SC, Vaadia E, Schulze-Bonhage A, Aertsen A, Ball T. Comparing information about arm movement direction in single channels of local and epicortical field potentials from monkey and human motor cortex. J Physiol Paris, 2004; 98: 498-506.

Mehring C, Rickert J, Vaadia E, Cardosa de Oliveira S, Aertsen A, Rotter S. Inference of hand movements from local field potentials in monkey motor cortex. Nat Neurosci, 2003; 6: 1253-4.

Mellinger J, Schalk G, Braun C, Preissl H, Rosenstiel W, Birbaumer N, Kubler A. An MEG-based brain-computer interface (BCI). NeuroImage, 2007; 36: 581-93.

Merchant H, Battaglia-Mayer A, Georgopoulos AP. Effects of optic flow in motor cortex and area 7a. J Neurophysiol, 2001; 86: 1937-54.

Middendorf M, McMillan G, Calhoun G, Jones KS. Brain-computer interfaces based on the steady-state visual-evoked response. IEEE Trans Rehabil Eng, 2000; 8: 211-4.

Miller KJ, Zanos S, Fetz EE, den Nijs M, Ojemann JG. Decoupling the cortical power spectrum reveals real-time representation of individual finger movements in humans. J Neurosci, 2009; 29: 3132-7.

Miltner WHR, Braun CH, Coles MGH. Event-Related Brain Potentials Following Incorrect Feedback in a Time-Estimation Task: Evidence for a “Generic” Neural System for Error Detection. Journal of Cognitive Neuroscience, 1997; 9: 788-98.

Moran D. Evolution of brain-computer interface: action potentials, local field potentials and electrocorticograms. Curr Opin Neurobiol, 2010; 20: 741-5.

Moran DW, Schwartz AB. Motor cortical representation of speed and direction during reaching. J Neurophysiol, 1999; 82: 2676-92.

Moritz CT, Perlmutter SI, Fetz EE. Direct control of paralysed muscles by cortical neurons. Nature, 2008; 456: 639-42.

Muller T, Ball T, Kristeva-Feige R, Mergner T, Timmer J. Selecting relevant electrode positions for classification tasks based on the electro-encephalogram. Med Biol Eng Comput, 2000; 38: 62-7.

Naito E, Ehrsson HH, Geyer S, Zilles K, Roland PE. Illusory arm movements activate cortical motor areas: a positron emission tomography study. J Neurosci, 1999; 19: 6134-44.

Nawrot MP, Aertsen A, Rotter S. Elimination of response latency variability in neuronal spike trains. Biol Cybern, 2003; 88: 321-34.

Niedermeyer E, Lopes da Silva FH. Electroencephalography : basic principles, clinical applications, and related fields, 5th ed. ed. Lippincott Williams & Wilkins: Philadelphia ; London, 2005.

Nunez PL, Srinivasan R. Electric fields of the brain : the neurophysics of EEG, 2nd ed. / Paul L. Nunez, Ramesh Srinivasan. ed. Oxford University Press: Oxford, 2006.

Ojemann G. The neurobiology of language and verbal memory: observations from awake neurosurgery. International journal of psychophysiology : official journal of the International Organization of Psychophysiology, 2003; 48: 141-6.

Ojemann G, Schoenfield-McNeill J, Corina D. Different neurons in different regions of human temporal lobe distinguish correct from incorrect identification or memory. Neuropsychologia, 2004; 42: 1383-93.

Parra L, Spence C, Gerson A, Sajda P. Response error correction--a demonstration of improved human-machine performance using real-time EEG monitoring. IEEE transactions on neural systems and rehabilitation engineering : a publication of the IEEE Engineering in Medicine and Biology Society, 2003; 11: 173-7.

Pfurtscheller G, Flotzinger D, Kalcher J. Brain Computer-Interface - a New Communication Device for Handicapped Persons. J Microcomput Appl, 1993; 16: 293-9.

Pfurtscheller G, Neuper C. Future prospects of ERD/ERS in the context of brain-computer interface (BCI) developments. Prog Brain Res, 2006; 159: 433-7.

Pistohl T, Ball T, Schulze-Bonhage A, Aertsen A, Mehring C. Prediction of arm movement trajectories from ECoG-recordings in humans. J Neurosci Methods, 2008; 167: 105-14.

Pistohl T, Schulze-Bonhage A, Aertsen A, Mehring C, Ball T. Decoding natural grasp types from human ECoG. NeuroImage, 2012; 59: 248-60.

Quiroga RQ. Spike sorting. Curr Biol, 2012; 22: R45-6.

Radons G, Becker JD, Dulfer B, Kruger J. Analysis, classification, and coding of multielectrode spike trains with hidden Markov models. Biol Cybern, 1994; 71: 359-73.

Rana P, Lipor J, Lee H, van Drongelen W, Kohrman M, VanVeen B. Seizure Detection using the Phase-Slope Index and Multichannel ECoG. Biomedical Engineering, IEEE Transactions on, 2012; PP: 1-.

Ray S, Niebur E, Hsiao SS, Sinai A, Crone NE. High-frequency gamma activity (80-150Hz) is increased in human cortex during selective attention. Clin Neurophysiol, 2008; 119: 116-33.

Requin J, Riehle A, Seal J. Neuronal activity and information processing in motor control: from stages to continuous flow. Biol Psychol, 1988; 26: 179-98.

Richmond BJ, Optican LM. Temporal encoding of two-dimensional patterns by single units in primate primary visual cortex. II. Information transmission. J Neurophysiol, 1990; 64: 370-80.

Rohde MM, BeMent SL, Huggins JE, Levine SP, Kushwaha RK, Schuh LA. Quality estimation of subdurally recorded, event-related potentials based on signal-to-noise ratio. IEEE Trans Biomed Eng, 2002; 49: 31-40.

Rose C, Smith MD. Mathematical statistics with Mathematica. Springer: New York, 2002.

Rotermund D, Ernst U, Pawelzik K. Towards on-line adaptation of neuro-prostheses with neuronal evaluation signals. Biological cybernetics, 2006; 95: 243-57.

Rubehn B, Bosman C, Oostenveld R, Fries P, Stieglitz T. A MEMS-based flexible multichannel ECoG-electrode array. J Neural Eng, 2009; 6: 036003.

Santhanam G, Ryu SI, Yu BM, Afshar A, Shenoy KV. A high-performance brain-computer interface. Nature, 2006; 442: 195-8.

Savitzky A, Golay MJE. Smoothing and Differentiation of Data by Simplified Least Squares Procedures. Analytical Chemistry, 1964; 36: 1627-39.

Schafer RW. What Is a Savitzky-Golay Filter? Ieee Signal Proc Mag, 2011; 28: 111-7.

Schalk G. Can Electrocorticography (ECoG) Support Robust and Powerful Brain-Computer Interfaces? Front Neuroeng, 2010; 3: 9.

Schalk G, Kubanek J, Miller KJ, Anderson NR, Leuthardt EC, Ojemann JG, Limbrick D, Moran D, Gerhardt LA, Wolpaw JR. Decoding two-dimensional movement trajectories using electrocorticographic signals in humans. J Neural Eng, 2007; 4: 264-75.

Schalk G, Leuthardt EC. Brain-Computer Interfaces Using Electrocorticographic Signals. Biomedical Engineering, IEEE Reviews in, 2011; 4: 140-54.

Schalk G, Miller KJ, Anderson NR, Wilson JA, Smyth MD, Ojemann JG, Moran DW, Wolpaw JR, Leuthardt EC. Two-dimensional movement control using electrocorticographic signals in humans. J Neural Eng, 2008; 5: 75-84.

Schalk G, Wolpaw JR, McFarland DJ, Pfurtscheller G. EEG-based communication: presence of an error potential. Clinical neurophysiology : official journal of the International Federation of Clinical Neurophysiology, 2000; 111: 2138-44.

Schwartz AB, Cui XT, Weber DJ, Moran DW. Brain-controlled interfaces: Movement restoration with neural prosthetics. Neuron, 2006; 52: 205-20.

Seal J, Commenges D, Salamon R, Bioulac B. A statistical method for the estimation of neuronal response latency and its functional interpretation. Brain Res, 1983; 278: 382-6.

Seidemann E, Meilijson I, Abeles M, Bergman H, Vaadia E. Simultaneously recorded single units in the frontal cortex go through sequences of discrete and stable states in monkeys performing a delayed localization task. J Neurosci, 1996; 16: 752-68.

Sellers EW, Kubler A, Donchin E. Brain-computer interface research at the University of South Florida Cognitive Psychophysiology Laboratory: the P300 Speller. IEEE Trans Neural Syst Rehabil Eng, 2006; 14: 221-4.

Serruya MD, Hatsopoulos NG, Paninski L, Fellows MR, Donoghue JP. Instant neural control of a movement signal. Nature, 2002; 416: 141-2.

Shain W, Spataro L, Dilgen J, Haverstick K, Retterer S, Isaacson M, Saltzman M, Turner JN. Controlling cellular reactive responses around neural prosthetic devices using peripheral and local intervention strategies. IEEE Trans Neural Syst Rehabil Eng, 2003; 11: 186-8.

Slutzky MW, Jordan LR, Krieg T, Chen M, Mogul DJ, Miller LE. Optimal spacing of surface electrode arrays for brain-machine interface applications. J Neural Eng, 2010; 7: 26004.

Smith M. Shedding light on the adult brain: a review of the clinical applications of near-infrared spectroscopy. Philos Transact A Math Phys Eng Sci, 2011; 369: 4452-69.

Sokolova M, Japkowicz N, Szpakowicz S. Beyond Accuracy, F-Score and ROC: A Family of Discriminant Measures for Performance Evaluation. AI 2006: Advances in Artificial Intelligence, 2006; %6: 1015--21 %&.

Solis-Escalante T, Muller-Putz G, Pfurtscheller G. Overt foot movement detection in one single Laplacian EEG derivation. J Neurosci Methods, 2008; 175: 148-53.

Staba RJ, Wilson CL, Bragin A, Fried I, Engel J, Jr. Quantitative analysis of high-frequency oscillations (80-500 Hz) recorded in human epileptic hippocampus and entorhinal cortex. J Neurophysiol, 2002; 88: 1743-52.

Stark E, Abeles M. Predicting movement from multiunit activity. J Neurosci, 2007; 27: 8387-94.

Steinier J, Termonia Y, Deltour J. Smoothing and Differentiation of Data by Simplified Least Square Procedure. Analytical Chemistry, 1972; 44: 1906-9.

Suminski AJ, Tkach DC, Hatsopoulos NG. Exploiting multiple sensory modalities in brain-machine interfaces. Neural Netw, 2009; 22: 1224-34.

Taylor DM, Tillery SI, Schwartz AB. Direct cortical control of 3D neuroprosthetic devices. Science, 2002; 296: 1829-32.

Thongpang S, Richner TJ, Brodnick SK, Schendel A, Kim J, Wilson JA, Hippensteel J, Krugner-Higby L, Moran D, Ahmed AS, Neimann D, Sillay K, Williams JC. A micro-electrocorticography platform and deployment strategies for chronic BCI applications. Clin EEG Neurosci, 2011; 42: 259-65.

Treves A, Panzeri S. The Upward Bias in Measures of Information Derived from Limited Data Samples. Neural Comput, 1995; 7: 399-407.

Uematsu S, Lesser R, Fisher RS, Gordon B, Hara K, Krauss GL, Vining EP, Webber RW. Motor and sensory cortex in humans: topography studied with chronic subdural stimulation. Neurosurgery, 1992; 31: 59-71; discussion -2.

Ullsperger M, von Cramon DY. Error monitoring using external feedback: specific roles of the habenular complex, the reward system, and the cingulate motor area revealed by functional magnetic resonance imaging. J Neurosci, 2003; 23: 4308-14.

Unnikrishnan R, Lalonde JF, Vandapel N, Hebert M. Scale selection for the analysis of point-sampled curves. Third International Symposium on 3D Data Processing, Visualization, and Transmission, Proceedings, 2007: 1026-33.

Vaadia E, Kurata K, Wise SP. Neuronal activity preceding directional and nondirectional cues in the premotor cortex of rhesus monkeys. Somatosens Mot Res, 1988; 6: 207-30.

van Schie HT, Mars RB, Coles MG, Bekkering H. Modulation of activity in medial frontal and motor cortices during error observation. Nat Neurosci, 2004; 7: 549-54.

van Veen V, Carter CS. Error detection, correction, and prevention in the brain: a brief review of data and theories. Clin EEG Neurosci, 2006; 37: 330-5.

Vansteensel MJ, Hermes D, Aarnoutse EJ, Bleichner MG, Schalk G, van Rijen PC, Leijten FS, Ramsey NF. Brain-computer interfacing based on cognitive control. Ann Neurol, 2010; 67: 809-16.

Vargas-Irwin CE, Shakhnarovich G, Yadollahpour P, Mislow JM, Black MJ, Donoghue JP. Decoding complete reach and grasp actions from local primary motor cortex populations. J Neurosci, 2010; 30: 9659-69.

Velliste M, Perel S, Spalding C, Whitford A, Schwartz A. Cortical control of a prosthetic arm for self-feeding. Nature, 2008; 453: 1098-101.

Victor JD. Asymptotic bias in information estimates and the exponential (Bell) polynomials. Neural Comput, 2000; 12: 2797-804.

Vidal JJ. Toward direct brain-computer communication. Annu Rev Biophys Bioeng, 1973; 2: 157-80.

Waldert S, Pistohl T, Braun C, Ball T, Aertsen A, Mehring C. A review on directional information in neural signals for brain-machine interfaces. J Physiol Paris, 2009; 103: 244-54.

Waldert S, Preissl H, Demandt E, Braun C, Birbaumer N, Aertsen A, Mehring C. Hand movement direction decoded from MEG and EEG. J Neurosci, 2008; 28: 1000-8.

Walton ME, Devlin JT, Rushworth MF. Interactions between decision making and performance monitoring within prefrontal cortex. Nat Neurosci, 2004; 7: 1259-65.

Wang W, Collinger JL, Perez MA, Tyler-Kabara EC, Cohen LG, Birbaumer N, Brose SW, Schwartz AB, Boninger ML, Weber DJ. Neural interface technology for rehabilitation: exploiting and promoting neuroplasticity. Phys Med Rehabil Clin N Am, 2010; 21: 157-78.

Wang W, Degenhart AD, Collinger JL, Vinjamuri R, Sudre GP, Adelson PD, Holder DL, Leuthardt EC, Moran DW, Boninger ML, Schwartz AB, Crammond DJ, Tyler-Kabara EC, Weber DJ. Human motor cortical activity recorded with Micro-ECoG electrodes, during individual finger movements. Conf Proc IEEE Eng Med Biol Soc, 2009; 2009: 586-9.

Weiskopf N, Mathiak K, Bock SW, Scharnowski F, Veit R, Grodd W, Goebel R, Birbaumer N. Principles of a brain-computer interface (BCI) based on real-time functional magnetic resonance imaging (fMRI). IEEE Trans Biomed Eng, 2004; 51: 966-70.

Weliky M, Fiser J, Hunt RH, Wagner DN. Coding of natural scenes in primary visual cortex. Neuron, 2003; 37: 703-18.

Wisneski KJ, Anderson N, Schalk G, Smyth M, Moran D, Leuthardt EC. Unique cortical physiology associated with ipsilateral hand movements and neuroprosthetic implications. Stroke, 2008; 39: 3351-9.

Wolpaw JR, Birbaumer N, McFarland DJ, Pfurtscheller G, Vaughan TM. Brain-computer interfaces for communication and control. Clin Neurophysiol, 2002; 113: 767-91.

Wolpaw JR, McFarland DJ. Control of a two-dimensional movement signal by a noninvasive brain-computer interface in humans. Proc Natl Acad Sci U S A, 2004; 101: 17849-54.

Wolpaw JR, McFarland DJ, Neat GW, Forneris CA. An EEG-based brain-computer interface for cursor control. Electroencephalogr Clin Neurophysiol, 1991; 78: 252-9.

Wood F, Black MJ, Vargas-Irwin C, Fellows M, Donoghue JP. On the variability of manual spike sorting. IEEE Trans Biomed Eng, 2004; 51: 912-8.

Zanolie K, Van Leijenhorst L, Rombouts SA, Crone EA. Separable neural mechanisms contribute to feedback processing in a rule-learning task. Neuropsychologia, 2008; 46: 117-26.

Zhuang J, Truccolo W, Vargas-Irwin C, Donoghue JP. Decoding 3-D reach and grasp kinematics from high-frequency local field potentials in primate primary motor cortex. IEEE Trans Biomed Eng, 2010; 57: 1774-84.